



**CLOSE-RANGE PHOTOGRAMMETRY AND
GAIT PRESSURE FOR PERPETRATOR
IDENTIFICATION**

A thesis submitted by

Ammar Sabri Majeed Al-Hammashi

For the award of

Doctor of Philosophy

2021

ABSTRACT

Human gait identification is a potential new tool for identifying individuals. The emergence of motion capture techniques provides high accuracy identification because completely recorded gait information can be compared with gait information obtained by security cameras. The emergence of motion capture techniques provides high accuracy identification because recorded gait information can be compared and matched with gait information obtained by security cameras.

This research aimed to build a practical method of gait identification and investigate the individual characteristics of gait and find new identification factors that can be extracted from gait features. A gait identification method was proposed, several studies of individual gait characteristics were performed, and a number of methods were used to compare the identification results.

The project was conducted in three parts. First, it identified the most suitable digital video camera to record the subjects' gait using close-range photogrammetry. Five types of digital video cameras with various specifications and costs were tested, calibrated and analysed. These tests found the most suitable video cameras to capture the gait of the recruits during walking. Second, it used photogrammetry to identify individuals from their gait via a novel set of features based on 3-D motion capture data such as the knee-ankle joint. Analysis of the identification factors was based on three phases of gait: a) heel-down, b) mid-stance and c) toe-off, and statistical analysis was used to validate the identification factors extracted from the gait features. Third, the footprint data of the same recruits was analysed using the RSSCAN International footprint sensing platform. Data, such as total force value for one gait cycle, was extracted from the footprint platform and synchronised with the data extracted from the photogrammetry part of the methodology. The two sets of data (photogrammetry and footprint) were obtained at the same time during walking on the sensing platform. Identification factors obtained from the footprint sensing mat were added to the identification factors from the photogrammetry part.

The resulting factors were found to increase the accuracy of the human identification technique explored in this research. Using statistical analysis, we identified the most significant gait analysis factors for use in human identification. The average identification rate was over 95%, with the best result close to 100%. This high

identification rate is the result of the two correlated identification techniques. Thus , This identification technique could help the crime investigators to identify the perpetrator because of many identification , authenticated factors included.

CERTIFICATION OF THESIS

This thesis is the work of Ammar Sabri Majeed except where otherwise acknowledged.

The work is original and has not previously been submitted for any other award, except where acknowledged.

Dr Albert K. Chong

Principal Supervisor:

Dr Xiaoye Liu

Associate Supervisor:

Dr Shahab Abdullah

Associate Supervisor:

Student and supervisor's signatures of endorsement are held at the University.

ACKNOWLEDGEMENTS

In the first place, I humbly thank Allah the Almighty, who gave me the health and thoughts to achieve this goal. Next, I would like to acknowledge and thank those who gave their valuable time and assisted me throughout my PhD journey. I would like to thank and express my sincere gratitude to Dr Albert K. Chong, my principal supervisor, for his guidance, help, patience, and encouragement. It would have been very difficult to complete my goal without his support.

Special thanks to my associate supervisors Dr Xiaoye Liu and Dr Shahab Abdullah for their assistance and support during the PhD journey .

I would like to dedicate this work to my parents, specifically my Father and my Mother who left us earlier and will not see me graduate. They raised me with a love of science and supported me in all my pursuits. Without their support and their prayers, I could not have completed this work. There are not enough words to describe what a powerful influence they continue to have on me. Many thanks.

It goes without saying that the assistance of my wife was vital. She helped and supported me throughout my journey. There were a lot of ups and downs in our life in Australia, but she was determined to keep me motivated and she believed that this PhD could be completed. It is now done and dusted. My daughters, I love you and this is for you. I would like to thank all my brothers and sisters back home in Baghdad. Without their prayers and positive influence in my life, I would not be where I am now. I would like to thank the support of my friends and colleagues who provided me with technical support. Special mention goes to Dr Mustafa Allame, Dr Mohammed Al-azzawi, and Dr Redha Alrikabi.

I would like to acknowledge the editorial support provided by the English editor, Ms Sandra Cochrane who reviewed the earlier version of this thesis for proofreading. Thank you. I also want to express my thanks to the Republic of Iraq Ministry of Higher Education and Scientific Research and Baghdad University for supporting me and for giving me the opportunity to do my best. I also wish to express my appreciation to the University of Southern Queensland (USQ). It has provided great support which has helped me to overcome the challenges I have faced during my academic study.

Finally, I would like to acknowledge the support of the Australian Commonwealth Government through the Research Training Program (RTP) Fees Offset scheme.

May the Almighty Allah richly bless all of you.

PUBLICATIONS

1. **Majeed, A. and Chong, A.K., 2021**, August. Study of CCTV Footage Based on Lower-Limb Gait Measure for Forensic Application. In *2021 IEEE 12th Control and System Graduate Research Colloquium (ICSGRC)* (pp. 160-164). IEEE.
2. **Majeed, A. and Chong, A.K., 2021**, April. Forensic perpetrator identification utilising foot pressure under shoes during gait. In *2021 IEEE 11th IEEE Symposium on Computer Applications & Industrial Electronics (ISCAIE)* (pp. 123-126). IEEE.
3. **Majeed, A. and Chong, A.K., 2020**, April. Advanced computing and image processing utilised in dashcam imagery study. In *2020 IEEE 10th Symposium on Computer Applications & Industrial Electronics (ISCAIE)* (pp. 211-214). IEEE.
4. **Majeed, A. and Chong, A.K., 2020**, April. Two measures of foot pressure image to detect foot drop of elderly diabetes sufferers. In *2020 IEEE 10th Symposium on Computer Applications & Industrial Electronics (ISCAIE)* (pp. 224-228). IEEE.
5. **Mnati, M.N., Chong, A.K. and Majeed, A., 2019**, July. Smartphone Sensor vs Photogrammetry for Gait Analysis. In *2019 3rd International Conference on Imaging, Signal Processing and Communication (ICISPC)* (pp. 130-133). IEEE.
6. **Majeed, A., Chong, A.K. and Abdulla, S., 2017**, December. Person identification by gait analysis using photogrammetry techniques and foot pressure sensing matt. In *Proceedings of the 1st MoHESR and HCED Iraqi Scholars Conference in Australasia 2017 (ISCA 2017)* (pp. 282-288). Swinburne University of Technology.

Table Of Contents

ABSTRACT	i
CERTIFICATION OF THESIS	iii
ACKNOWLEDGEMENTS	iv
PUBLICATIONS	vi
Table Of Contents	vii
LIST OF FIGURES	xi
LIST OF TABLES.....	xv
LIST OF ACRONYMS & ABBREVIATIONS.....	xviii
1 CHAPTER 1	1
1.1 Introduction	1
1.2 Overview	1
1.3 Research gap	5
1.4 Research questions.....	5
1.5 Objectives	6
1.6 Research outcomes and significance	6
1.7 Thesis structure.....	7
2 CHAPTER 2	9
2.1 Introduction	9
2.2 The content of gait analysis.....	11
2.2.1 Gait animation.....	11
2.2.2 Gait attractiveness.....	12
2.2.3 Gait pattern analysis and recognition.....	13
2.2.4 Gait identification	14
2.3 Human gait applications.....	15
2.3.1 Clinical purposes	15
2.3.2 Sports purposes.....	17
2.3.3 Forensic purposes.....	18
2.4 Common human gait identification technologies	19
2.4.1 Motion capture cameras.....	19
2.4.2 Inertial system.....	22
2.4.3 Electrogoniometer	23
2.4.4 Gait mat/pressure mat	24
2.4.5 Force sensing shoes.....	24

2.4.6	Force plates mechanism	26
2.5	Human gait identification techniques	29
2.5.1	Close-range photogrammetry	29
2.5.1.1	Collinearity Equations	30
2.5.1.2	Radial Distortion.....	32
2.5.1.3	Decentring Distortion.....	33
2.5.1.4	Linear Distortion.....	33
2.5.1.5	Bundle adjustment.....	34
2.5.1.6	Calculation of gait biometric and joint angles using 3- dimensional measurements.....	36
2.5.2	Footprint analysis	38
2.5.2.1	Pressure sensing systems	38
2.5.2.2	In-shoe systems.....	40
2.5.2.3	Footprint characteristics for identification	41
2.5.2.4	Identification using spatio-temporal parameters.....	44
2.6	Summary.....	48
3	CHAPTER 3	50
3.1	Introduction	50
3.2	Research methodology.....	50
3.3	Photogrammetry methodology.....	53
3.3.1	The process of camera calibration.....	53
3.3.2	Three-Dimensional calibration and measurement with iWitnessPRO .	54
3.3.2.1	Significance of camera calibration using iWitnessPRO.....	57
3.4	A process of camera calibration	57
3.4.1	Spy camera calibration	58
3.4.2	Calibration of UNIDEN closed-circuit television (CCTV) camera.....	60
3.4.3	Calibration of JVC handheld video camera.....	62
3.4.4	Calibration of Panasonic digital camera DMC-FZ300	64
3.5	Gait data collection using photogrammetry	67
3.5.1	A step before collecting data	67
3.5.2	Photogrammetry data analysis with the adopted human identification factors.....	69
3.5.3	Calculation of 3-D distances for the subjects at the heel-down stage .	71
3.5.4	Calculation of identification factors for subjects at the mid-stance stage 73	
3.5.4.1	Calculation of knee – inner ankle joint at mid-stance phase 74	
3.5.4.2	Calculation of knee–outer ankle joint at mid-stance phase	75

3.5.4.3	Calculation of knee angle at mid-stance stage	75
3.5.4.4	Calculation of knee-fore foot 3-D distance at mid-stance stage	76
3.5.5	Calculation of identification factors for the subjects at toe-off stage	77
3.5.6	Conclusions of photogrammetry methodology	79
3.6	Human identification using RSSCAN International platform	79
3.6.1	Human identification using force foot value.....	81
3.6.2	Human subject identification using force/pressure foot distance.....	83
3.6.3	Identification factor using temporal, spatial and ground force reaction parameters for human recognition.....	85
4	CHAPTER 4	87
4.1	Research results	87
4.2	Video camera calibration	87
4.2.1	Camera calibration parameters.....	89
4.2.2	Camera calibration data	91
4.2.2.1	Spy camera calibration data results.....	91
4.2.2.2	JVC digital camera calibration data results	96
4.2.2.3	Calibration results of closed-circuit television (CCTV) camera	99
4.2.2.4	Calibration results of Panasonic Lumix DMC-FZ300 digital video camera.....	102
4.3	Photogrammetry results.....	105
4.3.1	Calculation of photogrammetry three dimensions measurements at heel-down stage	105
4.3.1.1	Knee-inner ankle joint 3D distance data with ANOVA analysis	105
4.3.1.2	Knee-outer ankle joint 3D distance data with ANOVA analysis	109
4.3.2	Calculation of 3-D photogrammetry measurements at mid-stance phase.....	113
4.3.2.1	Calculation of knee-inner ankle joint 3-D dimensions distance parameter at midstance stage.....	114
4.3.2.2	Calculation of knee-outer ankle joint 3-D distance parameter at mid-stance stage	117
4.3.2.3	Calculation of knee-angle in 3-D measurements at mid-stance phase	120
4.3.3	Calculation of 3-D photogrammetry measurements at toe-off phase..	122
4.4	Data results and analysis of the footprint using RSSCAN International platform.....	126

4.4.1	Calculating of the Ground Reaction Force (GRF) of a foot during walking	126
4.4.2	Calculation and analysis of foot force/pressure distance identification factor.....	130
4.4.3	Analysis and normalization data of spatial and temporal gait cycle ...	133
5	CHAPTER 5	136
5.1	Discussion.....	136
5.1.1	Overview	136
5.2	Human gait analysis using photogrammetry	136
6	CHAPTER 6	141
6.1	Conclusions	141
6.2	Footprint analysis.....	142
7	REFERENCES.....	144
8	Appendix.....	165

LIST OF FIGURES

Figure 2.1: A taxonomy and timeline of gait recognition. On the left side is a list of enabling technologies. On the right, gait recognition and its advancements over time are shown divided into three main areas: gait analysis, gait forensics and gait biometrics. Some of the images used in this and other figures are from the Internet (Connor and Ross, 2018)..... 10

Figure 2.2: Gait with mood Angry, Sad and happy (Granieri et al., 1995). 11

Figure 2.3: Retargeting process which adapts the motion as the character morphs to 60% of its original size (Granieri et al., 1995). 12

Figure 2.4: Application of data analysis (Prakash et al., 2018). 15

Figure 2.5: Planting sensors on the runner to record movement data (Wahab and Bakar, 2011). 18

Figure 2.6: Sample frame images from crime scene CCTV cameras (Bouchrika et al., 2011). 19

Figure 2.7: Knee kinematics resulting from the proposed protocol during an illustrative gait cycle (Cocchi et al., 2019)..... 21

Figure 2.8: Foot contour (in blue), shank and thigh models (in blue), relevant stick segments (in black) connected through the joint centers (in red) resulting from the proposed ML protocol are superimposed onto the relevant RGB frame (Cocchi et al., 2019)..... 21

Figure 2.9: H-Gait and STEP32 sensor positioning. The images show the: (a) frontal, (b) lateral and (c) rear view of a subject prepared for the bi-instrumented gait analysis. The MIMU sensor positioned below the medial malleolus is shown in panel (d), the footswitches in panel (e) (Agostini et al., 2017). 23

Figure 2.10: A insole sensor GRF sensing device (Yang et al., 2019). 25

Figure 2.11: Instrumented insole is divided into 3 discrete zones, the hind-, mid- and forefoot (A). The load applied to each of these zones occurs at a constant distance from the ankle joint centre which is considered to be the zone centre of pressure (COP) (B). Moment arms (r) are calculated as the difference of these centres of pressure with the distance from the posterior aspect of the sensor to the ankle joint centre (x_{offset}). Plantar flexion moment is calculated as the sum of the scalar products of the moment arm and force applied to each zone.(Hullfish and Baxter, 2020)..... 26

Figure 2.13: Prototype floor sensor carpet (Chaccour et al., 2015)..... 28

Figure 2.12: RSscan international foot pressure mat (author owns this image)..... 28

Figure 2.14: Relationship between image and object point coordinates (Chong et al., 2014).	31
Figure 2.15: Multi-station bundle adjustment.	35
Figure 2.17: Comparison of body morphology of perpetrator and suspect.(Lynnerup and Vedel, 2005)	37
Figure 2.16: Screen shot of Photomodeler Pro R _ interface showing placing of reference points of various bodily features in the left panel and the resultant 3D scale “stickmen” of the perpetrator (Lynnerup and Vedel, 2005).	37
Figure 2.18: Inverted ankle during stance, (Kelly, 2020).	38
Figure 2.19 (a) : . An in-shoe based foot plantar pressure sensor by(Yang et al., 2019). (b) An in shoe based foot plantar pressure sensor F-Scan® System by Tekscan (Hullfish and Baxter, 2020).	40
Figure 2.20: Foot anatomical areas (Shu et al., 2010)	41
Figure 2.22: Clustering and tracking results over about 1.5 gait cycles: (a) through (f) show snap shots of observed floor data and corresponding COPs (red dots) and their ID numbers (white digits) (Andries, 2015).	43
Figure 2.23: Both perpetrator (to the left) and suspect showed inverted left ankle (white arrow) during left leg's stance phase and markedly outward rotated feet.	45
Figure 2.24: (a) Photogrammetric measurement of the perpetrator in the bank. (b) The suspect with measures of stature, eye height and left /right shoulder (Larsen et al.,2008).	48
Figure 3.1: Subjects test position using five digital video cameras and foot pressure sensing mat.	50
Figure 3.2: Four types of cameras used in this research. 1: Panasonic Lumix, 2: JVC handheld video camera, 3: Uniden CCTV camera and 4: Digital spy camera.	52
Figure 3.3: Camera calibration process using iWitness cardboard distributed on 3D surface (author's own image).	53
Figure 3.4: Focal length with x_p and y_p where c =focal length (Chong et al., 2014).	54
Figure 3.5: Photogrammetric triangulation, XYZ coordinates determined from intersecting rays (Chong et al., 2014).	55
Figure 3.6: The camera as an angle measuring device. (Chong et al., 2014).	56

Figure 3.7: Spy camera image extracted during calibration process - curved edge due to lens distortion (author's own image).	58
Figure 3.8: Calibration process in iWitnessPRO using images extracted from spy camera (author's own image).	59
Figure 3.9: Radial and decentring distortion grid of the spy camera (author's own image).	59
Figure 3.10: (a) Uniden CCTV camera and (b) Radial and decentring distortion grid of the UNIDEN CCTV camera (author's own image).	61
Figure 3.11: Calibration process for CCTV UNIDEN camera (author's own image).	62
Figure 3.12: Radial and decentering distortion grid for JVC video camera (author's own image).	63
Figure 3.13: JVC hand-help FHD video camera (author's own image).	63
Figure 3.14: Calibration of JVC video camera. Digitizing has a small number of non-digitizing points (author's own image).	64
Figure 3.15: Panasonic Lumix DMC-FZ 300 used to collect data (author's own image).	64
Figure 3.16: Panasonic digital camera while recording a subject gait. (author's own image)	65
Figure 3.17: Radial and decentering distortion grid for Panasonic Lumix DMC-FZ300 digital camera (author's own image).	66
Figure 3.18: 3-D model showing data collection with the distribution of the Panasonic cameras. Black mat refers to the RS scan foot pressure mat (author's own image).	66
Figure 3.19: Clock screen used in data recording, the three screens are synchronized and showing minutes, seconds and three digits of milliseconds (author's own image).	67
Figure 3.20: Capturing two images with clear view of the lowe-limb with the corresponding 3-D model of the points selected (author's own image).	69
Figure 3.21: Two images extracted from two different cameras: a- Image with blurry taken from JVC hand-held digital camera, b- Non-blurry image extracted from Panasonic digital cameras which were used in this research (author's own image).	71
Figure 3.22: Calculating real measurement of knee-inner/outer ankle joint to be compared with photo measurement to obtain error difference (author's own image).	72
Figure 3.23: Calculation of identification factors at heel-down stage. (a) Distance from knee-inner ankle joint, (b) Distance from knee-outer ankle joint (author's own image).	73

Figure 3.24: Calculations of identification factors at mid-stance stage. Measurements from two cameras views: a) measurements of knee-outer ankle joint, b) measurements of knee-inner ankle joint (author's own image).	74
Figure 3.25: Two extracted images with their corresponding 3-D modelling. Points 13, 14 and 15 to calculate the knee angle (author's own image).	76
Figure 3.26: The knee-forefoot 3-D distance at mid-stance stage (author's own image).....	77
Figure 3.27: Five different views for the toe-off stage for a recruit (author's own image). ...	78
Figure 3.28: RSScan International foot pressure mat with high speed 500frame/sec, 2.0 m.	80
Figure 3.29: Frame points which contain information of force, 2-D coordinates and time for the foot during walking (author's own image).	83
Figure 3.30: Force/pressure line (a,b) for recruit Number 9. We can see the similarity of the force line direction. (c,d) force/pressure line for subject number 15, and we can see the similarity of the force line direction. (a,b) has a different footprint shape and is different from (c,d) in regards to the force line direction. (author's own image).....	84
Figure 3.31: Temporal analysis diagram with factors related to temporal analysis (author's own image).....	85
Figure 4.1: Camera calibration (Fraser, 2013).....	89
Figure 4.2: (a) and (b) Panasonic Lumix DMC-FZ300 parameters after successful calibration a- at 4K resolution (3840x2160) pixel, b- at low resolution (1280x720) pixel.	90
Figure 4.3: Spy Camera parameters.....	92
Figure 4.4: Radial and decentring distortion for Spy camera.....	93
Figure 4.17: Knee-inner and outer joint ankle at heel down stage.	113
Figure 4.18: 3-D distance parameters at mid-stance stage.	114
Figure 4.19: Scatter plot of knee-inner ankle joint mean distance (mm) with standard deviation at mid-stance stage.	117

LIST OF TABLES

Table 3.1: Subjects' information.....	68
Table 3.2: Photogrammetry factors used in the research methodology	70
Table 3.3: Specifications of the RSSCAN foot scan mat used in this research (http://www.rsscan.com).....	80
Table 3.4: Example of data extracted from each frame while subject walked on force/pressure platform.	82
Table 3.5: Frame no. with the sum of 110 points distances in (mm) compared to the shoe length	84
Table 4.1: Spy camera parameters	94
Table 4.2: Spy camera radius with the corresponding radial distortion according to formula (4.1).	95
Table 4.3: JVC GZ-HD260 video camera specification (http://everio.jvc.com/).....	96
Table 4.4: Calibration parameters for JVC GZ-HD260 digital video camera.....	98
Table 4.5: Radial distortion correction parameter for JVC GZ-HD260 digital video camera	98
Table 4.6: Radial distortion correction parameter for UNIDEN CCTV digital video camera.	101
Table 4.7: Specifications of Panasonic Lumix DMC-FZ300 digital camera used to collect subjects' data	102
Table 4.8: Radial correction parameters calculated using formula 4.4 for the Panasonic digital camera.....	104
Table 4.9: ANOVA analysis knee-inner ankle joint distance (mm) with standard deviation at heel-down stage	107

Table 4.10: ANOVA analysis of Knee_inner_joint_Ankle_Heel_down_distance_(mm) showing the significance value.....	108
Table 4.11: ANOVA analysis knee-outer ankle joint distance (mm) with standard deviation at heel-down stage.....	111
Table 4.12: ANOVA analysis of Knee_outer_joint_ankle_at Heel_down_distance_(mm) showing the significance value.....	112
Table 4.13: ANOVA analysis knee-inner ankle joint distance (mm) with standard deviation at mid-stance stage	116
Table 4.14: ANOVA calculation for Knee to Inner-Joint_Ankle_Mid-stance.....	117
Table 4.15: The mean value of the 3-D measurements of knee-outer ankle joint parameters	118
Table 4.16: ANOVA Knee_outer_Joint_Ankle_Mid-stance.....	119
Table 4.17: 3-D knee angle at mid-stance phase with a standard deviation	121
Table 4.18: ANOVA analysis for 3-D knee angle at mid-stance phase.....	122
Table 4.19 a: ANOVA analysis knee-inner ankle joint distance (mm) with standard deviation at toe-off stage.....	123
Table 4.20b: ANOVA analysis knee-outer ankle joint distance (mm) with standard deviation at toe-off stage.....	124
Table 4.21: ANOVA analysis for the Knee_Inner_Joint_Ankle at Toe-off_stage..	125
Table 4.22b: ANOVA analysis for the Knee_outer_Joint_Ankle at Toe-off_stage	125
Table 4.23: Calculating foot force of one recruit for one step, value shown for each frame.	127
Table 4.24: Indicates that this similarity factor is significance while s too high within the group of subjects.	129

Table 4.25: ANOVA analysis for foot force_(KN)	130
Table 4.26: Statistical analysis for the foot force-distance with standard deviations	132
Table 4.27: ANOVA analysis for distance_Foot_force_or_Pressure_data with similarity significance factor threshold value 0.005	133
Table 4.28: Statistical analysis of normalized (Gait cycle /Ambulation time) X total foot pressure.	134
Table 4.29: ANOVA analysis of gait cycle normalized ambulation time then multiply by total foot pressure.....	135

LIST OF ACRONYMS & ABBREVIATIONS

Acronyms and abbreviations	Meaning
PP	Peak pressure
PTI	Pressure-time integral
CA	Contact area
CT	Contact time
COP	Centre of pressure
kPa.sec	Kilopascals multiplied by seconds
ms	Milliseconds
mm	Millimeter
ACL	Anterior cruciate ligament
RTS	Return-to-sport
ki	Coefficients of radial distortion
r_o	Radial distance from the principal point
EO	Exterior Orientation
IO	Interior orientation
GRF	Ground Reaction Force
ANOVA	Analysis Of Variance
DNA	Deoxyribonucleic acid
COP	Centre of pressure
CCTV	Closed circuit television
RGB	Red Green Blue
EGM	Electrogoniometer
pEGM	Potentiometric
fEGM	Flexible EGM
DoF	Degree of Freedom
FSR	Force Sensitive Resistors

3D	Three dimensions
FHD	Full high definition
DVR	Digital Video recorder
RTS	Return-To-Sport
ACL	Anterior Cruciate Ligament
ML	MarkerLess

CHAPTER 1

1.1 Introduction

This chapter provides a general overview of the research topic. It presents the research gap, objectives, questions, significance and the scope of the research. It also outlines the structure of the thesis.

1.2 Overview

Security has become a significant concern in modern society. This is due to the proliferation of crimes and terror attacks, and the need to provide a safer environment. Because of the rapid growth of security cameras and the lack of manpower to supervise them, the integration of biometric technologies into surveillance systems is a critical factor for the automation of security and forensic analysis (Nurse et al., 2017; Harrati et al., 2017). More importantly, with the early recognition of suspicious individuals (who may pose security threats) via the use of biometrics, a security system would be able to deter future crimes due to the identification of perpetrators as soon as possible, thus preventing further offences and to allowing justice to be administered (Christensen et al., 2021; Leipold, 2021).

Biometrics is concerned with deriving a descriptive measurement based on either human behavioural or physiological characteristics which distinguish one person from other people (Bouchrika, 2018; Bouchrika, 2017). Examples of physiological-based biometrics include the face, ear, fingerprint and DNA, whilst behavioural features include gait, voice and signature. Apart from being unique, the biometric description should be universal and permanent. The universality condition implies that measures can be taken from the entire population, while permanence signifies that the biometric signature should stay the same over time.

Unlike traditional identification or verification methods such as passports, passwords or personal identification numbers (PINs), biometrics cannot be transferred, forgotten or stolen, and should ideally be obtained non-intrusively (Tvoroshenko and Kukharchuk, 2021). Biometrics can work in either verification or identification mode. For verification, the system performs a one-to-one match for the newly acquired person's signature against a pre-recorded signature in a database to verify the claimed identity. A one-to-many matching process is conducted for identification against all

subjects already enrolled in the database to infer the subject's identity (Gautam et al., 2019).

Biometrics is now in regular use; deployed in various applications such as immigration border control, forensic systems and payment authentication (Sabhanayagam et al., 2018). The use of biometrics for people identification is considered to be a vital tool for forensic investigation.

Forensic science can be defined as a gathering, analysing and interpreting past information related to criminal, civil or administrative law. This includes the perpetrator identity and modus operandi (Lynnerup and Vedel, 2005). Forensics involves investigation, evaluation, forensic intelligence, automated surveillance and forensic identity management (Tistarelli et al., 2014). Forensic analysis is performed to conclude further evidence to exonerate the innocent and corroborate the perpetrator's identity by producing well-supported evidence.

The term "evidence" spans physical evidence, scientific statements and expert witness testimony (Harrati et al., 2017). Scientific statements are usually supported by hypotheses and experiments driven by statistical-based evidence and biometrics. Forensic biometrics is the scientific discipline concerning the use of biometric technologies to determine whether a perpetrator's identity (recorded during the crime scene) can be identified or excluded via a process of matching against a list of suspects (Bouchrika, 2017).

Many biometric features can be used in forensic analysis, such as the face, ear (Eftekhari et al., 2015), speech and gait (Bouchrika et al., 2011). However, the availability of biometric features for identification is limited to forensic experts, depending on the nature of the crime scene and perpetrators. An expert witness is usually based on a body of knowledge or experience provided by an individual who is formally qualified and broadly experienced in a particular domain. Important factors contribute to establishing an individual's credibility acting as an expert. These include educational qualifications and relevant experience. However, qualitative and descriptive-based expert opinions are argued to be insufficient and less credible (Biber, 2009;Edmond et al., 2014;Porter, 2009) compared to empirical-based statements that are gaining wider acceptance.

Human gait analysis, the systematic study of human walking, has been developed from early descriptive studies to newer studies involving mathematical analysis and modelling, and has become an important part of human motion analysis. Gait analysis has been applied in many areas including the biomechanical, psychological and security disciplines. The goal of researchers is to analyse a walker's status (such as gender, age and health) based on their gait (Jung et al., 2018;Prakash et al., 2018;Schülein et al., 2017;Smith-Ray et al., 2015). Furthermore, researchers aim to identify individuals (Khamsemanan et al., 2017;Wang and Yan, 2020;Song et al., 2019).

Recently, the use of soft biometrics for recognition has been studied. In Annamalai et al. (2018), a video analysis framework using soft biometric signatures such as skin tone and clothing colour was used for airport security surveillance. In (Kozlow et al. 2018), an efficient framework combining soft biometrics, such as height and stride length, along with gait features was proposed. With the development of gait recording techniques, research methods have also advanced. The question that was first proposed in the 1970s, “Can people recognise their friends or family by gait” has been developed to “Can we identify a particular person by gait” (Cutting and Kozlowski, 1977;Troje et al., 2005;Jokisch et al., 2006;Moustakas et al., 2010). Intuitively, we know that individual gaits are different and include some personal information. Can gait features be used like a 'biometric signature' to identify individuals, similar to DNA or handwriting? This question inspired the research aims of this thesis.

In this research, a novel approach for identifying individuals is proposed based on 3D motion capture data. A novel gait feature set is presented and evaluated. It investigates the different influences on gait features from three gait phases (heel-down, mid-stance and toe-off). The first part of this research which is close-range photogrammetry, as the name suggests, has been traditionally limited to short to medium camera-to-object distances. With the growing use of off-the-shelf digital cameras for photogrammetric measurement, however, requirements are emerging to perform measurements over: a) long distances, for applications in construction engineering, deformation monitoring and traffic accident reconstruction and b) very short distances for applications such as digital documentation and 3D measurements for forensic application via image-based approaches.

Such measurements often require long focal length lenses to keep the spatial resolution high and optimize the angular measurement precision. One of the most important factors of photogrammetry is camera calibration. Well calibrated cameras create images that are high precision, measurable and scalable objects. Different approaches to camera calibration depend on the type of project (Chong et al., 2014). For the close range photogrammetry used in this research, iWitness pro v.4.1 was used to obtain a well calibrated camera. The reason for the adoption of iWitness pro v.4.1 is described in detail in Chapter 3.

Human gait recognition has some challenges due to walking velocity changes (Heo et al., 2019). One possible way to solve this problem is to use the footprints remaining after human walking behavior. For this reason, we add to this research, a second identification technique to add more authenticated identification parameters to the photogrammetry using footprint features. Our study uses the footprints of recruits with their shoes on because this is an identification technique related to forensic applications.

Footprint-based person recognition methods began with Nakajima et al. (2000) who demonstrated an 85% recognition rate for ten men using normalized static footprints. Jung et al. (2003) showed the possibility of unconstrained person recognition using position-based quantisation of the centre of pressure (COP)_trajectory from shoe-type pressure sensors. Jung et al. (2003) tested five men's walking data and showed 100% recognition rate. But there was a problem that data are considerably correlated since all data were collected in a same day. Moreover, using a shoe-type sensor could be a serious constraint in the view of users.

In this research, one of the footprint identification parameters is calculating the total value of foot pressure for one complete step with shoes-on on a pressure sensing platform. In Chapter 3, we will describe in detail the identification parameters extracted by footprint data, and in Chapter 4 we will explain the statistical analysis of this data and evaluate the adoption of these parameters for human identification as an authenticated factor. For this research, a novel gait phases definition was proposed. The similarity and dissimilarity between gait features were investigated. The relationship between gait features and footprint features were analysed, and a predictable model for gait attractiveness was built.

1.3 Research gap

From a review of the literature (detailed in Chapter 2), it can be seen that the most common gait identification is using computer vision such as photogrammetry and silhouette to extract gait features and use them for human identification. The other application used is foot scan analysis for medical applications. In this research, we use a new approach for human identification. We correlate the two parts of human identifications. The first part uses computer vision close-range photogrammetry to capture images at specific gait phases and extracts gait features to use them in identification. The second part of this research uses footprint features for human identification. The new approach used in this research is to correlate these two parts to extract identification features simultaneously during walking on a force platform. The extracted identification factors from the two parts are combined and used as one set of human identification factors.

The existing literature has not reported any works that:

- a) correlate both photogrammetry techniques and Footprint techniques for human identification
- b) use the RSSCAN international footprint scan for human identification while shoes are on
- c) use gait features as in this research to extract identification factors such as knee-inner joint ankle 3-D distances and force foot 2-D distance.

These strategies can help to increase the accuracy of human identification from 95%-100% because they combine two different techniques and correlate their identification factors to become one set of identification techniques.

1.4 Research questions

This research has several questions which are:

1. Photogrammetry camera calibration:
 - a) What type and configuration of photogrammetric control is required to calibrate the cameras used in this research?
 - b) Does the configuration of camera tripods affect optimum 3-D images?
 - c) What is the minimum number of cameras that can provide the highest accuracy to obtain the subject's identification data?

2. Gait and plantar pressure test:

Does 20-30 subjects are enough to obtain their identification information accurately?

3. Plantar pressure:

a) What are the most reliable footprint parameters that give the most accurate data for the subject?

b) What is the minimum number of gait cycles that can be used to achieve the highest accuracy for the subject?

4. Close-range photogrammetry:

a) Is the accuracy of subject identification affected if the data is captured using different cameras or CCTV systems?

b) Will data accuracy be affected when cameras are not frequently calibrated?

1.5 Objectives

The main aim of this study is to introduce a more efficient approach for identifying a human subject. In order to achieve this aim, four objectives were formalised:

1- Determine the most reliable video camera features for human gait recording. This includes finding the most suitable digital video cameras. Also, finding the best calibration techniques to ensure that accurate data is extracted from gait recordings

2- Demonstrate an innovative alternative methodology to extract human identification parameters by analysing gait features using photogrammetry techniques

3- Demonstrating the effectiveness of the innovative methodology using the footprint features for human identification. This can be proved by extracting the footprint features data using the force foot platform

4- By The correlation of force/pressure and physical three - dimensional measures , we can obtain a huge potential in finding suitable ways to separate perpetrator from suspects. These potentials provide excellent research opportunities for the betterment of forensic sciences.

1.6 Research outcomes and significance

Completing this research may bring a number of substantial benefits. These are:

1. Assist criminal investigators to identify criminal suspects using this new technique
2. Increase the security of the interior and exterior of places such as government buildings and banks by adding the designed system to the main entrance of these buildings
3. Can be used when other facial recognition techniques fail
4. Help to detect suspects by combing data from more than one position that uses the same system
5. Can be applied to individuals wearing shoes or trousers
6. Low-cost equipment compared with other security systems.

1.7 Thesis structure

This thesis consists of six chapters, and each chapter provides essential information on the study. The rest of the thesis is structured as follows:

Chapter 1: The introductory chapter explains the background and definition of human gait and gait identification, photogrammetry techniques and the footprint force platform. The research problems and aims, research objectives, significance of the research, expected outcomes of the research and the thesis structure are also discussed

Chapter 2: Presents the literature review which considers the importance of human gait analysis, human identification methods using gait analysis, and close-range photogrammetry with the footprint force platform

Chapter 3: Divided into two parts, it describes the instrumentation used to perform the study's experiments. The first part shows the measurement systems used to measure kinematics of the lower limb movements, the test protocol, camera calibration and photogrammetric data capture, data collection from the recruits' gait, calculation, and statistics. The second part describes the materials used for the practical application of the research. It also describes the method of data collection using both regions, photogrammetry and the foot force platform. This chapter shows participants, protocol tests, data collection and processing, and statistical analysis.

Chapter 4: Presents the results of the photogrammetry testing, including camera calibration, force foot platform testing and the statistical analysis that reveals the identification parameters used to validate the research techniques used to evaluate and validate the presented methods

Chapter 5: Presents the main discussions points of the research conducted

Chapter 6: Presents the conclusion of the thesis and the future work.

CHAPTER 2

2.1 Introduction

The increase in the number of crimes worldwide has led researchers to explore new methods of identifying crime suspects. A traditional identification method is recognition by gait pattern. Another approach is using biometric devices to analyse footprint features. A new method, proposed in this study, is correlating lower limb gait analysis with footprint features analysis to obtain more accurate, authentic and reliable data that helps forensic investigators detect crimes quickly and accurately.

The development of gait recognition is shown in Figure 2.1. Unique walking patterns such as lower limb movement patterns and ground reaction forces (GRFs) have been used to identify individual humans through biomedical and forensic experiments. These patterns have helped with individual gait recognition (Tao et al., 2007). Ground reaction force (footprints) has also been used to identify criminals (Tao et al., 2012). The cumulative foot pressure record image system provides a lot of information for identifying the different walking patterns compared to the simple 2D system (Sivapalan et al., 2011). The cumulative system has also been used in biomedical assistants and forensic investigations.

Combining evidence from different sources has been achieved by proposing a multimodal biometric system (Jain et al., 2004). These sources come from other sensors (Poon et al., 2006), different classification algorithms (Shan et al., 2008), or directly from diverse biometric trails (Lanitis, 2010).

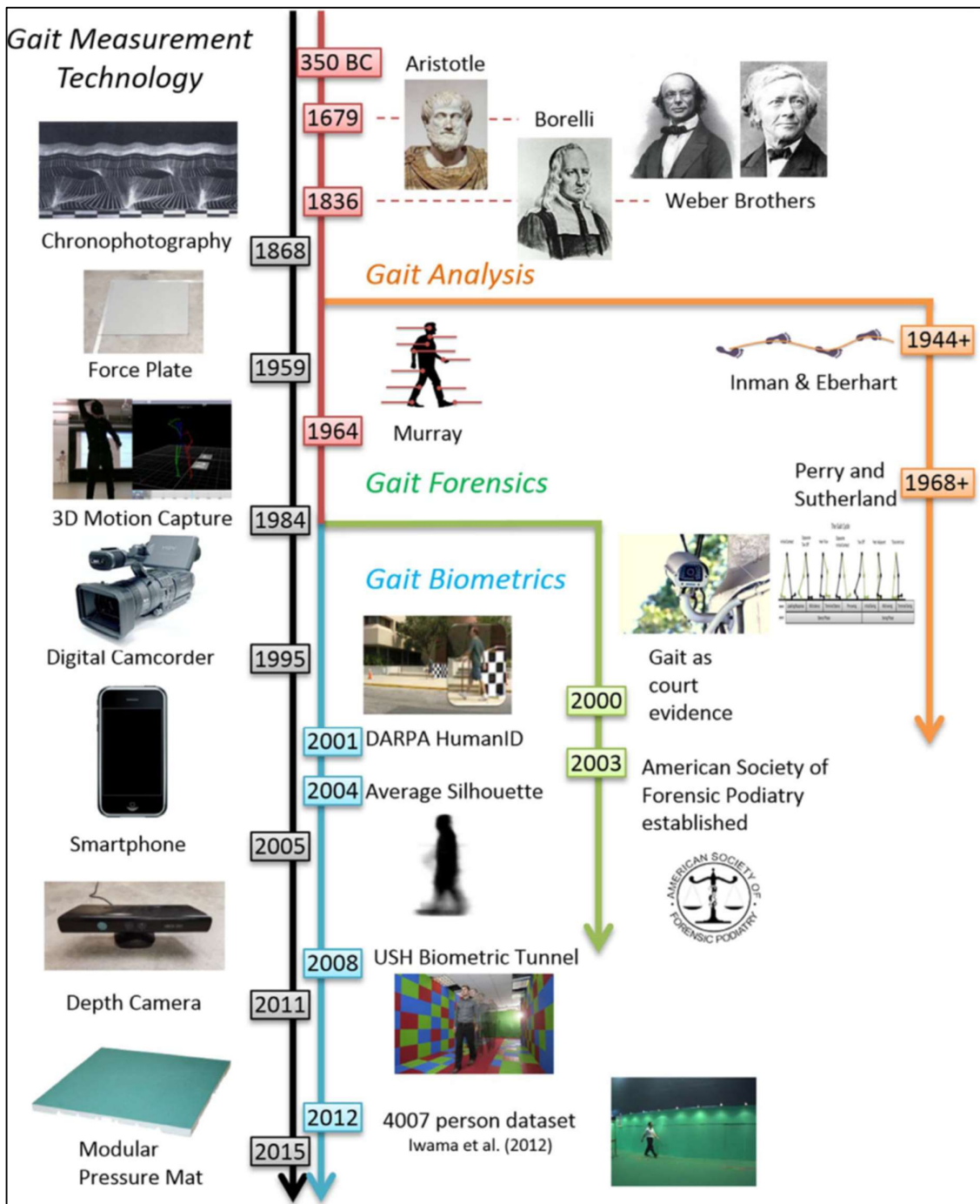


Figure 2.1: A taxonomy and timeline of gait recognition. On the left side is a list of enabling technologies. On the right, gait recognition and its advancements over time are shown divided into three main areas: gait analysis, gait forensics and gait biometrics. Some of the images used in this and other figures are from the Internet (Connor and Ross, 2018).

2.2 The content of gait analysis

Human walking is a simple process that involves a large amount of information. The analysis of quantitative gait data has mainly focused on the identification, animation, pattern analysis and recognition, attractiveness, and other specific factors.

2.2.1 Gait animation

Gait animation has been observed in a variety of application fields including computers, game design, advertising and simulation. Gait animation has attempted to create a virtual human that seems more like an actual human. The problem of human motion animation is the requirement for reality and complexity. Human motion animation ranges from very subtle motions such as smiling to whole-body motions such as dancing and running. Much previous research has focused on modifying and rebuilding existing movements based on motion capture data. Motion editing methods have been surveyed in Balazia and Plataniotis (2016). The generation of synthetic walkers was investigated as early as 1978 (Cutting et al., 1978).

Research related to articulated figure motion expanded the range of possible motion (Kaufman et al., 1999). Generating motion with mood, such as a “tired” walk, from a normal motion was studied via Fourier principle methods in Granieri et al. (1995). Research has also attempted to retarget motion to new characters by re-establishing constraints while maintaining the frequency characteristics of the original motion (Kleissen et al., 1998). Figures 2.2 and 2.3 illustrate an example of animation.

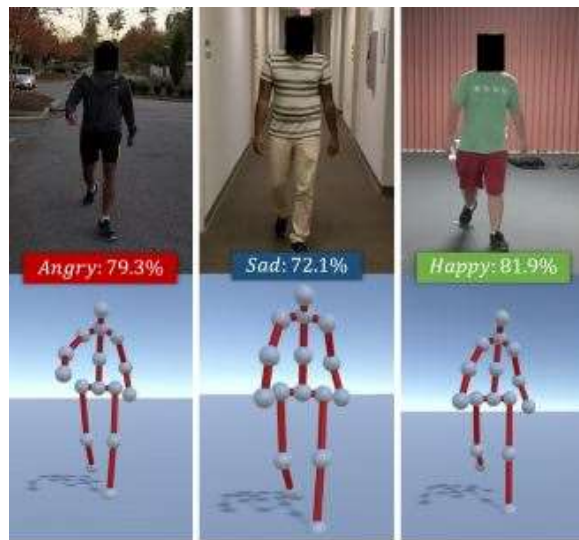


Figure 2.2: Gait with mood Angry, Sad and happy (Granieri et al., 1995).

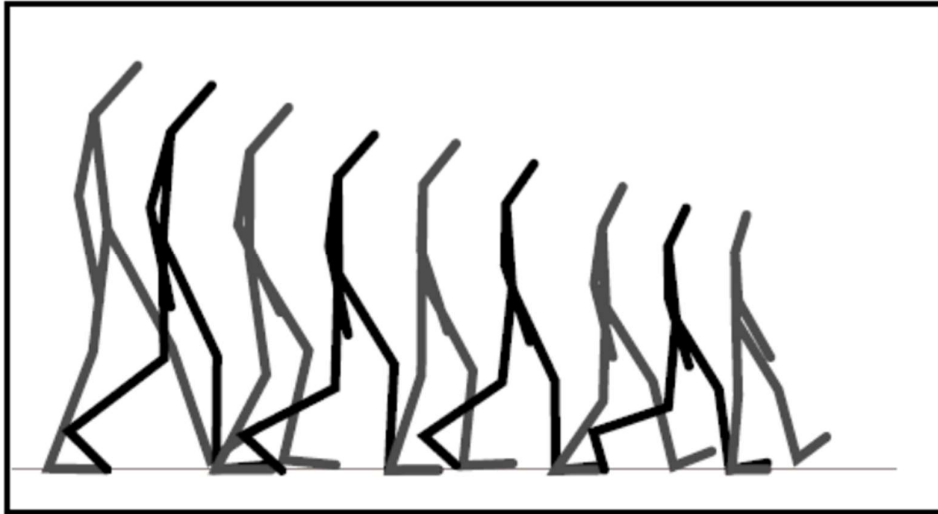


Figure 2.3: Retargeting process which adapts the motion as the character morphs to 60% of its original size (Granieri et al., 1995).

2.2.2 Gait attractiveness

Psychologists have long been interested in how people assess the attractiveness of others. Body shape is static, but the gait is dynamic. People continuously perceive gait attractiveness, whether this perception is conscious or not, because in real life, human figures are active most of the time, and walking is a common movement. As early as the 1930s, some researchers considered the factors influencing gait movement attractiveness (Allport and Vernon, 1933; Wolff, 1935; Eisenberg and Reichline, 1939). One study demonstrated that the gait of dominant women were rated as more attractive than those of non-dominant women, but these results were not conclusive because of methodological difficulties such as how to present the behavioural component of gait separately (Eisenberg and Reichline, 1939). At that time, the medium used to record gait was motion pictures. After the development of the point-light kinematic display method, it became possible to establish that people can indeed infer various traits of a subject based solely on movement cues from gait (Kozlowski and Cutting, 1977; Cutting et al., 1978). Some point-light research investigated the vulnerability

cues in the gait of target choices for assault (Grayson and Stein, 1981; Gunns et al., 2002).

Experimental results showed that the impression of awkward movement as a kinematic gait quality is related to both a higher feminine impression as well as a higher likelihood of being a target for sexual advances (Sakaguchi and Hasegawa, 2006). Computer animation technology has also provided new methods of gait analysis that have been used to explore gait attractiveness. Johnson et al. (2007) found that animated walkers were rated as more attractive by the opposite sex if they exhibited more sex-typical walking movements. The emergence of 3D motion capture techniques has improved the quality of data that can be used to analyse the gait attractiveness of real human walkers. For example, (Provost et al., 2008; Sheng et al., 2008) used motion capture to analyse variations in gait between women at high and low probability of conception and the attractiveness ratings that men assigned to these variations.

They found that the gait of women not using hormonal birth control were slightly more attractive during the luteal stage than in the late follicular phase.

2.2.3 Gait pattern analysis and recognition

Gait is related to a variety of information including health status, medical disease, age, gender, emotion and so on. Pattern analysis studies the gait patterns of a particular type of subject to reveal the relationship between this information and gait. Pattern analysis focuses on revealing the difference in gait pattern and the factors that affect a particular gait pattern, such as elder gait, female/male gait, patient gait and so on. For example, much research has focused on the effect of gender on gait (Cho et al., 2004; Murphy et al., 2005; McKean et al., 2007; Kobayashi et al., 2014). The gait of healthy subjects and patients has received increasing attention since the emergence of the motion capture technique (Woollacott and Shumway-Cook, 2002; Aminian and Najafi, 2004; Zhou and Hu, 2008; Aich et al., 2018).

In medicine, gait research is normally based on a single type of subject to investigate the difference between their gait and normal gait. In 1994, Hennekes and Nigg researched the gait characteristics of age and gender (Hennekes and Nigg, 1994). Age-related changes in gait were researched in 2005 (Kovacs, 2005). In 2009, researchers investigated the effect of walking surfaces, footwear and age on gait (Menant et al., 2009). Gait recognition is one important part of gait analysis and has attracted much

attention since the beginning of gait analysis. Gait recognition is a broad topic that includes gender recognition, age recognition, medical recognition, action recognition, and other recognitions depending on the characteristic used as the classification standard. Gait recognition is highly related to pattern analysis.

Pattern analysis analyses the different patterns of different groups compared the differences in the appearance of different groups of walkers and investigates the factors that affect gait. Gait recognition identifies the group to which the walker belongs. For example, there are some common types of recognition such as gender recognition, age recognition and health recognition.

2.2.4 Gait identification

A particular area of gait recognition research is gait identification which identifies individuals. In gait recognition, different subjects are classified by type. Gait identification research aims to identify individuals. It is only recently that identification by human gait has become an active area of study. Early medical studies demonstrated that individual gaits are unique, varying from person to person, and difficult to disguise (Murray et al., 1964). Kich showed that this personal identification ability also extends to the recognition of friends (Kich, 1992).

Stevenage et al. (1999) demonstrated that the individual human subject could be identified on the basis of their gait signature, without reliance on body shape, in the presence of lighting variations and under brief exposures. A novel technique for analysing moving shapes is presented using area-based metrics for automatic gait recognition (Kim and Paik, 2009). This technique is also used to discriminate between male and female subjects.

The field of security has also utilised gait analysis techniques. Scientists have been investigating the use of gait for personal identification and have tried to identify gait signatures that are specific to individuals. Security and biometrics aim to identify an individual through their actions. In 1988, the recognition of friends had already been researched from a medical/behavioural perspective (Norman, 1988). Later, several attempts were made to investigate the gait recognition problem from the perspective of capturing and analysing gait signals (Boulgouris et al., 2005). In 2014 and 2015, the identification of individuals was investigated based on walking pattern (Lee et al., 2014; Sprager and Juric, 2015) and area-based metrics (Foster et al., 2003).

Researchers have attempted to extract gait signature (Raj et al., 2010) or some combinations of gait and force foot signatures (Balazia and Plataniotis, 2016). Most recent work investigating the appropriateness of gait as a biometric for human identification has been performed in the context of the Human ID project sponsored by the U.S. Defense Advanced Research Project Agency (Bouchrika, 2017).

2.3 Human gait applications

Early work by Vasconcelos and Tavares (2008) discuss the application domains in gait analysis. In this section, we discuss the state of the art in the possible application of gait analysis. Gait analysis applications can be clustered under five applications: analysis, biometric, artificial gait, control based and other applications as shown in Figure 2.4.

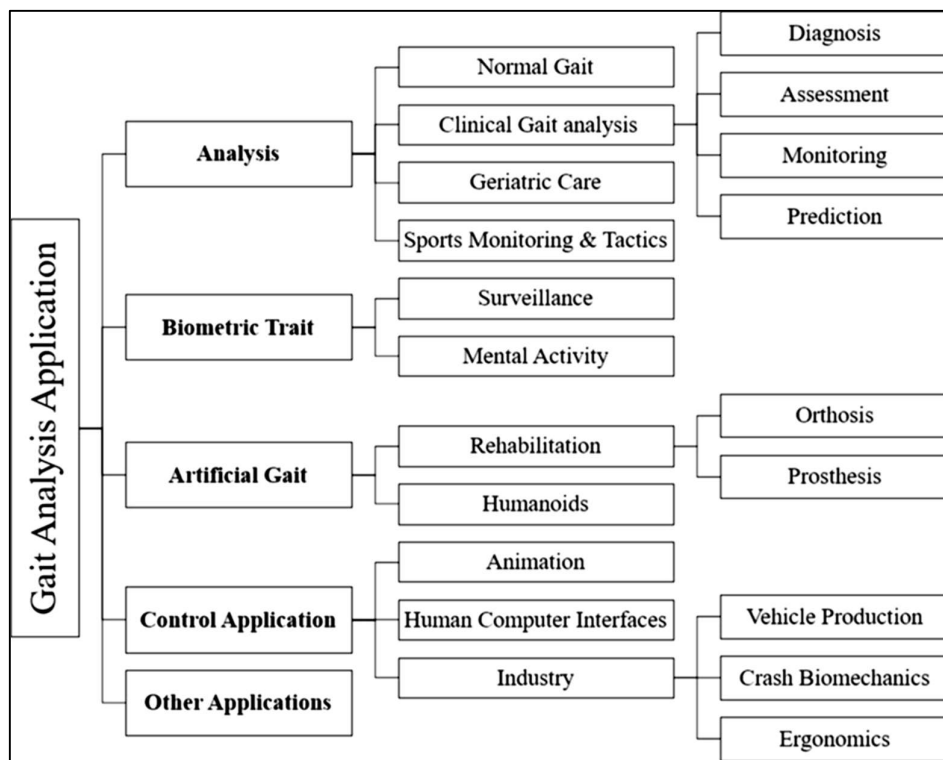


Figure 2.4: Application of data analysis (Prakash et al., 2018).

2.3.1 Clinical purposes

As stated earlier, evaluating some aspects of quality of life can be achieved by examining peoples' gait. According to (Muro-De-La-Herran et al.2014), gait analysis

becomes of particular interest when considering some special health situations and diseases that negatively impact a person's ability to walk normally; for instance, some neurological and systemic diseases or those caused by aging. From a clinical point of view, knowing and monitoring patients' gait characteristics can help specialists diagnose some diseases earlier and recommend better treatments. Zhou et al. (2020) have used some gait characteristics with machine learning techniques to predict falling behaviour in the elderly. Some gait parameters showed more significant associations with fall prediction as found with the study of the gait of 12 young and 12 elderly participants. This study concluded that injuries could be prevented by early identification of changes in gait.

Brehm et al. (2008) employed gait analysis to examine the effect of the so-called ankle-foot orthoses on walking efficiency in a heterogeneous group of children with cerebral palsy. They analysed the data of 172 children with spastic cerebral palsy (Kerkum et al., 2015; Ridgewell et al., 2010; Brehm et al., 2008). By analyzing and studying some gait parameters, the researchers concluded that the energy cost of walking of quadriplegic children with cerebral palsy decreased with the use of an ankle-foot orthosis. On the other hand, in diplegic and hemiplegic children with cerebral palsy the energy cost of walking was not affected. Another study showed the importance of gait analysis in rehabilitation (Schmid et al., 2013). The effect of two orthoses on gait in 12 hemiplegic cerebral palsy patients was examined. Gait analysis tools helped the researchers reveal that the hinged-foot orthosis resulted in significant gait improvement, while the dynamic-foot orthosis did not.

Martínez et al. (2018) examined some parameters of the pressure beneath the foot of 24 patients with Parkinson's disease. They wanted to determine the characteristics of the heel to toe motion of these patients. They found that these patients have a characteristic heel to toe motion pattern. It was also stated that the determination of such a pattern could be helpful for diagnostic, treatment and rehabilitation purposes.

Research by Majeed and Chong (2020b) used the foot pressure image to detect the foot drop of elderly diabetes sufferers. They found that a number of important measures can be determined based on plantar pressure and recorded time in the foot pressure image or pedobarographic. These variables are peak pressure (PP), pressure-time integral (PTI), contact area (CA), contact time (CT) and COP.

An in-sole pressure sensor provides accurate PP, PTI and CT, and these plantar pressure measures are available for standing still, walking and running (Maetzler et al., 2010;Keijsers et al., 2009;Tong and Ng, 2010). Accordingly, PP is the single most commonly reported measure and represents the maximum load in the plantar surface of the foot or a given area of the foot (Keijsers et al., 2009;Bus and Waaijman, 2013;Melai et al., 2011). This measure is clinically significant because the magnitude of PP can be localized when standing and walking (Melai et al., 2011). PTI is defined as the area under the pressure-time curve within each mask and expressed in kilopascals multiplied by seconds (kPa.sec) (Rao et al., 2011). Studies have found that those with forefoot pain had significantly higher PTI levels than healthy controls (Keijsers et al., 2013;Burns et al., 2005). The CT is a crucial measure as it indicates the time in milliseconds (ms) that each area of the foot is in contact with the pressure pad during the stance phase (Maetzler et al., 2010), as shown in Figure 2.5.

2.3.2 Sports purposes

Another crucial use of gait analysis is for sports purposes. Athletic performance can be improved and injury can be prevented using gait analysis (Suchomel et al., 2016). It has been applied in sports such as golf, running and basketball training (Chow et al., 2014). According to Viteckova et al. (2018), examining an athlete's running gait, whether it has a natural or any abnormal running pattern, might be conducted by employing human gait analysis techniques. Monitoring the pattern and improving it, will lead to better performance and lower injury possibilities if there are any movement abnormalities. Preatoni et al. (2013) used gait analysis, particularly kinematical study, to introduce a method that helps make proper measurements to evaluate sports skills quantitatively.

Losciale et al. (2021) studied the differences between the gait characteristics of two groups of athletes, namely those who passed and those who did not pass the return-to-sport (RTS) criteria six months after anterior cruciate ligament (ACL) reconstruction. They found that there are some differences between the two groups. In addition, they observed that those who did not pass the criteria of RTS had more abnormal and asymmetrical gait behaviours. These findings enable clinicians to have a testing criterion to recognise athletes with such abnormalities after ACL construction. They The return-to-sport (RTS) criteria may also improve the sports medicine specialist's

ability to identify athletes with a higher risk of secondary injury as shown in Figure 2.5.

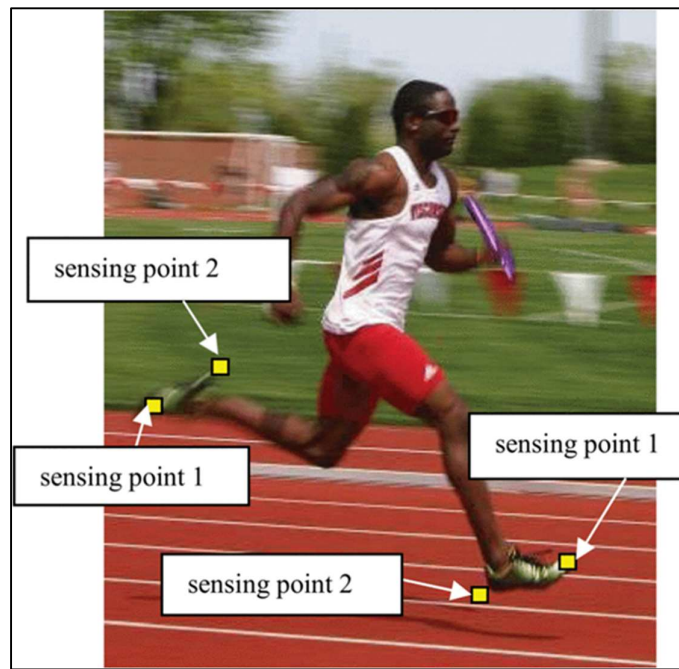


Figure 2.5: Planting sensors on the runner to record movement data (Wahab and Bakar, 2011).

2.3.3 Forensic purposes

Gait is a reliable tool for recognising people at a distance, which is very helpful in the security field. According to Rouzbeh and Babaei (2015), recognising people by gait refers to identifying them by their walking style. In this case, a person's gait is used as a biometric measure (Randhavane et al., 2019). According to Bhatia (2013), biometric means a measure obtained from a person to be used as a recognition or identification tool such as fingerprints, faces, irises, voices etc. Gait is a more valuable biometric than the others because surveillance applications do not easily recognise biometrics such as iris and face details at low resolution (Buciu, 2014). Gait, however, can be easily detected and measured by low-resolution surveillance applications (Reid et al., 2013), as shown in Figure 2.6. As a result, researchers have benefited from its parameters for security purposes. For instance, Lebleu et al. (2020) used gait features, namely ankle elevation, knee elevation, ankle stride width and knee stride width, along

with a locomotion human model to propose a novel recognition approach. Teufl et al. (2019) described an automated system to classify gender by using general (temporal and spatial) parameters, kinematic parameters, and moments.



Figure 2.6: Sample frame images from crime scene CCTV cameras (Bouchrika et al., 2011).

2.4 Common human gait identification technologies

2.4.1 Motion capture cameras

One of the established techniques of gait analysis is the use of motion capture cameras. Although a number of researchers are trying to establish various strategies in representation, characterisation and recognition of human gait, extracting suitable, targeted features from an image sequence is a very challenging task. Targeted features can be joint positions, joint motion trajectories and joint angle variations during walking.

Gait motion can be analysed with or without having any marker attached on human body (Colyer et al., 2018; Nagymáté and Kiss, 2019). This technique can be used both for 2D or 3D analysis of human gait. A single camera is commonly used to acquire data for 2D analysis (Castelli et al., 2015; Colyer et al., 2018). In this case, the camera is placed parallel with the subject's plane of motion of interest.

One of the limitations of this technique is out-of-plane movement which leads the analysis to unusual outputs. This problem can be overcome using treadmill walking. For 3D analysis, more than one camera with a complex setup is required as the observation should focus on all planes of movements (Majeed et al., 2017;Peyer et al., 2015). As 3D analysis requires the reconstruction of the points of interests on the subject for all the time, the points should be visible for at least two cameras for every moment (Schepers et al., 2018;Colyer et al., 2018). When using markers, the skin movement artifacts over the musculoskeletal system should be eliminated from the captured data before the reconstruction of motion. Benoit et al. (2015) consider that 60 Hz is adequate for kinematic analysis while the subject is walking at normal speed. But for faster locomotion it needs to increase the frequency of data sampling rate where extra lighting mechanism is required. Another challenge of camera use is the angle of view and focal distance which impose limits on capture volume. In order to account for parallax errors and body segment deformation, joint kinematics curves obtained for each lower limb model are averaged using a multiple anatomical calibration approach (Montefiori et al., 2019;Cereatti et al., 2015). For each joint kinematics the mean value was calculated. In Figure 2.7, a lower limb multi-segmental model resulting from the processing of the RGB-D recordings is superimposed to the RGB image in a gait cycle illustrative frame. Figure 2.8 shows the estimated knee angle pattern during a patient's gait cycle obtained using the marker less protocol.

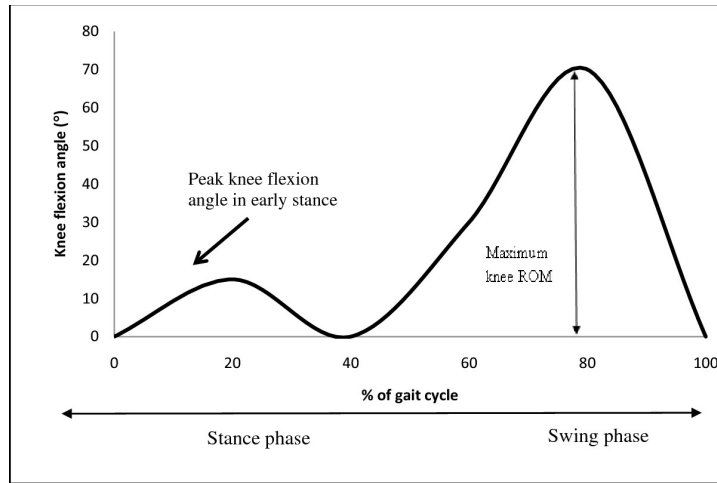


Figure 2.7: Knee kinematics resulting from the proposed protocol during an illustrative gait cycle (Cocchi et al., 2019).

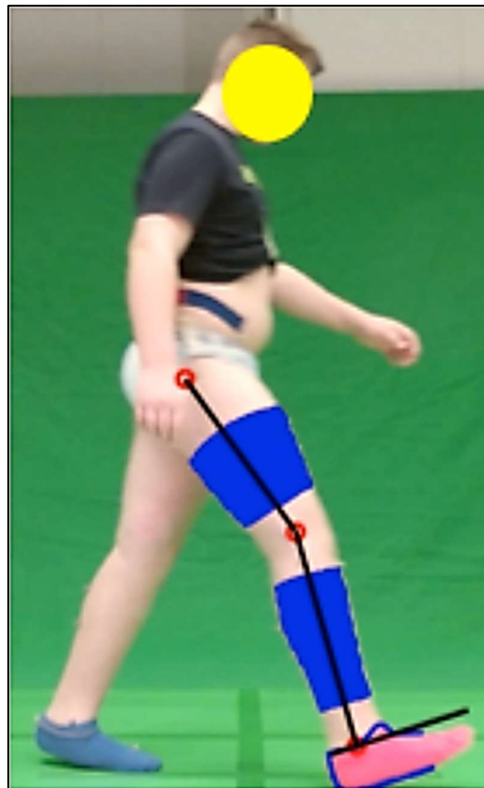


Figure 2.8: Foot contour (in blue), shank and thigh models (in blue), relevant stick segments (in black) connected through the joint centers (in red) resulting from the proposed ML protocol are superimposed onto the relevant RGB frame (Cocchi et al., 2019).

2.4.2 Inertial system

The inertial system combines accelerometers and gyroscopes and works on the principle of inertial measurements. The accelerometer and gyroscope provide the data of acceleration and orientation of the attached point through which segment acceleration, segment orientation and joint position can be achieved for gait analysis, see Figure 2.9. The sampling rate for both the accelerometer and gyroscope are same, and vary from 100 Hz to 10 KHz.. The tri-axial acceleration and gyration capabilities provide the facilities to analyse human locomotion in a 3D environment (Sheng et al., 2008; Sant'Anna et al., 2012; Lemoyne et al., 2009). The sensors are small, lightweight and capable of detecting a large range of angular velocity and acceleration (Rundo et al., 2018). The use of smartphones and portable media devices with integrated inertial sensors offer a new dimension in gait analysis and monitoring. The disadvantage of using this system is the skin movement artifacts which can affect the reading of acceleration and gyration (LeMoyne and Mastroianni, 2015; Morris and Lawson, 2010). Identification of the segment length and exact rotational axis is also challenging. Acceleration is relative to the position of the Inertial Measurement Unit (IMU) system (Lopez-Nava and Munoz-Melendez, 2016).

2.4.3 Electrogoniometer

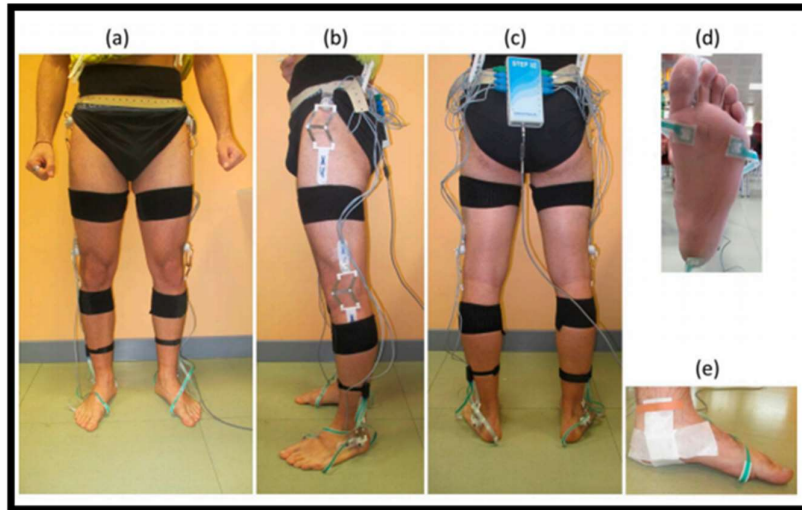


Figure 2.9: H-Gait and STEP32 sensor positioning. The images show the: (a) frontal, (b) lateral and (c) rear view of a subject prepared for the bi-instrumented gait analysis. The MIMU sensor positioned below the medial malleolus is shown in panel (d), the footswitches in panel (e) (Agostini et al., 2017).

An electrogoniometer (**EGM**) is an electro-mechanical instrument that measures angles of joint movements and is used in gait analysis. Two types of EGM are used: potentiometric EGM (**pEGM**) and flexible EGM (**fEGM**) (Roetenberg, 2006). For pEGM, a potentiometer is used at the joint rotational axis of two arms (Piriyaprasarth et al., 2008). These arms are normally attached with the two segments of a particular joint of the musculoskeletal system, especially at the knee (Akhtaruzzaman et al., 2015). The major challenge in capturing knee movement data for walking is to correlate the knee-joint axis with the system joint axis. To provide this facility, some flexibility is necessary at the attachment point of the instrument with limb segments. This problem can be overcome with the fEGM system as a flexible spring transducer and optical fiber are used with a fixed end and a telescopic end block. For both systems (pEGM and fEGM), when the leg moves, EGM converts the mechanical signals into electrical signals (Lopez-Nava and Munoz-Melendez, 2016). The drawbacks of the systems are that the angle movements can be measured only for one plane and accurate calibration is needed for the joint axis. Moreover, the instrument is uncomfortable to wear and very difficult to fit with a joint (such as hip or ankle) having more than one Degree of Freedom (DoF) (Roetenberg, 2006). Research shows that, although the

system produces good results for the elbow joint, it does not offer the same good quality data when used at the knee joint (Morris and Lawson, 2010).

2.4.4 Gait mat/pressure mat

A gait mat is a special kind of carpet where an arrangement of sensors is embedded. The geometry of the mat is pre-determined and the sensors of the mat are able to sense the foot contact as well as the GRF while walking (DeLisa, 1998). The uses of the gait mat and pressure mat are almost similar to the force plate. Portability, low cost and nonactive attachments to the subject are the advantages of using this system (Mariani, 2012). Most importantly, the system provides a good dataset of foot contact, step and stride length, distributed pressure and GRF. The limitation of these systems is the resolution of sensing points because of the finite size of the sensors. Moreover, increased resolution decreases the scan rate and raises the processing capabilities of the system (Zang et al., 2015).

2.4.5 Force sensing shoes

Force sensors like Force Sensitive Resistors (FSR) are arranged in the soles of shoes in such a way that the distributed foot pressure can be measured. As the GRF begins at the point of heel contact and ends at the point near toe, force shoes can provide a good dataset for gait analysis. In this context, FSR sensors may not be enough to measure tri-axial force and moment information (Zijlstra and Aminian, 2007; Castro et al., 2014). Parallel force sensor technology attached at the heel and forefoot regions could provide a reliable dataset for motion dynamic analysis (Castro et al., 2014; Liu et al., 2004; Tao et al., 2012). Force shoes data also need to be combined with limbs' kinematic data to identify and characterise human locomotion (Tao et al., 2012; Akhtaruzzaman et al., 2015).

The schematic of a wearable GRF sensing example is illustrated in Figure. 2.10. The force plate is attached to the bottom of the shoe. The X axis is in line with the moving direction, while the Z axis is the vertical, and Y forms a right-handed coordinate system together with the other two axes. According to Koch et al. (2016) and Niu et al. (2014) the maximum vertical GRF is about 120% of the body weight during the loading response. The maximum of antero-posterior GRF is about 25% of the bodyweight, while the mediolateral GRF is the lowest in amplitude and directed

laterally. Regarding the lower-limb as a musculoskeletal functional unit, the combined effort of the locomotion system can be recorded by the gait on force plates. However, there is no general agreement on the parameterisation of GRF. The indices for 3-D parameters vary considerably.

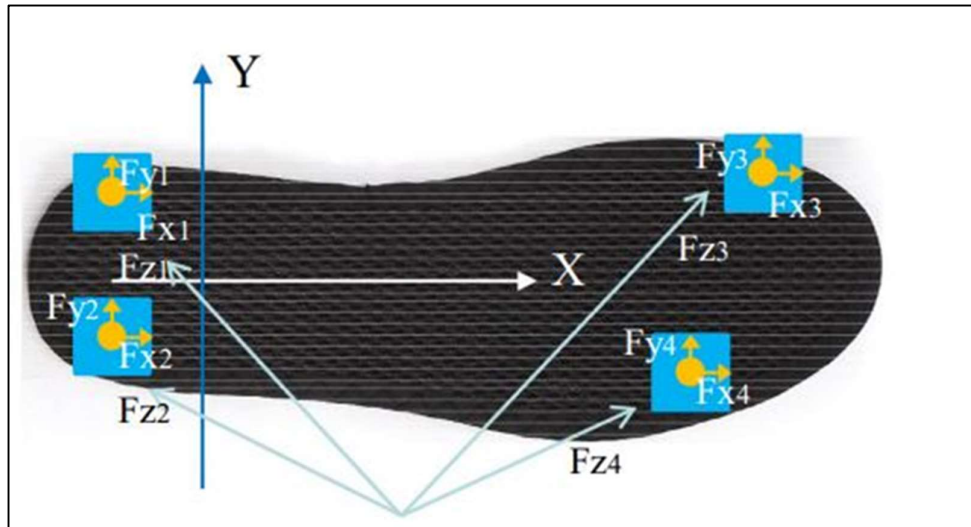


Figure 2.10: A insole sensor GRF sensing device (Yang et al., 2019).

In recent years, force sensors emerged due to their embedded footwear to realise ambulatory measurements of GRF (Ramirez-Bautista et al., 2017; Yang et al., 2019). Force sensors are usually employed to distinguish the pressure of different parts directly from insole sensing elements. Force sensors suitable for measuring consecutive gait cycles (Song and Kim 2017) on uneven and bumpy surfaces such as ascending and descending stairs (Figueiredo et al., 2018). Wearers do not have to focus on their steps which improves the accuracy and reliability of gait recognition (Shen et al., 2018). Figure 2.11 shows an instrumented insole constructed by embedding force sensors. Each insole consists of seven sensing elements pasted on the insole, one conditioning circuit for signal formulating and one battery for the power supply. Based on the data obtained in Shen et al. (2018), the value of foot pressure is highest at the heel, forefoot and hallux, and that of the mid-foot and lateral border is relatively low. The lowest pressure exists beneath the posterior metatarsal.

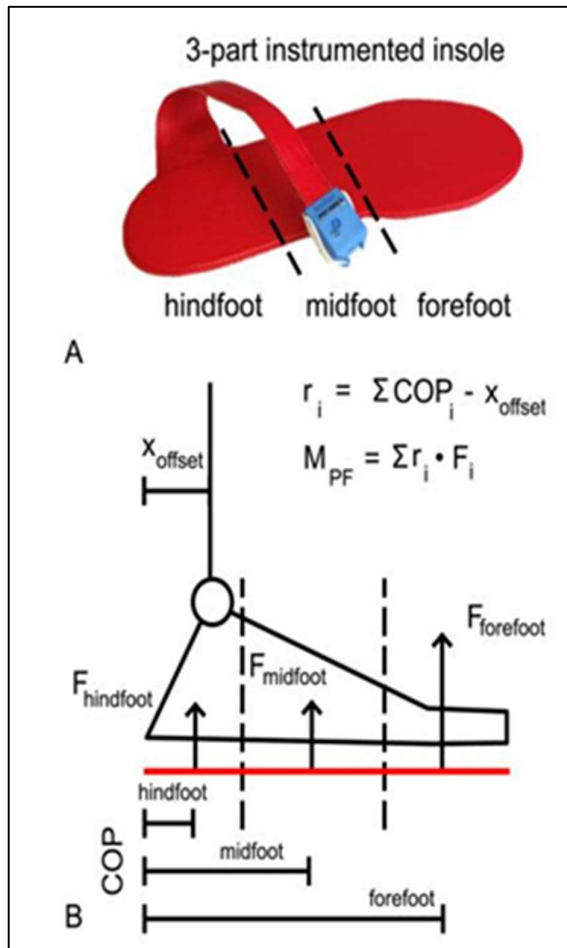


Figure 2.11: Instrumented insole is divided into 3 discrete zones, the hind-, mid- and forefoot (A). The load applied to each of these zones occurs at a constant distance from the ankle joint centre which is considered to be the zone centre of pressure (COP) (B). Moment arms (r) are calculated as the difference of these centres of pressure with the distance from the posterior aspect of the sensor to the ankle joint centre (x_{offset}). Plantar flexion moment is calculated as the sum of the scalar products of the moment arm and force applied to each zone. (Hullfish and Baxter, 2020).

2.4.6 Force plates mechanism

This technique consists of metal plates having load cell (most commonly) at each corner of the plates. This mechanism is used to measure the GRF caused by standing or moving. The shape of the force plate can vary based on design: square or triangular. Sensors (resistive, capacitive, piezoelectric, piezoresistive, strain gauge, etc.) used in the force plate can also vary based on pressure range, sensitivity and linearity. The

force plate mechanism provides the facility to measure the force induced on the plate and its directions. As the force plates are placed on a fixed location on the ground, the CoP of the subject's body can easily be calculated but for a long force platform it may lead to increase its cost. Moreover, the suitable position of footsteps on the plate may not be followed properly which could lead to the wrong calculation of the CoP point. Data captured from foot plates should be combined with limb kinematics information to analyse the principles of gait (Refai et al., 2017).

In the systems based on this technique, sensors are placed along the floor on the so-called force platforms or instrumented walkways where gait is measured by pressure or force sensors and moment transducers when the subject walks on them. There are different types of floor sensing platforms depending of the manufacturer design. Floor sensing platforms vary in size, length and number of sensors per cm^2 . When the venue has a length of 2 meters, the subject can walk for two gait cycles. An increase in the number of sensors leads to an increase in the frames extracted per second (i.e. increasing of the accuracy). There are two types of floor sensors: force platforms and pressure measurement systems, see Figure 2.12. Force platforms should be distinguished from pressure measurement systems, although they too quantify the CoP but do not directly measure the force vector applied. Pressure measurement systems help quantify the pressure patterns under a foot over time but cannot quantify horizontal or shear components of the applied forces (Refai et al., 2017). An example of an instrumented floor sensor and the acquired data from research conducted at the University of Southampton is depicted in Figure 2.13.

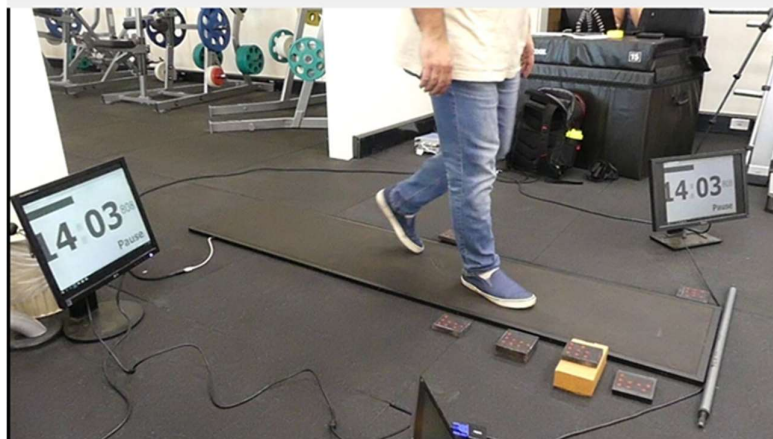


Figure 2.13: RSscan international foot pressure mat (author owns this image).

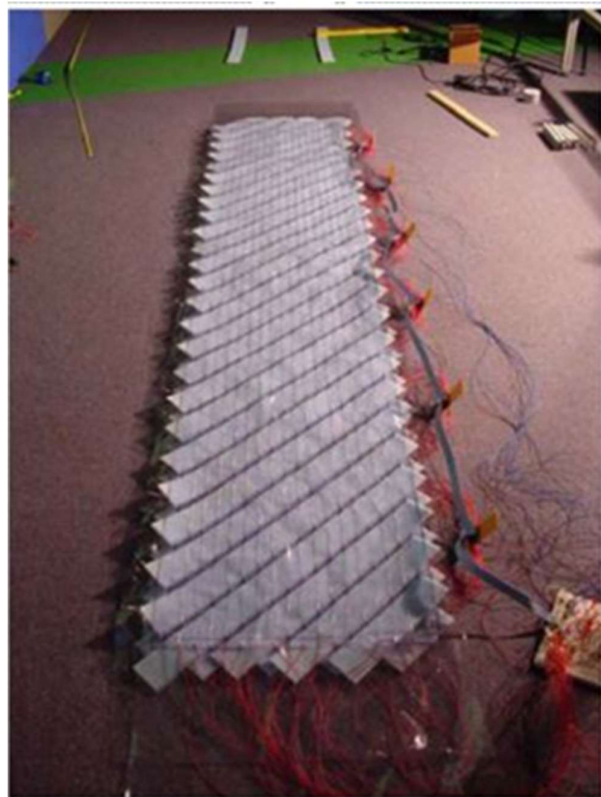


Figure 2.12: Prototype floor sensor carpet (Chaccour et al., 2015).

The characteristic that distinguishes floor sensors (FS-based) systems from IP-based systems is the analysis of force transmitted to the floor when walking, known as GRF. This type of system is used in many gait analysis studies (Muro-De-La-Herran et al., 2014;Iwashita et al., 2013). Costilla-Reyes et al. (2018) performed a comparative assessment of spatiotemporal information contained in the footstep signals for person recognition, analysing almost 20,000 valid footstep signals. These devices are the most basic ones that can be used to obtain a general idea of gait problems. Since the reaction force is exactly the opposite of the initial force (Newton's Third Law), the specialist identifies the evolution of the foot's pressure on the floor in real-time. These data, added to the previous comparison, help specialists make diagnoses. Pressure is given in percentage of weight in order to compare the patients' data. Pressure varies during the time the foot is in contact with the floor. The maximum pressure occurs when the heel touches the floor and when the toes pushes off to take another step. During this time, pressure may reach up to 120%–150% of the patient's body weight.

2.5 Human gait identification techniques

2.5.1 Close-range photogrammetry

Close-range photogrammetry, as the name suggests, has traditionally been limited to short to medium camera-to-object distances. With the growing use of off-the-shelf digital cameras for photogrammetric measurement however, requirements are emerging to perform measurements over: a) long distances for applications in construction engineering, deformation monitoring and tracking accident reconstruction, and b) very short distances for applications such as digital documentation and 3D visualisation of cultural heritage objects via image-based approaches (Koeva, 2016). Such measurements often require long focal length lenses to keep the spatial resolution high and optimise angular measurement precision.

It has long been recognised that there can be practical photogrammetric impediments to the employment of very long focal lenses with small format cameras, centring principally upon potential difficulties in analytical orientation and subsequently self-calibration. As focal length increases, so the field of view becomes narrower. This can impact the performance of the conventional central perspective adversely (Chong et al., 2009). In applying network orientation with self-calibration to images with very narrow fields of view, problems can arise through over parameterization, ill-

conditioning and subsequent numerical instability in the ordinary equations of the bundle adjustment. Recovery of satisfactory camera calibration parameters is often precluded in such 'weak geometry' cases due to linear dependencies that arise between the interior and exterior orientation parameters. The non-linearity of the collinearity equations is considered an inherent obstacle when it comes to the self-calibration of long focal length lenses, since the deterioration of the linear independence of the interior and exterior orientation parameters can be anticipated (Chong, 2011).

This partially accounts for why recent research on this topic has focused more on the development of alternative linear models to accommodate such network geometries. For example, Bell et al. (2016) developed an orthogonal projection model to address the issue of long-distance measurements in close-range photogrammetry. Even though their model was successful, it had limitations in that calibration of interior orientation elements was ignored and object space control points were required for the calculation of the initial exterior orientation parameters.

For the measurement of small objects, Jia et al. (2015) implemented a parallel projection model that requires parallel projection images taken with telecentric lenses, with the bundle adjustment incorporating a simplified interior orientation model. For either of these cases, a fully automatic self-calibration procedure was not reported. Obtaining the most suitable digital camera with less distortion and high accuracy is the main topic of this part of the research.

2.5.1.1 Collinearity Equations

The mathematical formulation of the relationship between image and object space can be described by collinearity equations which derive from central projection. The fundamental characteristic of such a relationship is that the perspective centre, the image point and the corresponding object point all line up in a straight line in space. Perturbations to this relationship however, give rise to departures from collinearity. Figure 2.14 shows the relationship between the coordinates $x; y$ of an image point p and the coordinates $X; Y; Z$ of an object point P within a basic interior orientation model. This can be mathematically formulated as shown in equation (2.1):

$$\begin{aligned}
 x &= x_p - c \frac{r_{11}(X - X_0) + r_{12}(Y - Y_0) + r_{13}(Z - Z_0)}{r_{31}(X - X_0) + r_{32}(Y - Y_0) + r_{33}(Z - Z_0)} + \Delta x \\
 y &= y_p - c \frac{r_{21}(X - X_0) + r_{22}(Y - Y_0) + r_{23}(Z - Z_0)}{r_{31}(X - X_0) + r_{32}(Y - Y_0) + r_{33}(Z - Z_0)} + \Delta y
 \end{aligned}
 \tag{2.1}$$

..... (2.1)
(Stamatopoulos, 2011)

The parameters x_p and y_p are the coordinates of the principal point, and c is the principal distance or focal length. The parameters r_{ik} appearing in Equation (2.1) are the elements of the rotation matrix R , which describes the three-dimensional orientation of the image with respect to the XYZ object coordinate system. The inherent departures from collinearity, due mainly to lens distortion, must be considered for metric measurement with these perturbations to the collinearity equations described by the terms Δx and Δy .

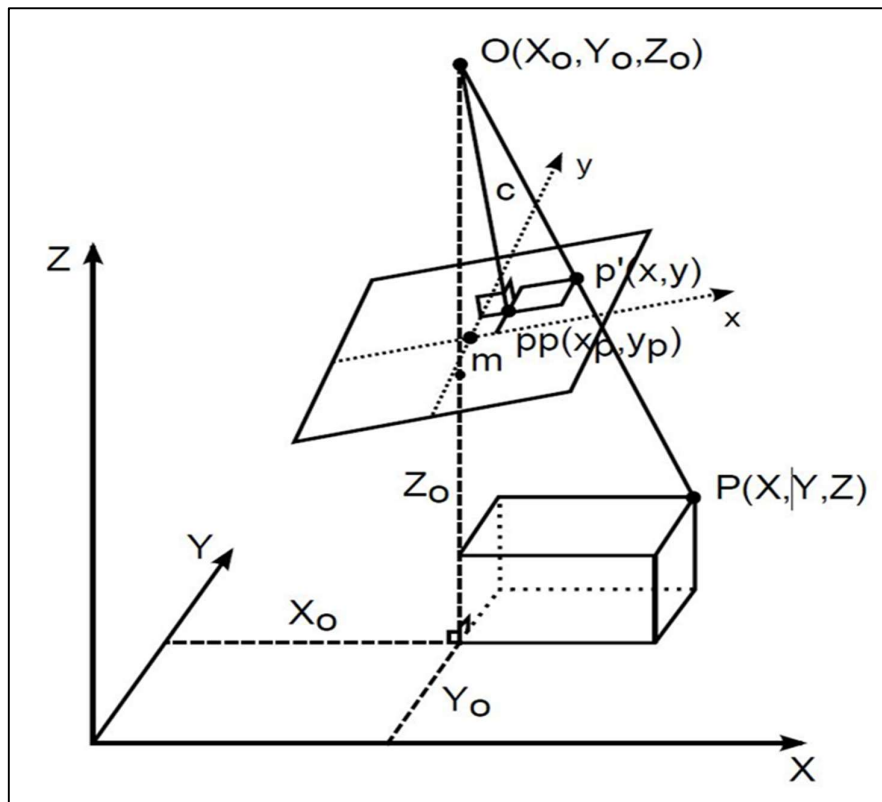


Figure 2.14: Relationship between image and object point coordinates (Chong et al., 2014).

2.5.1.2 Radial Distortion

Symmetrical radial distortion in photogrammetry is represented as an odd ordered polynomial series as a consequence of the nature of the Seidel aberrations (Stamatopoulos, 2011) equation 2.2:

$$\Delta r' = K_1 r'^3 + K_2 r'^5 + K_3 r'^7 + \dots \dots\dots(2.2)$$

where the K_i terms are the coefficients of radial distortion and r_0 is the radial distance from the principal point (Stamatopoulos, 2011) equation 2.3:

$$r' = \sqrt{x'^2 + y'^2} = \sqrt{(x - x_p)^2 + (y - y_p)^2} \dots\dots\dots(2.3)$$

Distortion can have both negative and positive values. Positive radial distortion is often referred to as pincushion distortion, while negative distortion is known as barrel distortion due to the resulting geometry deformation in the image plane. For wide-angle lenses, the third-, fifth- and seventh-order terms are often required. For most medium angle lenses employed in cameras nowadays, the third-order K term is sufficient to account for induced aberrations, at least for applications that do not demand the highest accuracy. Although radial distortion is present in long focal length lenses, its magnitude is generally tiny, and for metric applications, decreases with increasing focal length (Fraser, 2013). As the cubic component of radial distortion is the most significant, and the combined contribution of the K_2 and K_3 terms are generally relatively small, the distortion can be adequately profiled with just the K_1 term. Additionally, the projective coupling between the principal distance and lens distortion can help also in eliminating components of the error.

It is not uncommon for digital cameras to utilise only the central part of the available field of view, which in combination with long focal length lenses, can lead to a radial profile that may not depart from a linear function of the form $\Delta r = K_0$. This linear profile can be absorbed by a change in the principal distance which will, in turn, indicate that there is no significant radial distortion. From Equation 2.3, the necessary corrections to the x ; y coordinates follow as below (Stamatopoulos, 2011) equation 2.4:

$$\begin{aligned} \Delta x'_{radial} &= x' \frac{\Delta r}{r'} \\ \Delta y'_{radial} &= y' \frac{\Delta r}{r'} \end{aligned} \dots\dots\dots(2.4)$$

The coefficients K_i are usually highly correlated with each other. However, this does not typically affect their calculation.

2.5.1.3 Decentering Distortion

The misalignment of the individual elements of the lens along the optical axis introduces another error known as a decentering distortion. This can be compensated by the functions below derived by (Shah and Aggarwal, 1996) equation 2.5:

$$\begin{aligned} \Delta x'_{decentering} &= P_1(r'^2 + 2x'^2) + 2P_2x'y' \\ \Delta y'_{decentering} &= P_2(r'^2 + 2y'^2) + 2P_1x'y' \end{aligned} \dots\dots\dots(2.5)$$

Although not apparent from the above formulation, there is a strong coupling of the decentering distortion parameters with the principal point offsets x_p and y_p (Fraser, 2013). This correlation increases with increasing focal length, and it can be problematic for the calibration of long focal length lenses. Images with higher convergence angles can help in diminishing the coupling effect. The image coordinate correction values for decentering distortion rarely exceed a few pixels maximum and, as a consequence of this and the projective coupling to Interior Orientation (IO), decentering distortion is often ignored (Tang, 2013).

2.5.1.4 Linear Distortion

Digital imaging systems that have rectangular light-sensitive elements instead of a square can present deviations of the image coordinate system concerning orthogonality and scale uniformity. The metric consequences of such variations are described by two parameters: the affinity and shear, and can be modelled as shown below (Chong et al., 2014).

:

$\Delta x'_{linear} = B_1 x' + B_2 y'$ $\Delta y'_{linear} = 0$(2.6)
---	------------

Linear distortion is usually ignored in close-range photogrammetry because of the high geometric integrity of modern-day digital cameras with nominally square pixels (Chong et al., 2014) equation 2.6.

2.5.1.5 Bundle adjustment

This procedure is seldom used in practice except as a first step for generating approximations for a bundle adjustment, which is a general solution for the collinearity equations initially formulated by Duane Brown in 1958 (Brown and Cassells, 1971). The bundle adjustment refers to the bundle of rays of light leaving 3D object space and converging to each camera perspective centre. The bundle adjustment is essentially the simultaneous relative orientation of all bundles with respect to one another that leads to the optimal calculation of the EO (exterior orientation) parameters and the object point coordinates. Optionally, it can also include additional calibration parameters such as the camera IO (interior orientation) parameters to account for the departures from collinearity. This process is commonly called a self-calibrating bundle adjustment due to the inclusion of the camera calibration parameters. Figure 2.15 illustrates a typical case of a bundle adjustment where multiple stations, object points and possibly cameras form the photogrammetric network. The bundle adjustment constitutes a general solution of the collinearity equations.

Collinearity equations have to be linearized using the Taylor expansion series for the least-squares adjustment as they do not have a linear form. The calculation of the differential quotients needed for the linearization process requires approximate values of some of the unknown parameters which can be acquired with the methods presented in the previous sections. After the linearization process, the bundle adjustment will have the form of the unknowns of Equation 2.7 (Chong et al., 2014), and the unknowns of a bundle adjustment are the selected camera calibration parameters for each camera represented by the vector x_1 , the EO parameters.

$$A_1x_1 + A_2x_2 + A_3x_3 = b \quad \dots\dots\dots(2.7)$$

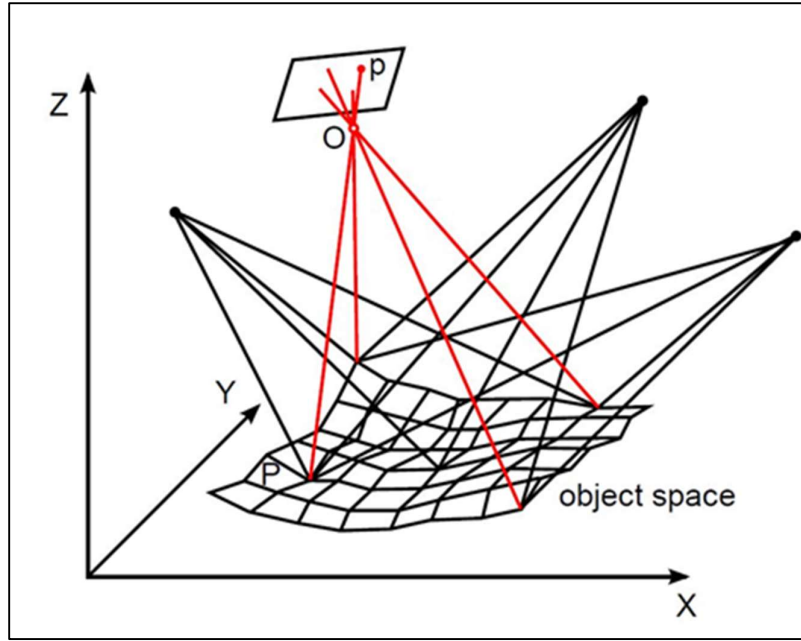


Figure 2.15: Multi-station bundle adjustment.

$x_2^T = [X_0 \ Y_0 \ Z_0 \ \omega \ \theta \ \kappa]$ for each image station and the object point coordinates.

$X^T_3 = [X \ Y \ Z]$ for each point. Usually, the vector x_1 consists of 8 parameters with $X^T_1 = [xp \ yp \ K_1 \ K_2 \ K_3 \ P_1 \ P_2]$. Thus, for a network of l cameras, m images and n points, the total unknowns are $8l + 6m + 3n$, should a basic 8-parameters camera calibration model be considered. The observations most of the time solely image coordinates measurements, so for a network of similar size as the one already mentioned, the number of observations is $2mn$ if all the points are visible in every image. Multi-image photogrammetric networks with many objects' points are usually highly redundant in observations.

2.5.1.6 Calculation of gait biometric and joint angles using 3-dimensional measurements

Photogrammetry means measuring by photography. As such, photogrammetry is a technique as old as photography. Photogrammetry is extensively used in surveying, mapping and architecture, but also more recently in forensic medicine, and may include measurement of unknown values by use of known values within single images (Ebert et al., 2016; Buck et al., 2018; Urbanová et al., 2015). Another basic application for photogrammetry is measuring objects in a three-dimensional space, using photographs of the object taken from different sides and angles. Similar points on the different photographs are identified, and a computer program can then calculate the x, y, z-coordinates of the points, thus creating a virtual model of the object. If the photographs of an object have been calibrated, a true scale model is made.

As a forensic case solution by photogrammetry, Lynnerup and Vedel (2005) used the above operations to identify perpetrators who robbed a bank on 21 June 2002; a bank in the town of Aalsgarde, Denmark. They used Photomodeler Pro V4, a software package to analyze the images captured by the CCTV cameras. They compared the images of the suspect with the perpetrator in order to note such bodily features and proportions that might indicate concordance as well as an incongruity. Obviously, due to the use of helmets (unlike, e.g., a tight-fitting stocking or balaclava) and loose-fitting clothing, only very general bodily features could be noted. However, several physical features did seem fairly concordant. The researchers noted a similarity in body proportions, stance and general features, e.g., the back and shoulders (Figure 2.16). Both suspect and perpetrator displayed rather rounded shoulders with a wide neck. Likewise, the waist–shoulder proportions were consistent. The curvature of the spine and resultant morphology of the back was also very similar Figure 2.17.

The photogrammetry method as used in this case, had an advantage in that there was no need to ascertain the position of the perpetrator in relation to a measuring device. As a result of this case, the researcher measured the height of a desk (bolted to the floor and not moved between the incident and the analysis) by photogrammetry (result: 89.3 cm) and compared this to an actual physical measurement (result: 90.0 cm). The error was 7 mm or less than 1%.

Another photogrammetry technique for human identification presented by Larsen et al. (2010) combined the basic human ability to recognize other individuals with functional anatomical and biomechanical knowledge to analyze the gait of perpetrators

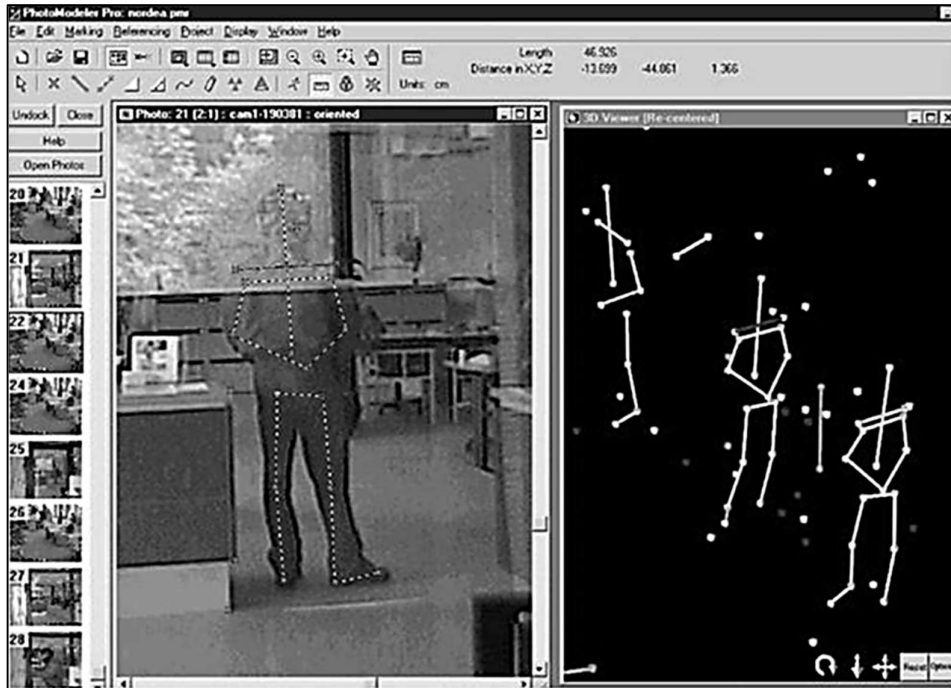


Figure 2.17: Screen shot of Photomodeler Pro R_ interface showing placing of reference points of various bodily features in the left panel and the resultant 3D scale “stickmen” of the perpetrator (Lynnerup and Vedel, 2005).



Figure 2.16: Comparison of body morphology of perpetrator and suspect.(Lynnerup and Vedel,

as recorded on surveillance video. The perpetrators are then compared to similar analyses of suspects. Using a structured checklist which addresses the single body segments during gait, the researchers identify whether the perpetrator has a characteristic gait pattern compared to normal gait, and if a suspect has a comparable gait pattern. Researchers also have found agreements such as limping, varus instability in the knee at heel strike, more significant lateral flexion of the spinal column to one side than the other, inverted ankle during stance (Figure 2.18), pronounced sagittal head movements, and marked head-shoulder posture. Based on these characteristic features, they can say whether suspect and perpetrator could be the same person, though it is not possible to positively identify the perpetrator (Kelly, 2020). Nevertheless, researchers have been involved in several cases where the court found that this type of gait analysis, especially combined with photogrammetry, was a valuable tool.



Figure 2.18: Inverted ankle during stance, (Kelly, 2020).

2.5.2 Footprint analysis

2.5.2.1 *Pressure sensing systems*

Feet provide the primary surface of interaction with the environment during locomotion. Thus, it is crucial to diagnose foot problems early for injury prevention, risk management and general wellbeing. One approach to measuring foot health, widely used in various applications, examines foot plantar pressure characteristics. It

is, therefore, important that accurate and reliable foot plantar pressure measurement systems are developed. One of the earliest applications of plantar pressure was the evaluation of footwear (Chatzistergos et al., 2020). Bus et al. (2016) examined the effectiveness of footwear and other removable off-loading devices as interventions for treating diabetic foot ulcers or the alteration of biomechanical factors associated with ulcer healing, and discussed the quality and interpreted the findings of research to that point. Since then, there have been many other studies of foot pressure measurement. For example, Zhang and Li (2013) applied plantar pressure to footwear design for people without impairments.

Furthermore, (Fuchs et al., 2020) ,(Coelho, 2018) found that the most effective method for reducing the pressure beneath a neuropathic forefoot was using rocker bottom shoes and claimed the rocker would decrease the pressure under the first and fifth ray (metatarsal head). Metatarsal heads are often the site of ulceration in patients with cavovarus deformity. DeBiasio et al. (2013) indicated that future shoe designs for preventing metatarsal stress fractures should be gender-specific due to differences in plantar loading between men and women.

Concerning application once involving disease diagnosis, many researchers have focused on foot ulceration problems due to diabetes that can result in excessive foot plantar pressures in specific areas under the foot. It is estimated that diabetes mellitus accounts for over \$1 billion per year in medical expenses in the United States alone (Hutton et al., 2014). Diabetes is now considered an epidemic and, according to some reports, the number of affected patients is expected to increase from 171 million in 2000 to 366 million in 2030 (Aboua et al., 2013).

Improvement in balance is considered important for both sports and biomedical applications. Notable applications in sport are soccer balance training (Ramizuddin and Washimkar, 2013) and forefoot loading during running (Bus et al., 2016). With respect to healthcare, pressure distributions can be related to gait instability in the elderly and other balance impaired individuals. Foot plantar pressure information can be used to improve balance in the elderly (Machado et al., 2016). Based on the above discussion, it is crucial to devise techniques capable of accurately measuring foot pressure.

2.5.2.2 In-shoe systems

In-shoe sensors are flexible and embedded in the shoe such that measurements reflect the interface between the foot and the shoe. The system is flexible making it portable which allows a wider variety of studies with different gait tasks, footwear designs, and terrains (MacWilliams and Armstrong, 2000).

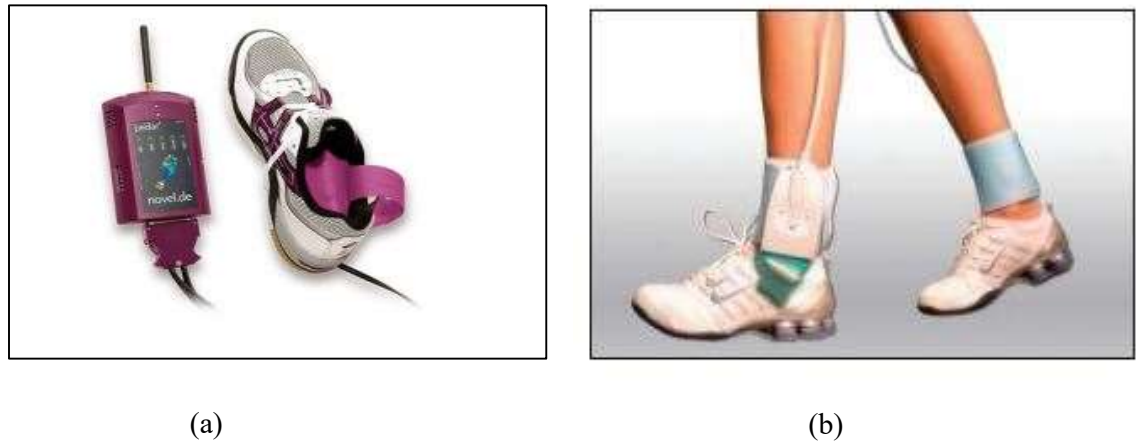


Figure 2.19 (a) : . An in-shoe based foot plantar pressure sensor by(Yang et al., 2019). (b) An in shoe based foot plantar pressure sensor F-Scan® System by Tekscan (Hullfish and Baxter, 2020).

Real-time measurement of natural gait parameters requires that sensors should be mobile, untethered, can be placed in the shoe sole, and can sample effectively in the target environment. The main requirements of such sensors are as follows:

- a- Very Mobile: To make a sensor mobile, it must be light and of small overall size [27,28], the suggested shoe mounted device should be 300 g or less.
- b- Limited Cabling: A foot plantar system should have limited wiring, wireless is ideal. This is to ensure comfortable, safe and natural gait.
- c- Shoe and Sensor Placement: To be located in the shoe sole the sensor must be thin, flexible and light(Lee et al., 2001). It is reported that a shoe attachment of mass 300 g or less does not affect gait significantly(Bamberg et al., 2008). Shu et al (2010) mentioned that the sole of foot can be divided into 15 areas: heel (area 1–3), midfoot (area 4–5), metatarsal (area 6–10), and toe (area 11–15), as illustrated in Figure 2.20. These areas support most of the body weight and are

adjusted by the body's balance; therefore, ideally the 15 sensors are necessary to cover most of the body weight changes based on the Figure 2.20 anatomy.

- d- Low Cost: The sensor must be affordable for general application to benefit from inexpensive, mass-produced electronics components combined with novel sensor solutions (Arafsha et al., 2018).
- e- Low Power Consumption: It should exhibit low power consumption such that energy from a small battery is sufficient for collecting and recording the required data(Tahir et al., 2020).

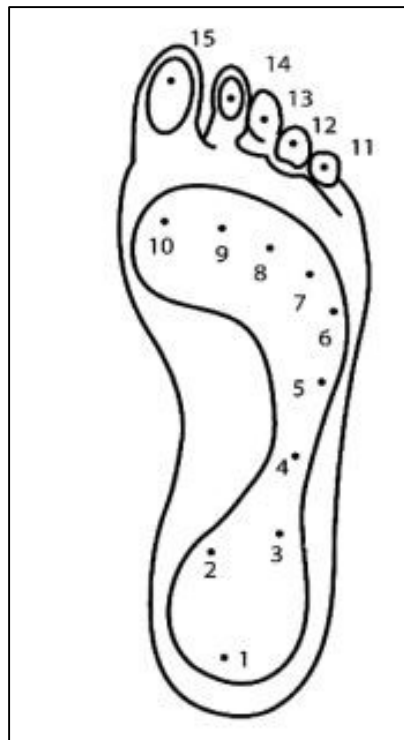


Figure 2.20: Foot anatomical areas (Shu et al., 2010)

2.5.2.3 Footprint characteristics for identification

There are many types of research for identification based on the foot pressure analysis approach. For example, (Wafai et al., 2015;Nagwanshi and Dubey, 2018;Jung et al., 2004;Orr and Abowd, 2000;Pirttikangas et al., 2003;Yun et al., 2003;Yun et al., 2005) researched person identification using foot pressure over time for the one-foot step when passing on a pressure sensor platform. The footprint profile features used in these approaches include the mean, standard deviation, duration of the pressure profile,

overall area under the profile, pressure value and the corresponding time of some key points such as the maximum point in the first and last halves of the profile and the minimum threshold between them. In these approaches, due to the nature of load-cell based pressure sensing, the spatial pressure distribution during a footstep is not measured, and only the amount of pressure and the corresponding time can be used for feature extraction and people identification. Therefore, the load-cell-based gait identification approaches do not consider spatial pressure distribution and features such as COP trajectories.

On the other hand, (Qiu and Xiong, 2015);(Karatsidis et al., 2017) used the 2D COP trajectory to recognize people using a mat-type pressure sensor. To identify a person based on the foot pressure measured during a gait cycle, it is crucial to extract both spatial features such as the trajectories of COP and footstep pressure profile features. To address this issue, Wang et al. (2018) developed a reliable approach for the identification of a group of twenty people. (Andries;2015) used a Tekscan floor mat consisting of a number of pressure sensing mats arranged in a rectangular shape spanning a total sensing area of about 180 square feet. Each pressure sensing mat had 2016 FSR based sensors in a resolution of over six sensors per square inch. By using this large area, high-resolution pressure sensing floor, the researcher extracted features from both the trajectories of the COP and the pressure profile of both the left and right footsteps during a gait cycle. They also used other gait features such as the stride length and cadence.

The Fisher linear discriminant is used as the classifier. Encouraging results were obtained using the proposed method with an average recognition rate of 94% and a false alarm rate of 3% using pair-wise footstep data from 10 subjects. Experimental results show that the proposed method achieves better or comparable performance compared to existing methods. However, the proposed approach is limited in a few aspects. (Andries, 2015) considered the identification of individuals through floor pressure when walking with shoes off. However, the identification technique used in our research considered the subjects wearing shoes as part of a forensic application. This advantage makes our research more valuable. Andries (2015) also assumed that people walk in a straight line at an average speed. In addition to these limitations, this approach needs to be further evaluated using floor pressure data collected at various walking speeds with a larger dataset of more subjects. The identification approach used

by Andries (2015) considered clustering and tracking of COP using mean-shift. The mean-shift algorithm Cheng (1995) was used to cluster floor pressure data and track the COP over time. Mean-shift is a repetitively shifting process to find the sample mean of a set of data samples. In this case the data samples are the 2D locations of points on the floor with active pressure readings as described in Figure 2.22.

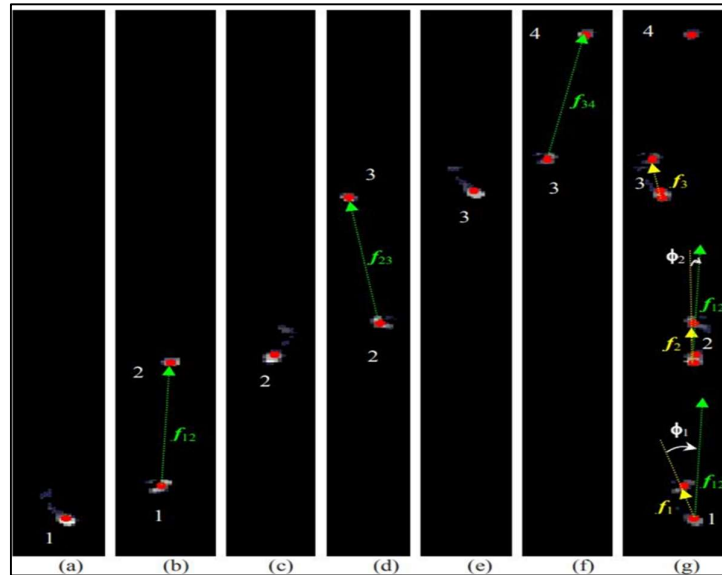


Figure 2.21: Clustering and tracking results over about 1.5 gait cycles: (a) through (f) show snapshots of observed floor data and corresponding COPs (red dots) and their ID numbers (white digits) (Andries, 2015).

For this identification approach, the data set was tightly packed into clusters, with all data points located closely to the center of that cluster (Andries, 2015). The process is said to have converged either after the maximum number of iterations defined by the algorithm is reached, or earlier when the mean shift of centres becomes less than the convergence threshold. After convergence, each cluster is assigned with a unique cluster ID number, and every data point has a ‘label’ associated with the corresponding cluster. For every subsequent pressure data frame, centres from the previous frame are updated through the mean shift algorithm (Rangarajan et al., 2007) using current observed pressure values as weights, and checked for convergence.

In practice, entirely new data points resulting in new cluster centres can occur if groups of data points are not assigned to any existing cluster centres. Figure 2.22 shows clustering and tracking results of the pressure data over about 1.5 gait cycles.

Qian et al. (2008) said that the red dots indicate the cluster centres, and the white digits their ID numbers. During a footstep, which is defined as the period between the heel-strike and the toe-off of a foot, COP can be correctly tracked using the mean-shift algorithm since the corresponding cluster-ID is maintained.

2.5.2.4 Identification using spatio-temporal parameters

Spatio-temporal parameters, walking velocity, cadence, and step and stride length, appear to be the most relevant biomechanical parameters in both individuals with a transtibial amputation and healthy adults. In addition, walking velocity is of even greater relevance since it also measures, and has a direct effect on, such parameters as cadence and stride length (Roberts et al., 2017;Larsen et al., 2010).

Additionally, these spatio-temporal parameters have a certain ease of measurement. Measuring simple spatio-temporal parameters such as walking velocity, would appear to be an effective and simple way to add objectivity to clinical gait analysis which is primarily aimed at ease of measurement (Roberts et al., 2017;Qiu et al., 2018;Vienne et al., 2017).

Three-dimensional motion analysis (3D-MA) provides objective and highly accurate information about the kinematics of gait in terms of both spatio-temporal parameters and joint excursions. However, although this approach is very informative, it is generally used to obtain only spatio-temporal parameters, thus missing the possibility of distinguishing primary abnormalities from active compensatory mechanisms (Rucco et al., 2017). In contrast, a kinematic analysis that includes the study of joint angular excursions allows the splitting of the movement into its individual elements; each of them with a precise biomechanical significance. Along the same line of reasoning, the most used concise indices of the quality of gait patterns are calculated almost exclusively with kinematic parameters (Rucco et al., 2017).

The GAITRite walkway system has been shown to be reliable for the measurement of spatio-temporal gait parameters (STP), giving an estimate of the quality of gait (Bzhikhatlov et al., 2019). This system has been validated in healthy children and adults, to analyze gait pathologies such as stroke and vestibular dysfunction (Roche et al., 2018;García-Soidán et al., 2021). To the best of our knowledge, one previous study reported the feasibility and repeatability of STP measurement with the GAITRite system in ataxic gait, which represents a very variable type of gait (Elharrouss et al., 2021;Roche et al., 2018)

Joint angles of subjects walking at a similar gait speed vary with a standard deviation of 2°–8° (Wilken et al., 2012; Chung and Wang, 2010; Bejek et al., 2006). However, larger inter-subject variability was found for the minimum and maximum hip angle (around 13) (Bejek et al., 2006) and more minor inter-subject variability for pelvic rotation and obliquity (around 1.5) (Bejek et al., 2006; Yang et al., 2014a). In forensic practice, however, the gait speed of a perpetrator and suspect are likely to differ. Therefore, Yang et al. (2014a) investigated whether and when a perpetrator and suspect's gait cycle joint angles can be compared if their speed differs. Importantly, comparing joint angles from two-dimensional (2D) video footage is meaningless with current techniques. Nevertheless, even for observer-based forensic gait analysis, knowledge of gait speed effects may be important. Yang et al. (2014a) found that joint angles were almost the same for gait speed at mid-stance and mid-swing (around 30% and 80% of the gait cycle). During the remainder of the gait cycle, especially at toe-off (50%–60% of the gait cycle), gait is too variable to compare joint angles separately. Front-view joint angles and higher gait speeds are more suitable for comparison than side-view angles and lower gait speeds (Yang et al., 2014a). Yang et al. (2014a) advised to compare gait joint angles of similar speeds if possible, and to select mid-stance or mid-swing video frames for comparison of joint angles otherwise. (Mutsavi, 2018) compared the posture of the perpetrator during robbery to the stance of the suspect based on a covert recording supplied with the images obtained for



Figure 2.22: Both perpetrator (to the left) and suspect showed inverted left ankle (white arrow) during left leg's stance phase and markedly outward rotated feet.

photogrammetric use, see Figure 2.25. It found concordances between perpetrator and suspect, such as restless stance, anterior positioning of the head showing a neck lordosis, and inversion in the left ankle joint. Larsen et al. (2010) also observed some incongruities. The perpetrator had a wider stance, truncus leaning slightly forward, elevated shoulders, and the arms were abducted compared to the suspect. They suspected that these incongruities could be the result of differences in the state of anxiety between the two recording situations. The results were presented to the police using a checklist for posture analysis similar to the list for gait analysis presented here. Larsen et al. (2008) developed a checklist for forensic gait analysis. They first describe the general characteristics of the perpetrator's gait and then analyse each of the joint rotations and segment movements (*by trial and error*) found relevant for forensic gait analysis. According to their research methodology, it used many video cameras recording from different positions to ensure accuracy using statistical calculation and not using trial and error.

Recordings from video surveillance systems are used as evidence from crime scenes. It would be useful to perform comparisons between disguised perpetrators and suspects based on their gait. Larsen et al. (2008) applied functional anatomical and biomechanical knowledge to analyse the gait of perpetrators, as recorded on surveillance video. Using a structured checklist, which addresses the single body segments during gait, it will be able to give a statement concerning the gait patterns (Cunado et al., 2003).

According to Larsen et al. (2008), in December 2004, a perpetrator robbed a bank in Noerager, Denmark. Researchers were contacted by the police to perform a gait analysis, as they thought the perpetrator had a unique gait. The robbery was recorded by two surveillance cameras. One camera was placed at the entrance, recording the perpetrator in frontal view: walking in, standing and walking in the bank during the robbery, and leaving the bank. The recording frequency was about 5 Hz. The other camera was placed inside the bank, recording the cashier's desk from behind and did not record the gait of the perpetrator. However, this camera could be used to measure the perpetrator by photogrammetry and to perform a posture analysis.

It was possible to derive several measures of the perpetrator such as stature, eye height and shoulder height, as shown in Figure 2.24, using photogrammetry in 2D (a

measuring frame was placed at the position of the perpetrator and used as drawing plane using the software package PhotoModeler Pro 5.0 (Sturzenegger and Stead, 2009). The suspect was recorded from three different cameras simultaneously, and a measurable 3D model was created in PhotoModeler Pro 5.0 as shown in Figure 2.24 (b). It can be seen that the static measures of the perpetrator and the suspect were in concordance within 3 cm. Furthermore, the differences in the measures can be explained by differences in posture between perpetrator and suspect: the perpetrator stood with the head bowed slightly forward (resulting in decreased stature and eye height), right shoulder elevated (increased right shoulder height), and lowered left shoulder (decreased left shoulder height) (Larsen et al., 2008).

According to the research methodology, the measurements were applied to the lower limb of the individual with more accuracy because the system would validate before being applied to the perpetrator and suspect.

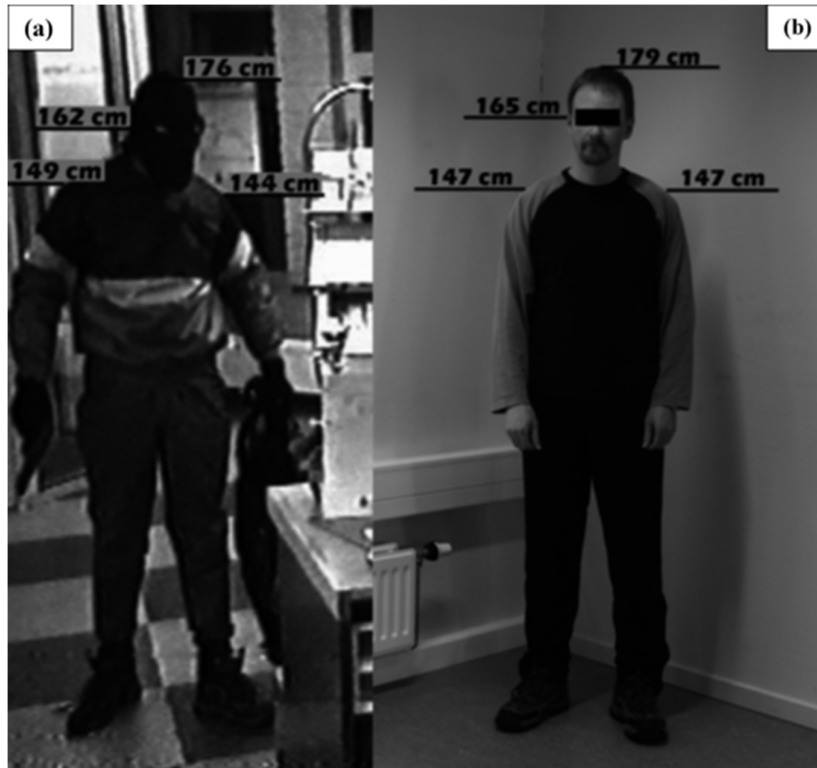


Figure 2.23: (a) Photogrammetric measurement of the perpetrator in the bank. (b) The suspect with measures of stature, eye height and left /right shoulder (Larsen et al.,2008).

2.6 Summary

This chapter addressed the importance of studying human movement and gait characteristics. It also demonstrated that many studies have used a variety of methods and techniques to analyse human movements and gait characteristics, and that many studies have used photogrammetry techniques in science and engineering to make accurate 3D measurements of objects.

The literature review has also explained gait analysis methods used in gait studies such as non-wearable devices and wearable devices. The advantages and disadvantages of both methods have been explained in detail. However, there is a lack of research investigating close-range photogrammetry with force foot platform in terms of biomedical information , and a new technique needs to be developed to evaluate the way of human identification in high accuracy data. The current work aims to fill this research gap by providing an understanding of the gait study methods using new strategies and different ideas.

This aim has been achieved by applying a set of objectives to introduce a new technique for human identification in Chapter 3. The first objective is to finding and calculating the most suitable cameras configurations to obtain a high resolution digital video image recording to obtain an accurate subject's data for identification. The second objective is demonstrating the most effective 3-dimensions measures and angles for the human gait using closed range photogrammetry. For the third objective, we calculate the most reliable, accurate parameters by using foot force/pressure data using force plate platform. This is a non-wearable sensors device that export foot-print data while walking on the platform and that why it can be used for security purposes. The fourth objective is correlate the two sets of data that obtained from objective two (the close range photogrammetry data) and objective three (the force foot data) .by combining these two sets of data, we can extract a new accurate, reliable and authenticated human identification data that used in this research. Finally, this study evaluated and validated the performance's quality of the proposed method by using different statistical methods and comparing the results of the innovative methodology with those of the most used methods in published works.

CHAPTER 3

3.1 Introduction

In this chapter , we will describe the process of methodology and the tools and equipment used and the steps applied for the recruits to obtain the data. The process under the Human ethics application issues by USQ with HREC ID; H21REA120.

3.2 Research methodology

This study offers a new human identification technique to be applied in forensic investigations. The system uses five video cameras and a foot pressure sensor mat brand (RSSCAN INTERNATIONAL). Both methodology parts (photogrammetry and foot pressure sensing mat) worked simultaneously to provide the data. Five video cameras were used. These five cameras sat on tripods surrounding the 2 meters long RSSCAN foot pressure mat located at a building entrance, as shown in Figure 3.1.

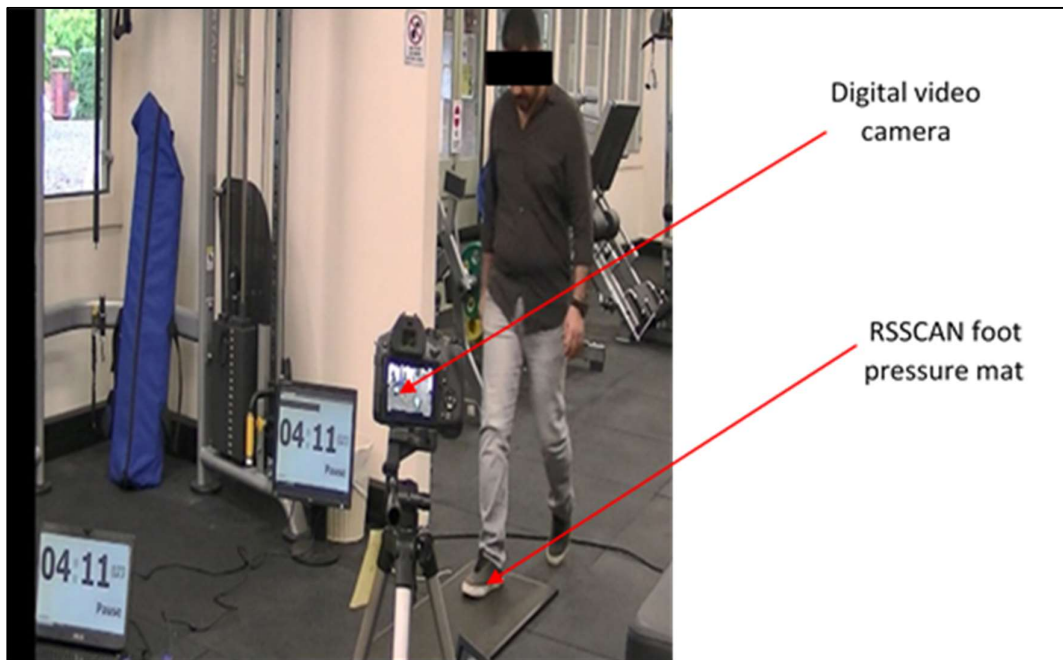


Figure 3.1: Subjects test position using five digital video cameras and foot pressure sensing mat.

Three digital timing screens were installed in different positions to ensure full location coverage by the cameras. The three timing displays were synchronized for minutes, seconds and three digits of milliseconds. The timing was used to extract the same frame from each camera. The photogrammetric foot pressure technique was verified by calculating the correlation between the morphological assessment of bodily features of the lower limb and the dynamic changes of the footprint at a different point on the time scale. Twenty-three (23) individuals were recruited to walk on the RSSCAN mat surrounding by five digital cameras to obtain two sets of data.

The first set of data was collected through photogrammetry. Using five video cameras, each subject's gait data was extracted and analysed from the digital camera footage. Physical features were calculated using photogrammetry at the stages of heel-down, mid-stance and toe-off. These features included knee to inner ankle joint, ankle to knee distance and knee angle. According to Lynnerup and Vedel (2005), a perpetrator's body measurements and leg joints show a strong resemblance to those of the suspect. Three-dimensional angles were also calculated at the three postures for the knee (heel-down, mid-stance and toe-off). In their study, van Mastrigt et al. (2018b) found that at the gait speed of the mid-stance and mid-swing stages (around 30% and 80% of the gait cycle), the joint angles are most stable.

To obtain accurate measurements, a complete calibration was applied to the four different types of cameras. These cameras had different specifications such as focal length, resolution and cost. Identifying the correct camera positively impacts cost and performance. As mentioned above, four types of video cameras were tested in this research. The first was the Panasonic Lumix DMC-FZ300 DSL camera with the capability of recording 4K streaming at a standard resolution of (4000x4000) pixels and 60 frames per second. The second camera was a handheld JVC video camera of full high definition (FHD) resolution of (1920x1080) pixel. The third type of camera was a closed-circuit television (CCTV) video surveillance camera Uniden brand with a recording capability Full HD (1920x1080) pixel but with a different lens focal length and cost from the JVC handheld cameras. The CCTV cameras need a digital video recorder (DVR) in order to transfer the recording from analogue to digital, and record the footage on a hard disk with a minimum 500 GB installed inside the DVR. The last type of camera was a spy camera, providing a low-resolution recording of 720-pixel,

small in size, low cost and lens focal length. Figure 3.2 shows the four types of the cameras tested before choosing the one most suitable for this study.



Figure 3.2: Four types of cameras used in this research. 1: Panasonic Lumix, 2: JVC handheld video camera, 3: Uniden CCTV camera and 4: Digital spy camera.

The methodology of this research is classified into two major parts. The first part is the photogrammetry analysis, including camera calibrations and video frames analysis and 3-D measurements of the subjects' lower limbs, including 3D angles. The second part is the footprint analysis using an RSSCAN INTERNATIONAL foot sensing platform which extracts the under shoe features to be used as human identification factors.

3.3 Photogrammetry methodology

In this section, we will describe the calibration steps for the four different types of video cameras, and introduce a photogrammetry technique to obtain the biological measurements of individuals.

3.3.1 The process of camera calibration

Camera calibration is a crucial stage in photogrammetric work as it improves the accuracy of measured imaged coordinates (x, y, z) . The calibration software was iWitnessPRO V4 licenced by Photometrix . This software is part of a photogrammetry package software called Australis. All cameras were calibrated by finding the interior orientation parameters (x_0, y_0, f) , radial distortion parameters (K_1, K_2, K_3) , and lens alignment (P_1, P_2, P_3) . The selected cameras were calibrated individually using a self-calibration technique based on iWitness cardboard at an object distance of 900-1000 mm, see Figure 3.3.

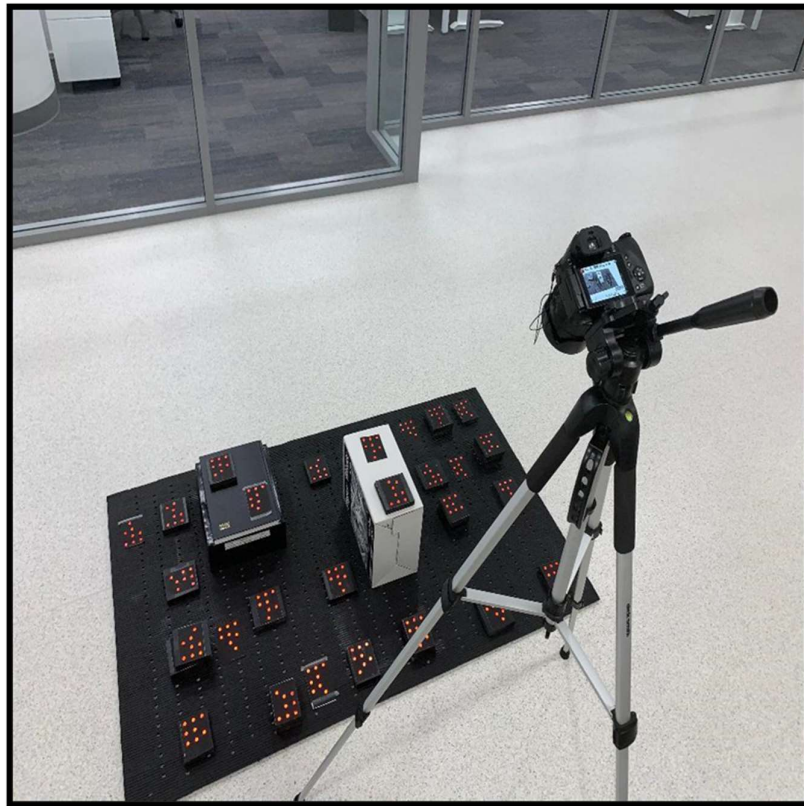


Figure 3.3: Camera calibration process using iWitness cardboard distributed on 3D surface (author's own image).

The calibration process began by capturing 24 sets of convergent video test clips. The cameras were positioned on each corner of the board and the middle of each side, each position had three clips, the first one at zero angles of the camera, 90° and -90° . Individual frames were extracted from each clip and the frames were processed by iWitnessPRO. The mathematical concepts of camera calibration are discussed in the following section of this chapter. The PLPC (Principal Lens Parameter Computation) technique (Chong 2011) was used to determine lens parameters during the imaging session, see Figure 3.4.

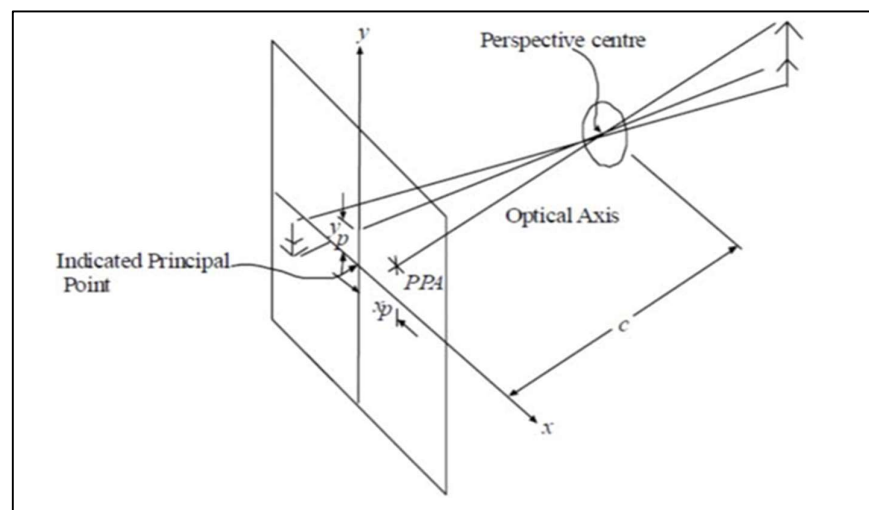


Figure 3.4: Focal length with x_p and y_p where c =focal length (Chong et al., 2014).

3.3.2 Three-Dimensional calibration and measurement with iWitnessPRO

iWitnessPRO is used to convert 2D coordinate (x,y) information of feature points on an object recorded in two or more images of a photographed scene into 3D coordinates (X, Y, Z) . The measurement process is illustrated in raw form in Figure 3.5. Imagine that three images of an object are recorded from three different viewing directions (with a consumer-grade digital camera,) such that feature points P1 to P5 appear in all photos. Intuitively, it is clear that if the positions of the camera stations S1, S2, and S3 are known in a 3D reference system, with the X, Y, and Z axes as illustrated, and the directions of the three imaging rays to a feature point are also known, then the position, say P1, will lie at the end of the intersection of the three rays at coordinates $(X1, Y1, Z1)$ (Chong et al., 2014). This part is straightforward. Unfortunately, the matter is

complicated because we generally do not know the camera stations' precise locations, and we do not directly measure the spatial directions of the imaging rays.

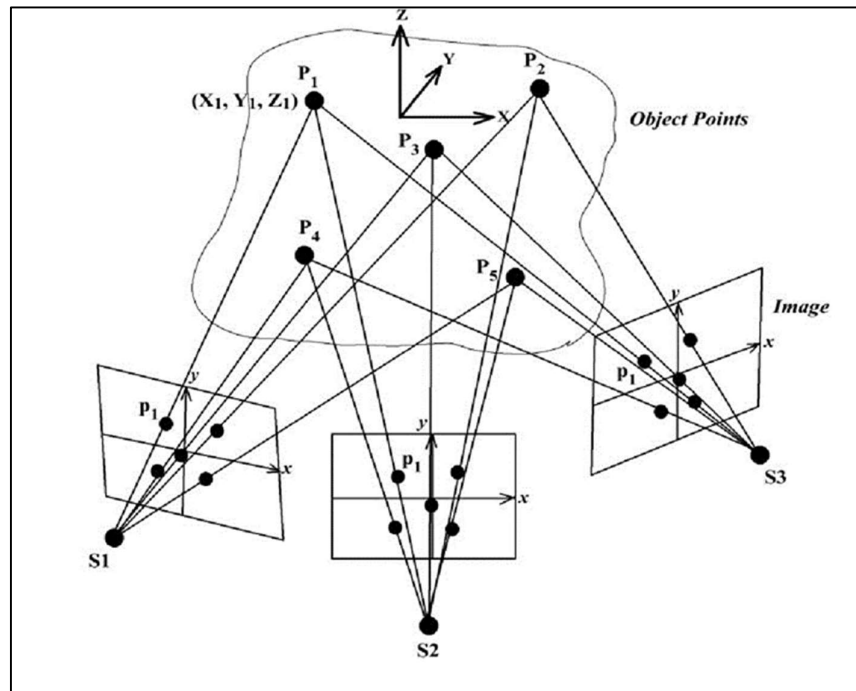


Figure 3.5: Photogrammetric triangulation, XYZ coordinates determined from intersecting rays (Chong et al., 2014).

This is where the technology of photogrammetry comes in. If you imagine Figure 3.5 as illustrating the mutual intersection of three bundles of imaging rays, then this assemblage of camera stations and object points forms a 3D shape. The bundles will only fit together in one way if the corresponding rays for each point intersect perfectly. To achieve this mutual intersection of all matching rays, it is necessary to recover the same 'relative orientation' between the images that they possessed at the time of photography. This reconstruction of the spatial orientation of images, with the 3D reconstruction of the true shape represented by the object points, is termed photogrammetric orientation.

The situation described is no different in principle to the way the human brain recreates 3D scenes from stereo-imagery, for example as with a 3D movie. But with iWitnessPRO any number of images, any number of points, and a wide variety of camera viewing directions are accommodated in the 3D coordinate determination. For the bundle of rays for each image to be established, it is necessary to determine the angular relationship between the rays which all pass through the perspective centre of

the camera lens. This is where the requirement to 'mark' (actually measure) image coordinates comes in. For although we might be marking the 2D location on an image, we are determining the angular direction of each ray with respect to the camera's pointing axis. This is illustrated in Figure 3.6.

By thinking of the image measurement process as the formation of a bundle of rays with known relative directions, we make it easier to visualise the mutual fitting together of these bundles to form a 3D shape. This shape can have an arbitrary scale (move the cameras stations apart and the shape enlarges) and an arbitrary 3D coordinate system. The assignment of scale, or size, and orientation and position of the intersected points P1 to P5 in a chosen XYZ coordinate system is termed 'absolute orientation' in photogrammetry.

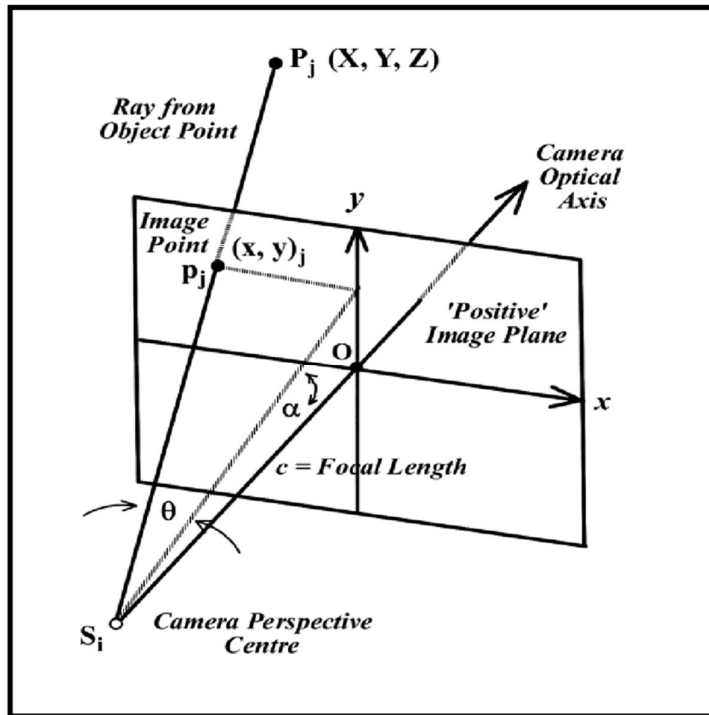


Figure 3.6: The camera as an angle measuring device. (Chong et al., 2014).

So, the 3D feature point determination can be viewed as a four stage process:

- 1- Record two or more images from practical camera viewpoints
- 2- Mark the x, y image coordinates to establish the angular relationship between rays forming each bundle of rays. The corresponding points are said to be

'referenced' when they are marked in two or more images. Note that with iWitnessPRO, this referencing process can be fully automatic when both coded and uncoded high-contrast targets are used as common points

- 3- Relatively orient the images, i.e. bundles of rays, to recreate the geometry at the time of photography and so define the 3D shape of the array of referenced feature points
- 4- Assign the desired scale and XYZ coordinate system to the relatively oriented assemblage of bundles of rays, thus producing the desired outcome: scaled XYZ feature point coordinates.

3.3.2.1 Significance of camera calibration using iWitnessPRO

We need to state at the outset that photogrammetric measurement is both accurate and reliable, and the orientation procedures in iWitnessPRO are more robust if the camera is calibrated (Luhmann et al., 2016). As mentioned, the purpose of marking/referencing x,y image coordinates is to determine the two angles θ and α shown for each ray. But, this cannot be done unless the distance S_i to O is precisely known and it happens to be the focal length of the camera lens. More strictly, we talk of principal distance, c , rather than focal length, which is typically a nominal value corresponding to infinity focus. Note that c changes with focusing, which is why images within a project must be recorded at a single focus and zoom setting.

Note also that the computation of the angles α and β will be influenced by how closely the camera optical axis intersects the assumed origin of the x,y coordinate axes (there are two IO parameters here). Furthermore, there is an assumption that the object point P, the image point p, and the camera station S form a straight line, but lens distortion causes the ray to deviate from a straight line, and thus, there is a need to correct for such distortion effects.

3.4 A process of camera calibration

Before describing the process of camera calibration, the following are some rules which apply to recording images for photogrammetric measurements with iWitnessPRO:

1. The camera lens should not refocus during the photography session to ensure the focal length does not change

2. The lens zoom should not be adjusted during the photography session
3. If the camera has an auto-rotate function, which digitally rotates the recorded image, the function must be turned OFF. In next sections, we will describe in detail the calibration of the four camera types and their limitations in order to calculate which cameras will be used to capture the gait of the subjects.

3.4.1 Spy camera calibration

This low-cost camera has a small focal length of lens with a high range of distortion, as shown in Figure 3.7. It also has a small lens angle, limited memory capacity, and a low-resolution recording.

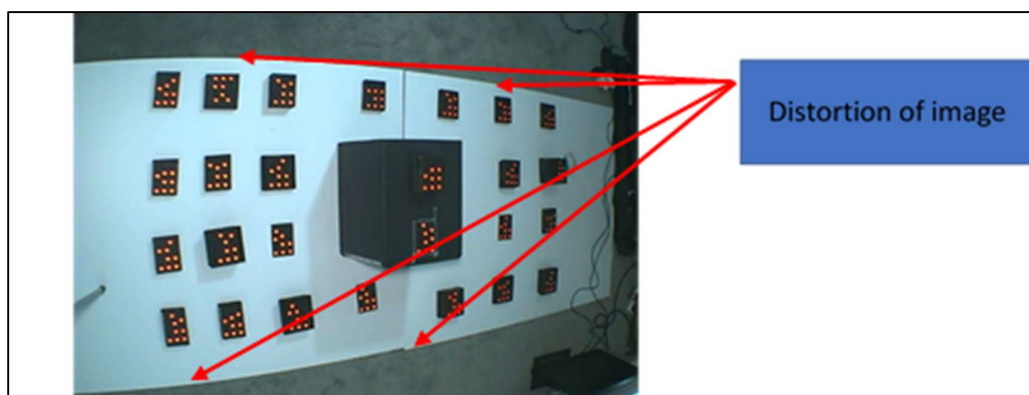


Figure 3.7: Spy camera image extracted during calibration process - curved edge due to lens distortion (author's own image).

The process of calibration by installing the camera on a tripod is shown in Figure 3.7 above. After extracting more than 20 images from different angles and positions, the calibration process was conducted (Figure 3.8). In this process, the green marks indicate a successful recognition of the cardboard known by iWitnessPRO, while the red marks show unsuccessful recognition. Recognition fails due to high lens distortion and low image resolution (Li and Liu, 2018).

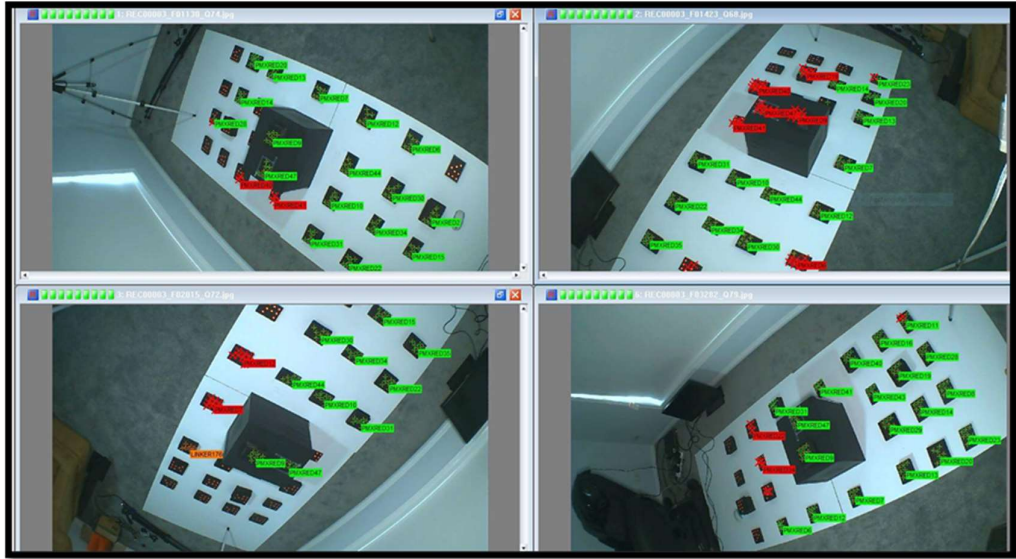


Figure 3.8: Calibration process in iWitnessPRO using images extracted from spy camera (author's own image).

Figure 3.9 shows the distortion grid of the spy camera and how the view of the camera focused on the centre of the lens while the outer space had a large amount of distortion. Focal length value and participants point with the radial distortion coefficients will be discussed in the next chapter.

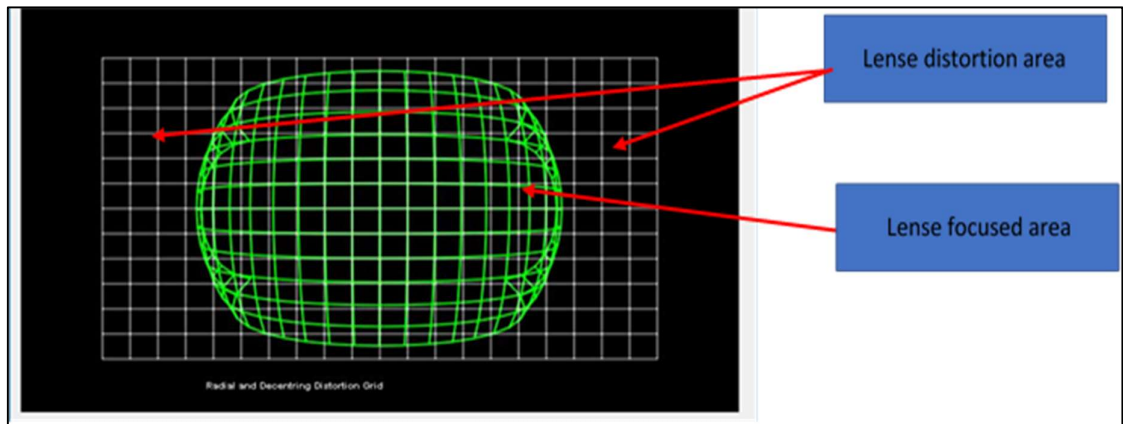


Figure 3.9: Radial and decentering distortion grid of the spy camera (author's own image).

3.4.2 Calibration of UNIDEN closed-circuit television (CCTV) camera

A CCTV camera can be defined as a system that captures (relates to optics and sensor) and records (pre-processes, encodes, compresses and records) its surrounding area for surveillance purposes (Doyle et al., 2013). The most important factor that controls the outcome of these cameras is the amount of lens distortion which affects the quality of video recording resolution (Wright et al., 2010). The radial and decentering distortion grid of this CCTV camera, Figure 3.10 (a and b), shows the distortion which is less than the previous type of camera (Spy camera).

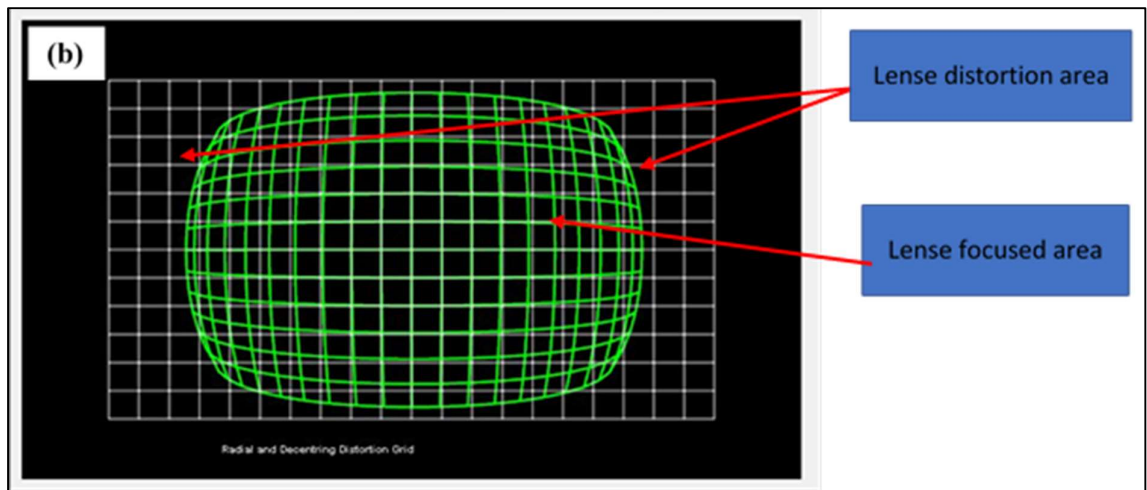


Figure 3.10: (a) Uniden CCTV camera and (b) Radial and decentering distortion grid of the UNIDEN CCTV camera (author's own image).

The extracted frame from the footage of these CCTV cameras had less distortion. Figure 3.11 shows one of the CCTV camera calibration process images. We can notice that the green marks of the calibration boards are not fully marked. This is because of distortion and the low resolution of those cameras.

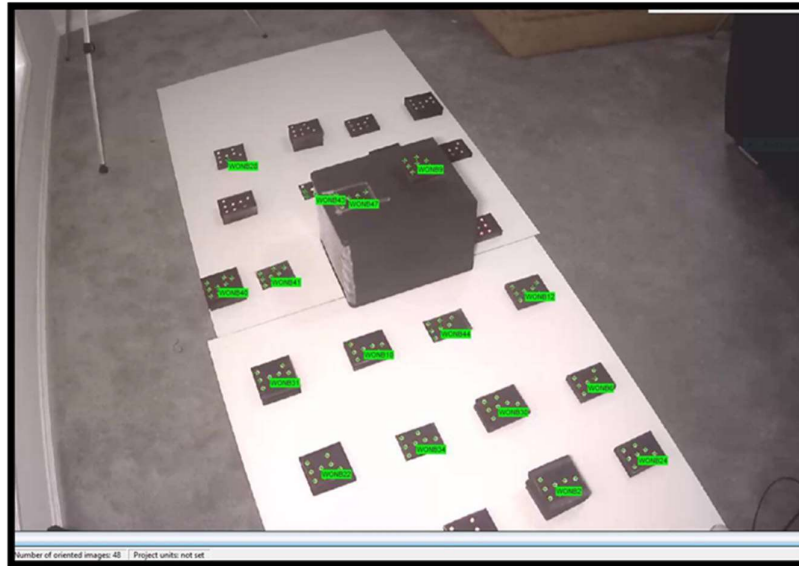


Figure 3.11: Calibration process for CCTV UNIDEN camera (author's own image).

3.4.3 Calibration of JVC handheld video camera

This type of camera has a good image quality with high resolution (1920x1080) pixel. The footage of this camera had less distortion than the two cameras discussed previously, see Figure 3.12.

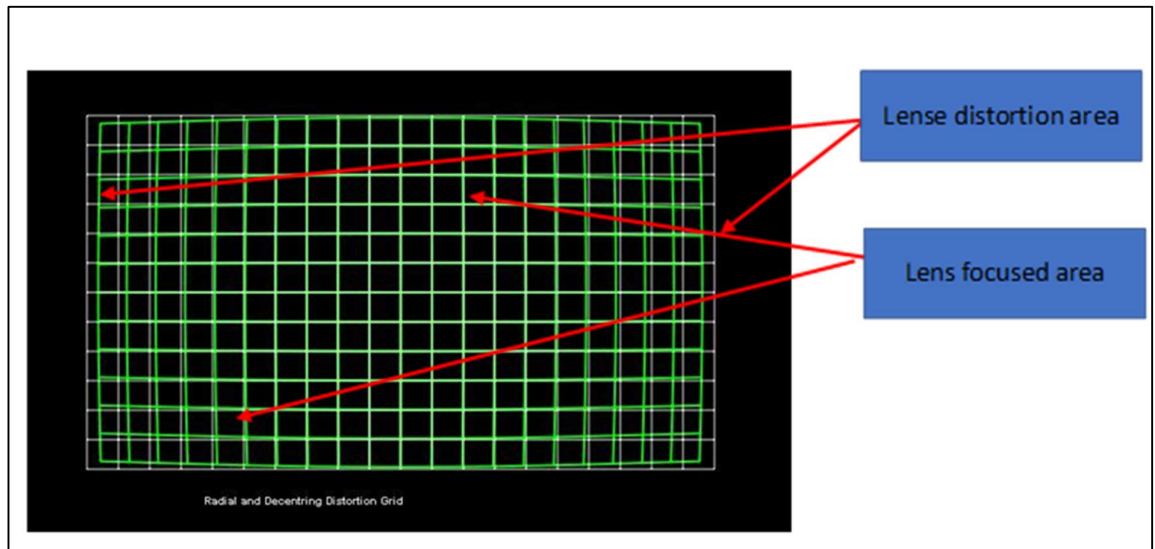


Figure 3.12: Radial and decentering distortion grid for JVC video camera (author's own image).

From Figure 3.12, it can be seen that the distortion area is too small, and the lens covers most of its view without distortion. During the calibration process (with iWitnessPRO), higher resolution images could lead to the cardboard being recognized easily and the camera parameters obtained more accurately. The calibration cardboard was recognized with a smaller number of rejection points, see Figure 3.14.



Figure 3.13: JVC hand-help FHD video camera (author's own image).

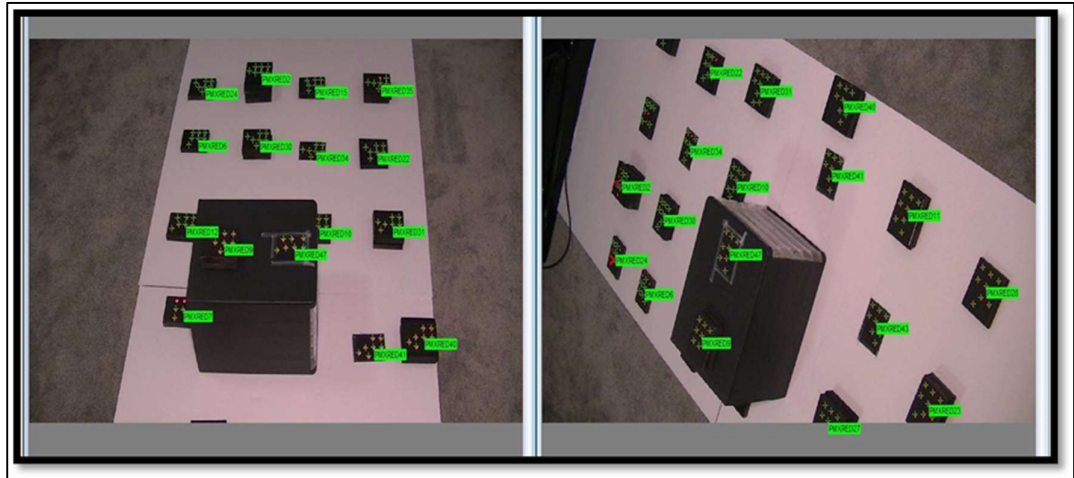


Figure 3.14: Calibration of JVC video camera. Digitizing has a small number of non-digitizing points (author's own image).

3.4.4 Calibration of Panasonic digital camera DMC-FZ300

This camera (Figure 3.15) was used to collect the data for this research. It can record 4k video streaming with a high resolution of 3840x2160 pixels. Pixel width = 0.0050mm and Pixel height = 0.0050mm.



Figure 3.15: Panasonic Lumix DMC-FZ 300 used to collect data (author's own image).

Before collecting data with this camera (Figure 3.16), the setting was set to FHD resolution (1980x1080) pixels, because this resolution is the most common in CCTV cameras. The difference in using these cameras is that they have less distortion and a wider lens angle.

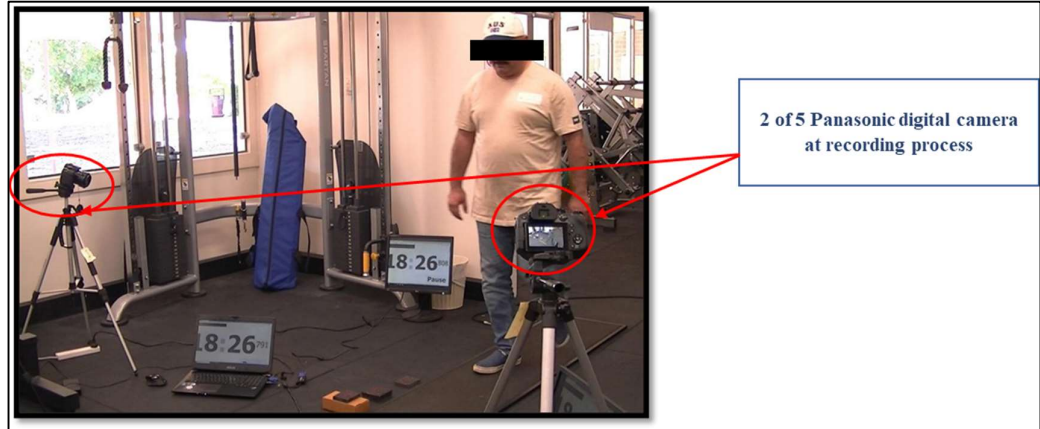


Figure 3.16: Panasonic digital camera while recording a subject gait. (author's own image)

According to Figure 3.17, the distortion area is smaller than the previous cameras. For the radial and decentering distortion grid of the Panasonic DMC-FZ300, the green area covered most of the grid, meaning less lens distortion during recording of the gait of subjects surrounded by five Panasonic cameras sitting on tripods (Figure 3.18).

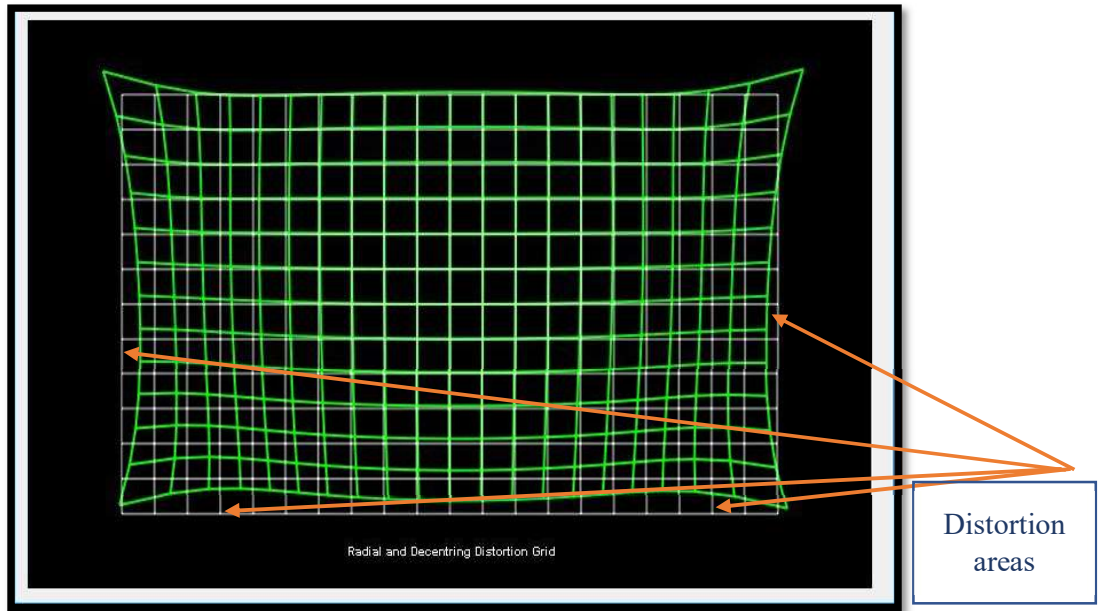


Figure 3.17: Radial and decentering distortion grid for Panasonic Lumix DMC-FZ300 digital camera (author’s own image).

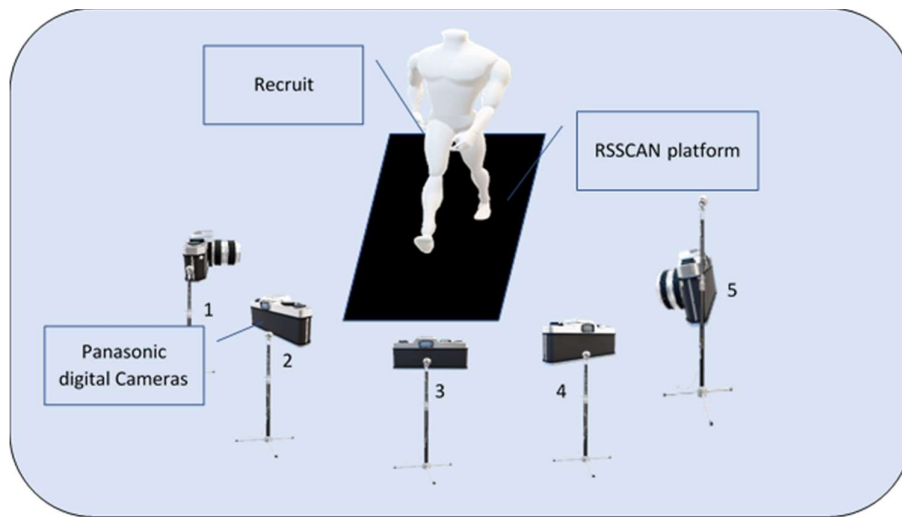


Figure 3.18: 3-D model showing data collection with the distribution of the Panasonic cameras. Black mat refers to the RS scan foot pressure mat (author’s own image).

In the next section, we describe the data collection procedure using the Panasonic digital video cameras using photogrammetry.

3.5 Gait data collection using photogrammetry

3.5.1 A step before collecting data

After calibrating the cameras, three clock screens were placed in different positions to ensure that at least one of them was viewed by the camera recording, see Figure 3.19. These clock screens are used to ensure that we extracted the same frame from the videos recorded by the five different camera positions. The figure also shows a scale bar of 846mm length. This scale bar was used as a reference scale set in the 3-D measurements using iWitnessPRO. The subjects were tested under the Ethics application issued by the University of Southern Queensland (USQ) of number: USQ HREC ID: H21REA120.

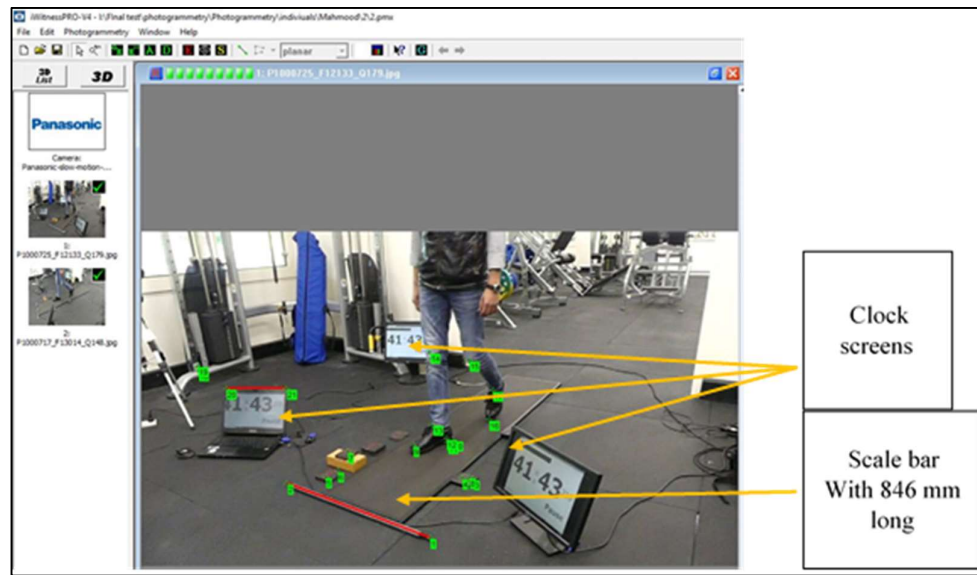


Figure 3.19: Clock screen used in data recording, the three screens are synchronized and showing minutes, seconds and three digits of milliseconds (author's own image).

This part of the research aimed to collect measurements data (3-D distances and angles) for the lower limb of the 23 subjects' information (presented in Table 3.1) at the three stages (heel-down, mid-stance and toe-off) and compare them with the other individual's data. The comparison was determined with the use of one-way ANOVA (analysis of variance) statistics, in order to obtain the similarities and differences of the factors that used in these calculations.

Table 3.1: Subjects' information

No.	Gender	Height (cm)	Weight (kg)	Age (year)	Shoe size (US)
1.	M	186	108	43	12
2.	M	176	100	48	10
3.	F	162	59	45	7
4.	M	178	107	38	11
5.	M	181	70	41	10
6.	M	174	85	39	9.5
7.	F	159	81	41	7
8.	F	155	45	14	6
9.	M	176	84	38	11
10.	M	180	92	39	10.5
11.	F	172	74	29	7
12.	F	166	58	26	7
13.	F	169	60	28	8
14.	M	176	72	45	10
15.	M	183	79	20	11
16.	M	178	69	18	10
17.	F	168	65	35	7
18.	M	178	86	42	10
19.	M	172	81	39	9.5
20.	M	176	88	37	11
21.	M	182	69	17	11
22.	M	178	73	25	10.5
23.	F	161	55	29	7

The photogrammetry software used in this research is called iWitnessPRO Version 4. With this software, we need at least two photos taken from different views of the cameras to obtain a 3-D model to calculate the 3-D measurements. The question now is, why we are using five cameras while we need only two photos to get the 3-D measurements. The answer to this question is that, during video analysis using

iWitnessPRO, we choose the most suitable captured photo that gives the measurements without challenges.

The captured images extracted three postures of the gait, heel-down, mid-stance and toe-off. At the mid-stance stage, the velocity of walking is almost stable (van Mastrigt et al., 2018a). Moreover, multi-captured images allowed digitization of the target points from the best view and uncovered by the other leg. see Figure 3.20.


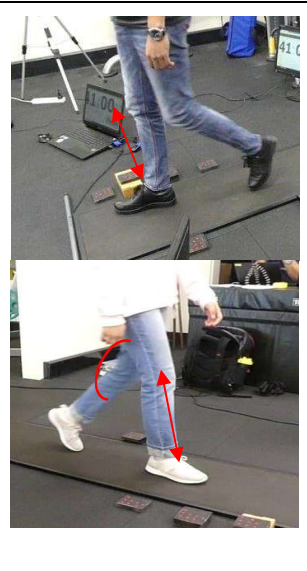
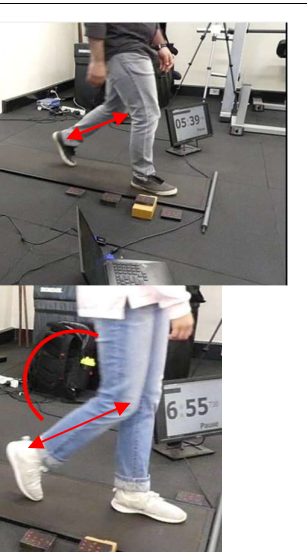


Figure 3.20: Capturing two images with clear view of the low-limb with the corresponding 3-D model of the points selected (author's own image).

3.5.2 Photogrammetry data analysis with the adopted human identification factors

The methodology of this part of the research provides multi-data collected from lower-limb 3-D measurements. We will consider the measurements as shown in Table 3.2.

Table 3.2: Photogrammetry factors used in the research methodology

No.	Stage	Factor name	Example
1	Heel-down	<ul style="list-style-type: none"> a- Knee-inner ankle joint distance b- Knee-outer ankle joint distance c- Knee angle 	
2	Mid-stance	<ul style="list-style-type: none"> a- Knee-inner ankle joint distance b- Knee-outer ankle joint distance c- Knee angle 	
3	Toe-off	<ul style="list-style-type: none"> a- Knee-inner ankle joint distance b- Knee-outer ankle joint distance c- Knee angle 	

Nine factors were used in the photogrammetry section of this chapter. Six different 3-D distances for the three phases (heel down, mid-stance and toe-off) and the knee angles for each stage. The outcome from footage analysis for the three resulted in the nine factors mentioned in Table 3.2 above. They show zero similarities within the group of twenty-three subjects. The 3-D angle for the knee at each stage also showed zero signs of similarities in the ANOVA calculation.

3.5.3 Calculation of 3-D distances for the subjects at the heel-down stage

Five cameras were used to record and register the subjects' gait while walking through the RSscan foot pressure mat. After extracting the images showing clear views of the knee-inner and outer ankle joints and knee angles, the 3-D measurements were processed with iWitnessPRO V.4. The selected digital cameras provided a non-blurry picture or a picture less blurry than the other cameras discussed in the calibration section. Non-blurry images help identify the target more accurately, see Figure 3.21.

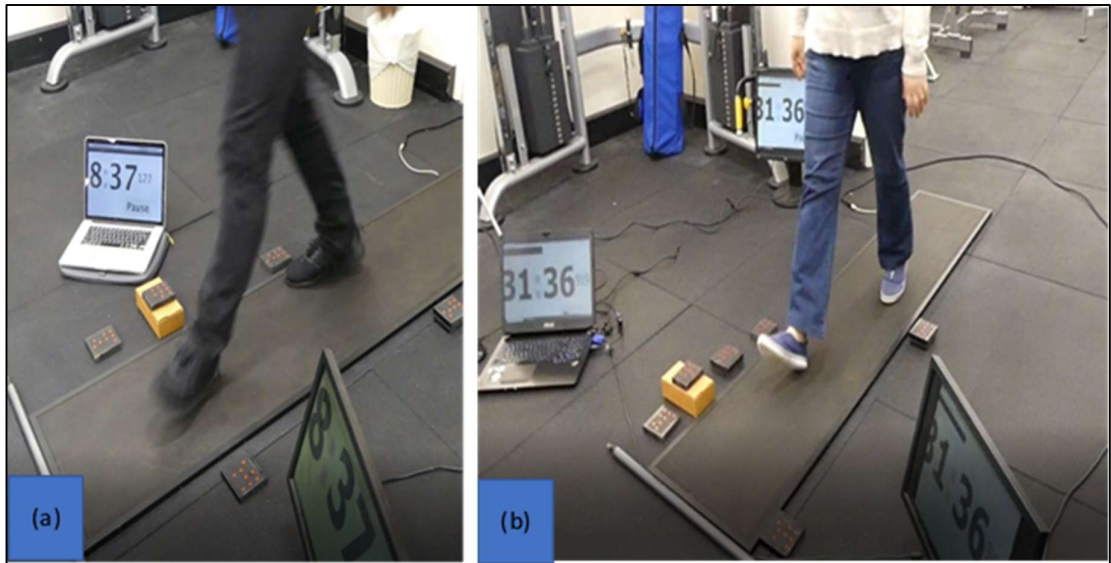


Figure 3.21: Two images extracted from two different cameras: a- Image with blurry taken from JVC hand-held digital camera, b- Non-blurry image extracted from Panasonic digital cameras which were used in this research (author's own image).



Figure 3.22: Calculating real measurement of knee-inner/outer ankle joint to be compared with photo measurement to obtain error difference (author's own image).

The 3-D measurements of the knee-inner ankle joint and the outer ankle joint are calculated by targeting the knee centre point to the inner ankle joint of the same leg for each recruit. Moreover, the images were used to measure the outer joint extracted from different cameras just as the inner ankle joint was calculated.

The view of the Knee- inner joint Ankle is different from the Knee to the outer joint Ankle. Next, the 3-D distance between these two points was calculated using iWitnessPRO. Each measurement was verified by comparing the actual measures with the photogrammetry measurements. The difference between these two measurements shows that less than 1 mm. According to calculations for the 3-D distances for multiple targets on the lower limb of the subjects, the most significant factors for this stage were the 3-D distance from the knee-inner ankle joint and knee-outer ankle joint. This is important because the ankle joints are stable during gait and not affected by ground level or feet deviations (Yang et al., 2014b).

The calculation of the 3-D knee angle at this stage starts by locating three target points on the leg, see Figure 3.23. The first point on the trap, the second target point on the centre of the knee, and the third point on the leg. By drawing two vectors from these three target points, we calculated the angle between these two vectors using the equation (3.1) below:

$$\theta = \cos^{-1}(\vec{a} \cdot \vec{b} / \|\vec{a}\| \|\vec{b}\|) \dots\dots\dots (3.1)$$

where \vec{a} is the 3-D vector from the knee target point to the target point of the trap, \vec{b} is the 3-D vector point from the knee target point to the target point on the leg. Data obtained from the 3-D measurements for the three identification factors showed a significant value for human identification. The similarity value with the ANOVA calculation was the low value when comparing the tested subjects with the data of the others (between-group). While the similarity factor was highest when comparing the ten trials' data for the same subjects (within a group).

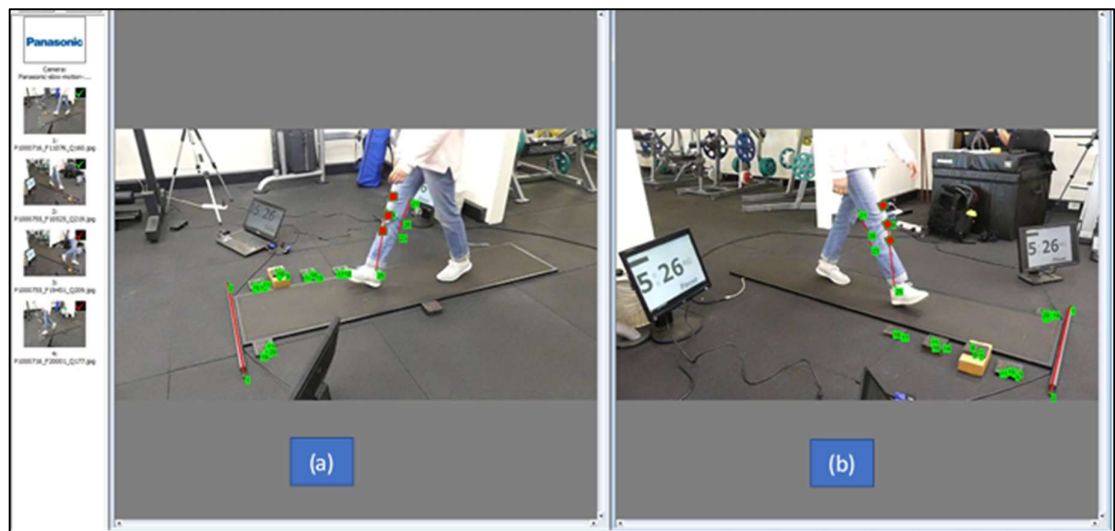


Figure 3.23: Calculation of identification factors at heel-down stage. (a) Distance from knee-inner ankle joint, (b) Distance from knee-outer ankle joint (author's own image).

3.5.4 Calculation of identification factors for subjects at the mid-stance stage

Calculation and analysis of extracted data for this stage were more reliable and accurate than the other two stages (heel-down and toe-off). This is important because the image was less blurry at this posture. Also, the recruit took a long time standing on their feet during the mid-stance stage compared with heel-down and toe-off (Hurd and Snyder-Mackler, 2007;Roca-Dols et al., 2018). Four different recruit identification factors were obtained from this stage (Figure 3.24):

- a) Knee-inner ankle joint 3-D distance
- b) Knee-outer ankle joint 3-D distance
- c) Knee angle in three dimensions
- d) Knee-fore foot 3-D distance.

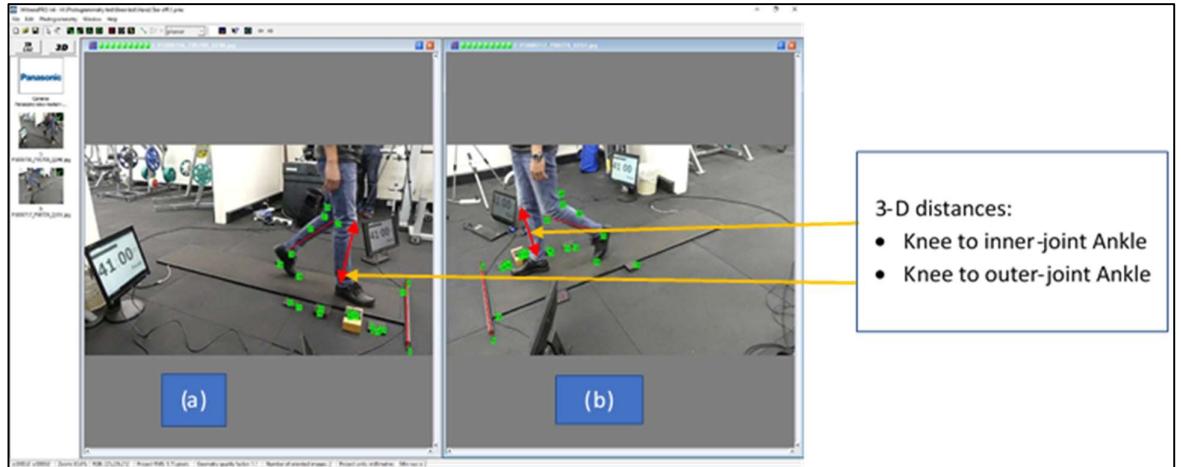


Figure 3.24: Calculations of identification factors at mid-stance stage. Measurements from two cameras views: a) measurements of knee-outer ankle joint, b) measurements of knee-inner ankle joint (author's own image).

3.5.4.1 Calculation of knee – inner ankle joint at mid-stance phase

To calculate this identification factor, we identified the cameras suitable for recording the space of the knee-inner ankle joint. From Figure 3.24(a) we determined that the cameras used were numbers 1 and 2 if we considered the distribution of the cameras as in Figure 3.18. While in Figure 3.24(b), Camera numbers 4 and 5 were used to extract the images. After extracting two images from Cameras 4 and 5 using iWitnessPRO, we targeted the knee and the inner ankle joint. After that, using iWitnessPRO, we calculated the distance between the two targets. This process was applied 10 times to each of the 23 subjects. The distances were measured in 3-D and each measurement was compared with the real distance taken from the subjects at the same stage. The difference factor between real and photogrammetry was $\pm 3\text{mm}$.

The obtained measurements were statistically calculated using one way ANOVA to check the significant of this identification factor. Results showed that the significant (p) value was 0.01 which means no similarities of the 3-D distances between the group of subjects, while this (p) value was 1.000 for the subjects (within a group of same subjects). The resulting data showed that this factor can be used for human identification because it is the difference significance is very high.

3.5.4.2 Calculation of knee–outer ankle joint at mid-stance phase

To calculate this identification factor, we used a different camera's view from the previous factor. As shown in Figure 3.24 (a), we used Cameras 1 and 2 or 1 and 3 to calculate this factor with high authentication. We will followed the same procedures as the previous step after obtaining the 3-D distances for the knee-outer ankle joint angles and calculated them using the ANOVA statistical analysis. The significance from this ANOVA calculation showed this factor could also be used as a human identification factor. The results will be discussed in detail in the next chapter. The significant value for the 23 subjects for this identification factor was around 0.003 if we compared the 3-D distances from the knee-outer ankle joint of each subject (between group). While this value was approximately 1.000, which considered insignificant if we compared these distances for the 10 trials of the same subjects (within a group).

3.5.4.3 Calculation of knee angle at mid-stance stage

For this identification factor, we used the same procedure as calculating the knee angle at heel-down. First, we identified three points, as shown in Figure 3.25. Points 13, 14, and 15 determined the knee angle by drawing two vectors. The first vector from Point 13 – 14. The second vector between Points 14 and 15. The value of the angle was as the equation (3.13), which was mentioned above:

$$\theta = \cos^{-1}(\mathbf{a} \cdot \mathbf{b} / |\mathbf{a}| |\mathbf{b}|) \dots \dots \dots (3.3) \quad \text{where}$$

\mathbf{a} : vector between Points (13-14)

\mathbf{b} : vector between Points (14-15).

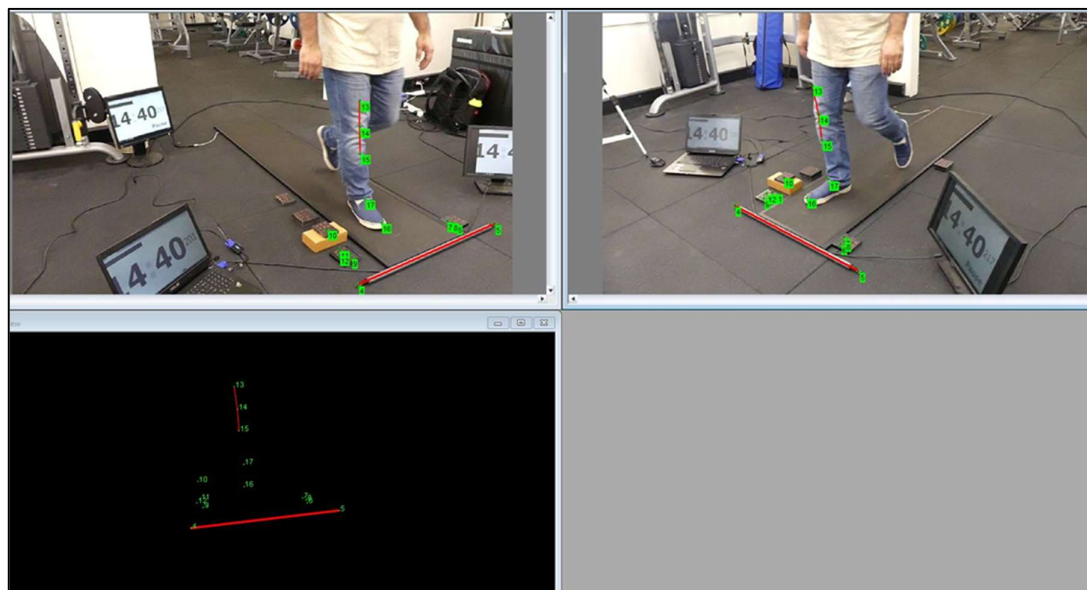


Figure 3.25: Two extracted images with their corresponding 3-D modelling. Points 13, 14 and 15 to calculate the knee angle (author’s own image).

The values of the knee angle were calculated for the 23 subjects and were determined statistically using ANOVA analysis and obtained the similarity significant value between the group (subjects) with a value 0.01 and 1.00 for the same recruit group (within the group). These calculations show that the 3-D knee angle for the subjects is a significant identification factor. This factor will be used with the other identification parameters to identify humans.

3.5.4.4 Calculation of knee–fore foot 3-D distance at mid-stance stage

The calculation of this parameter showed that it is significant for identification only in the mid-stance stage because the leg is more stable than in the other stages (Hurd and Snyder-Mackler, 2007). Figure 3.26 showed the knee-forefoot 3-D distance at the mid-stance stage. To calculate this distance, the Knee point was targeted and the front of the shoes that touching the toes. Next, these two points were connected by drawing a line and measuring it with iWitnessPRO. The statistical calculation of these distances for the 23 subjects showed that it is a significant identification factor. Calculations result 0.01 value of similarity is a significant factor between the group subjects and

around 1.00 when determining the significant similarity value by ANOVA calculation for the subjects (within the group).

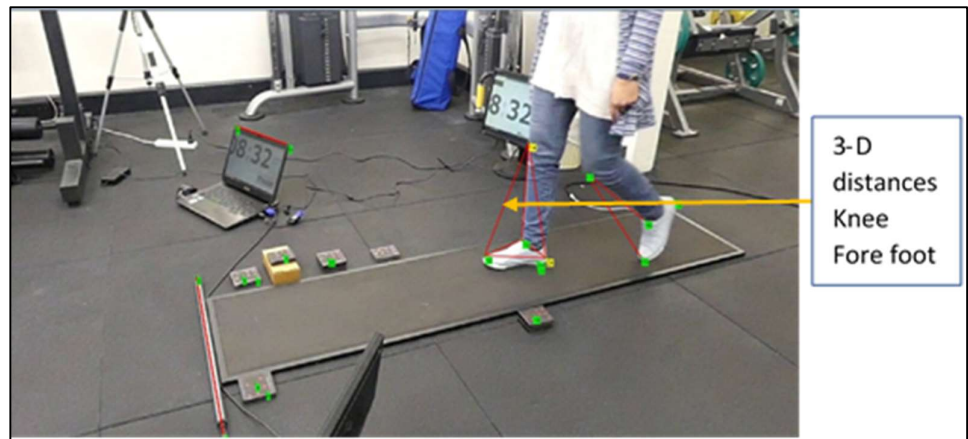


Figure 3.26: The knee-forefoot 3-D distance at mid-stance stage (author's own image).

3.5.5 Calculation of identification factors for the subjects at toe-off stage

This stage comes after the mid-stance stage. The time for this stage is less than the time at the mid-stance stage. As a result, the importance of the cameras chosen for this test was shown by the high possibility of obtaining blurry images. The cameras used in this research could reduce photo blurriness to identify the target points on the knee, inner ankle joint and outer ankle joint.

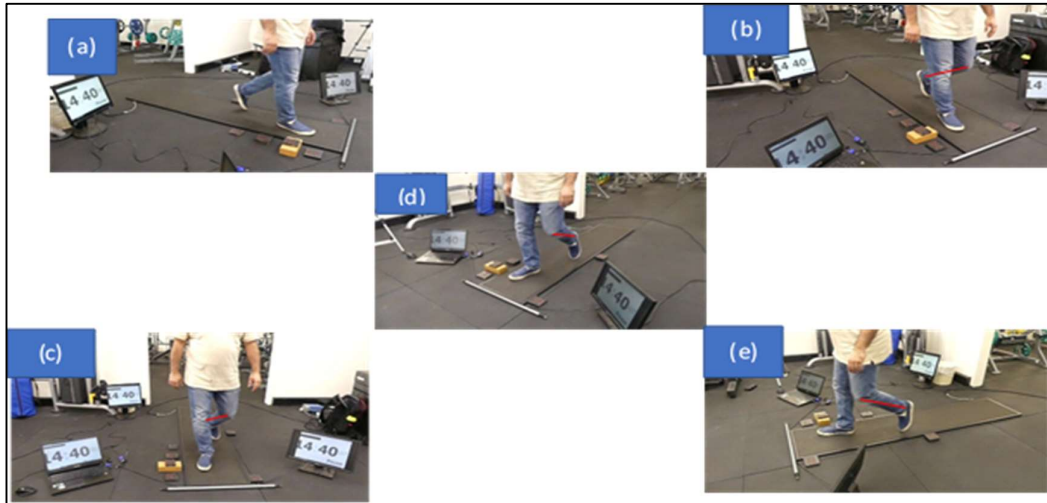


Figure 3.27: Five different views for the toe-off stage for a recruit (author’s own image).

From Figure 3.27 we can see that five different views were extracted from five different positions with the Panasonic cameras. Figure 3.27 (a) is a useless image because, at toe-off stage, the left knee was hidden by the right leg. As a result, we used the other four images to measure knee-inner ankle joint.

After calculating the 23 subjects’ measurements (ten tests per recruit) we obtained a set of measures data. These data were analysed using the statistical ANOVA analysis. The resulting data showed that the knee-inner ankle joint 3-D measures and the knee-outer ankle joint 3-D measures were significant identifications factors. These factors had a similarity factor of around 0.01 between the group of subjects. While the significant similarity factor was very high at around 1 for the ten tests of each recruit (within-group).

The third identification factor for this stage was the 3-D knee angle. To calculate this parameter, the same procedure was adopted as that used to calculate the 3-D knee angle for the heel-down and mid-stance phases. Three points were targeted. The first point was above the knee. The second target point was on the knee and the third was below the knee. Vector one was between Points 1 and 2. The second vector was between Points 2 and 3. The 3-D angle was calculated according to equation (3.3):

$$\theta = \cos^{-1}(\vec{a} \cdot \vec{b} / |\vec{a}| |\vec{b}|) \dots\dots\dots(3.3) \quad .$$

where \vec{a} is the vector between Points 1 and 2

\vec{b} is the vector between Points 2 and 3.

The values of this knee angle were subjected to ANOVA statistical analysis, which resulted in significant identification parameters which were added to the other photogrammetry identifications parameters.

3.5.6 Conclusions of photogrammetry methodology

Before applying the tests to the subjects, we had to find the most suitable video cameras that for recording the 23 subjects while walking on the RSSCAN force\pressure platform. Calibration data analysis showed the Panasonic Lumix cameras to be the most suitable for this research; obtaining reliable, scalable and authenticated 3-D measurements. More than 50 identification parameters were tested and evaluated, and only the mentioned factors (knee to inner/outer measurements, knee angle) for three stages (heel-down, mid-stance and toe-off) were chosen (according to the data analysis) to represent the adopted human identification technique of this study. There were some internal and external challenges. The external factors mostly imposed challenges to the recognition approach (or algorithm). For example, viewing angles (e.g., frontal view, sideview), lighting conditions (e.g., day/night), outdoor/indoor environments (e.g. sunny, rainy days), clothes (e.g. skirts). The internal factors were changes in natural gait, due to sickness (e.g. foot injury, lower limb disorder, Parkinson disease etc.) or other physiological changes in the body due to aging, drunkenness, pregnancy, gaining or losing weight and so on.

3.6 Human identification using RSSCAN International platform

Force plate-based biometrics is feasible to operate on authentication mode just like a sensor based gait recognition systems. Unlike the vision-based gait recognition systems where surveillance cameras and images are used to identify people by their gait, force plate biometrics has potential applications in user verification for limited access systems. They can even be used along with fingerprints or facial recognition in an integrated biometric system.

The force data biometric system proposed in this paper is simpler than the one described by Connor and Ross (2018) in terms of feature sets and recognition techniques. This identification technique is the second part of the proposed human identification system using gait analysis with the RSScan International foot scan

system (Figure 3.28). The specifications of this platform are shown in Table 3.3. This model was used to collect data for the same subjects in the photogrammetry data described in the previous part of this chapter. There is a correlation between collecting photogrammetry data and foot scan data.

During the trials, data was collected and processed for both video footage and the foot scan system. Four different parameters will be described in this part of the research. These parameters showed great advantages for identification. They showed a very high difference between groups of subjects and high similarities within the same individual's trials.



Figure 3.28: RSScan International foot pressure mat with high speed 500frame/sec, 2.0 m.

Table 3.3: Specifications of the RSSCAN foot scan mat used in this research (<http://www.rsscan.com>).

Specifications	Dimensions
Advanced & Hi-End 2m plate Dimensions (length x width x height):	2093 mm x 469 mm x 18 mm
Weight:	28.8 Kg
Number of sensors:	16384 (arranged in a 256 x 64 matrix)
Sensor dimensions:	7.62 mm x 5.08 mm
Active sensor area:	1950 mm x 325 mm
Sensor technology:	resistive
Data acquisition frequency:	up to 500 Hz or 500frame/sec
Pressure range:	1 – 127 N/cm ²
Operating temperature range:	+15 °C to +30 °C
Storage temperature range:	+0 °C to +40 °C
Relative humidity:	20% to 80% non-condensing
Plate cable length:	300mm +/- 50mm (integrated cable)

The collected data was analyzed using ANOVA just as it was used in the photogrammetry analysis. The parameters used in this analysis were as follows:

- 1- Force in Newton (N): This parameter is the sum of force in Kilo Newton KN for the foot from initial contact to toe-off
- 2- Force/pressure distance (mm): Data for each frame has the information of force in KN and the (X, Y) coordinates for these frames. By using equation (3.1), we calculated the total distance for the total frames scanned
- 3- Temporal parameter (ms): Calculations of gait cycle time in (ms) for subjects with all trials
- 4- Spatial parameter (mm): Calculation of gait cycle length
- 5- Total foot pressure data (N/m²): Calculation of the sum of foot pressure from initial contact to toe-off for each subject
- 6- Calculating the ambulation time in (ms) for the ten trials of each of the 23 subjects. The ambulation time was calculated for one gait cycle.

3.6.1 Human identification using force foot value

This identification parameter was obtained by collecting the data from the subjects through the RSScan International (specifications shown above). This device was calibrated before use by entering the weight of the subject before they walked on it. The 5m walkway was designed to provide approximately seven to eight continuous gait cycles including walking on the pressure plate. The foot scan system was calibrated before each measurement session.

To calibrate the device, a recruit's weight was entered as instructed by the software menu before the subject walked along the walkway at average speed while wearing shoes. This force/pressure mat is capable of recording 500 frames/sec. The frames were extracted and stored in the computer connected to the pressure platform using software named Foot Scan Gait.

According to Świtoński et al. (2011) dynamic plantar pressure measures have been captured using similar devices. Each recruit executed 10 trials starting with the left foot and another 10 trials starting with the right foot. The length of the pressure plate provided a three-four step steady gait. The data collected from the second step started with the left foot (from the right step). Gait is more stable from the second step (Larsen et al., 2008;Schöllhorn et al., 2002;Xu et al., 2017;Franklyn-Miller et al., 2014;Bus and de Lange, 2005). To obtain the identification factor from the force foot profile, we

combined all the force values from the extracted frames for one gait cycle for all 10 trials and calculated the mean value to be compared with the suspect data.

Table 3.4 shows the data extracted for each frame including force value in Kilo Newton (KN), time is taken in (ms), and the (X, Y) coordinated 2-D location for each frame.

Table 3.4: Example of data extracted from each frame while subject walked on force/pressure platform.

Frame	Time ms	X	Y	Force (N)
0	0	-12.93	17.68	45
1	7.94	-10.13	18.07	74
2	15.87	-8.68	18.84	90
3	23.81	-7.52	19.91	105
4	31.74	-5.96	21.74	130
5	39.68	-5.02	23.79	157

Figure 3.29 shows each frame point for the force foot of a subject. The number of frames varied between subjects depending on the foot dimension (Mostayed et al., 2008). We calculated the value of the force foot from initial contact (heel-down) to toe-off for the second step as it is more stable, as mentioned previously. In Table 3.4 the Force column shows an increase in the force value from zero to the peak value and then the force value decreases. This peak was due to increasing foot forces from initial contact, which had the least weight, to mid-stance posture representing the peak value. The foot force value started decreasing when foot posture transferred from mid-stance to toe-off or final shoe contact.

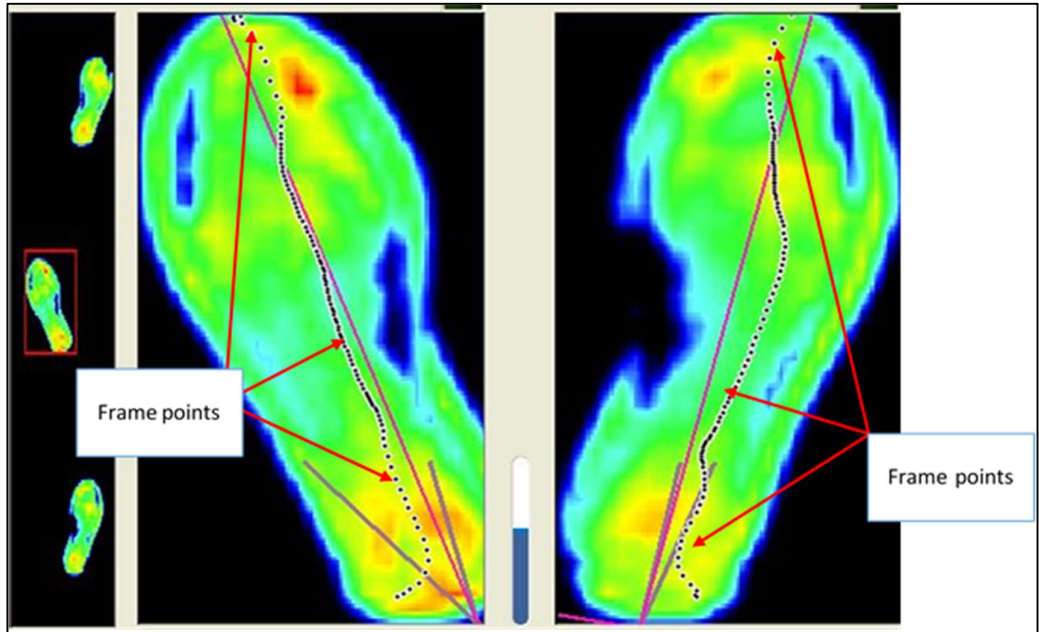


Figure 3.29: Frame points which contain information of force, 2-D coordinates and time for the foot during walking (author’s own image).

3.6.2 Human subject identification using force/pressure foot distance

This parameter showed significant results for the 23 subjects tested. These results were obtained by calculating the foot force/pressure distance shown in Section 3.5.1 Table 3.4, which delivers for each frame force value in (Newton) and (X, Y) coordinates. With this human identification parameter, we calculated the two dimensions’ distances using the Pythagorean Theorem to calculate the distance between two points, as shown in equation 3.4 below:

The distance equation 3.4 (Burgstaller and Pillichshammer, 2009)

Suppose P(x1,y1) and Q(x2,y2) are two points in the number plane. Then:

$$D = \sqrt{((X_n - X_{n-1})^2 + (Y_n - Y_{n-1})^2)} \dots \dots \dots (3.4)$$

Where n represents the number of points or frames on the force line. This distance is the same as the distance of the pressure line according to the physics equation 3.5 below:

$$P = F/A \dots \dots \dots (3.5)$$

where P is pressure, F is a force in Newton, and A is the area in m².

Table 3.5 the calculation of the force line distance for one trial to one subject.

Table 3.5: Frame no. with the sum of 110 points distances in (mm) compared to the shoe length

No. of frames	Total distance (mm)	Shoe length
110	312	320

From Table 3.5, the total force/pressure distance can be seen to be slightly less than the shoe length (312mm / 320). The difference in mm refers to the thickness of the shoes above the foot. Figure 3.30 below shows the footprint of two different subjects with two figures for each subject. Figure 3.30 (a) and (b) show the force/pressure frames path for two trials of Subject 9. Figure 3.30 (c) and (d) show the force/pressure frames route for Subject 15. We can see the similarity of the force frames route for (a) and (b) and the similarity of frames route between (c) and (d). There is a huge difference between the force line and footprint shape between the two subjects indicating the value of this factor as one of the identification factors identified by this research.

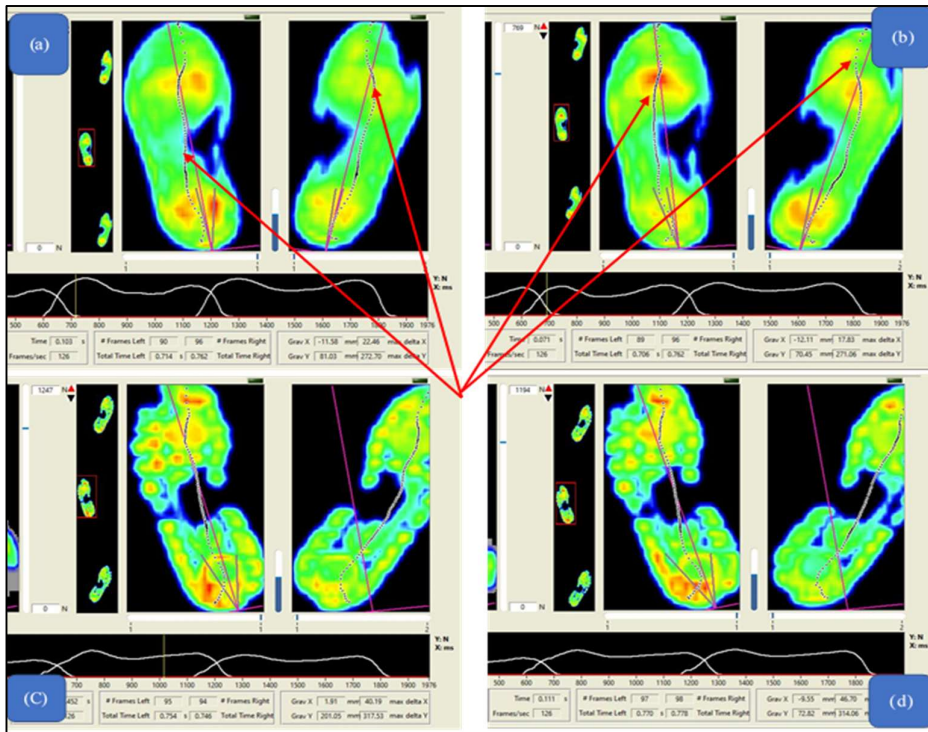


Figure 3.30: Force/pressure line (a,b) for recruit Number 9. We can see the similarity of the force line direction. (c,d) force/pressure line for subject number 15, and we can see the similarity of the force line direction. (a,b) has a different footprint shape and is different from (c,d) in regards to the force line direction. (author's own image).

3.6.3 Identification factor using temporal, spatial and ground force reaction parameters for human recognition

Another vital parameter used as a human identification factor is the timing sequence of human gait (temporal) (Zhu et al., 2018). In this research, we extracted many parameters related to the temporal parameter during the subjects walking across the RSSCAN INTERNATIONAL foot pressure mat, such as step time, gait cycle time and ambulation time, see Figure 3.31. After analysing each parameter for the subjects, the most significant parameter that could help with human identification was ambulation time. ANOVA analysis results showed that the ambulation time is valuable for recognition of subjects.

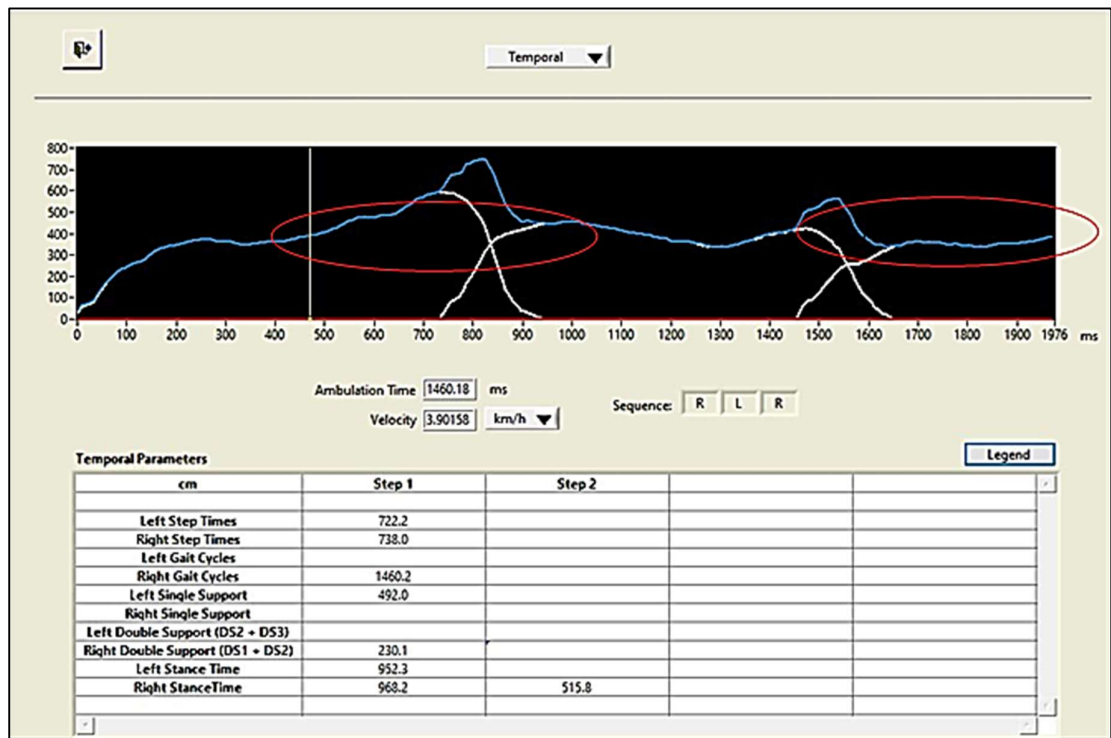


Figure 3.31: Temporal analysis diagram with factors related to temporal analysis (author's own image).

However, this factor varied with walking speed. An increase in gait speed was positively correlated with people's ambulation time (Benson et al., 2018). If we use this factor for identification, there will be some challenges: the walking time varied according to the changing gait speed. To solve this issue, we stabilized this factor with speed increasing or decreasing. One effective way is to normalise the correlated

temporal and special parameters (Bravi et al., 2020). For gait spatial calculation, we used the most significant value for identifying the subject: gait cycle distance. By normalizing these two values, we obtained a new significant factor that helps in human recognition.

However, this new value is still affected by the GFR during walking. According to Yamin et al. (2017), GFR is an essential parameter in kinetics response concerning gait movement on various surfaces. GFR has been widely used in numerous gait analyses related to running (Jafarnezhadgero et al., 2020;Teymouri et al., 2017) and walking (Wang et al., 2020;DiLiberto et al., 2018) on different gait patten. There is a strong correlation between ambulation time and the foot force reaction during running and walking (Yamin et al., 2017). According to the above, there is a strong correlation between spatial, temporal and foot force reaction, affecting both the running and walking of humans.

This correlation can be represented by normalizing the spatial factor represented by gait cycle distance, temporal (ambulation time) and foot reaction force. According to the results obtained in this research, we normalised the three factors (gait cycle, ambulation time and foot force reaction) as follows in equation (3.6):

$$(Gait\ cycle *Foot\ force\ reaction) / ambulation\ time)*100\%.....(3.6)$$

By subjecting the data obtained from the equation above to ANOVA statistics, we found significant values for human recognition. These significant values will be added to the previous factors to increase the accuracy of human identification identified in this research.

CHAPTER 4

4.1 Research results

In this chapter, we will discuss the results obtained from the experiments which we made on 23 subjects. Subject details were shown in Table 3.1. According to the research methodology described in Chapter 3, in this chapter we will classify the results into three main parts. The first part in Section 4.2 will be about the video camera calibrations and why we chose the Panasonic digital cameras to collect data, and the good and weak points for each camera considered. We will discuss camera specifications and show a distortion graph for each along with their weaknesses. Then we will move to Section 4.3 which is the photogrammetry part. This section represents the central part of the data collected as it has many items to discuss: knee to ankle distance, knee to front foot distance, knee to rear foot distance, knee angles and more will be described for the three postures of heell-down or first contact, mid-stance or full load and the toe-off. We will also consider the most significance factors used for human identification. The final part of this chapter, Section 4.4, will discuss the RSSCAN INTERNATIONAL foot pressure mat results. The data obtained will show the most positive factors used to identify the subjects, such as the foot force line value, foot pressure distance, and temporal and spatial statistics.

4.2 Video camera calibration

Camera calibration is always considered an essential factor for photogrammetric measurements, especially in high-accuracy close-range measurements (James et al., 2019). With the increasing use of off-the-shelf digital cameras for new 3D measurement applications, there are numerous circumstances where the image network calculation will not support robust recall for camera parameters during the calibration process.

As mentioned in the previous methodology chapter, the software used for calibration and photogrammetry is the iWitnessPRO V4.1. To realise maximum accuracy for 3D object feature measurements using photogrammetry, the camera or cameras employed must be calibrated. For optimal reliability and accuracy of measurement results, iWitnessPRO requires that accurate estimates of the camera's focal length (principal distance), lens distortion characteristics and other calibration coefficients are available. This calibration information can come from a prior full metric calibration of the camera, using either the full or semi-automatic processes. Alternatively, in certain

circumstances (and only in these circumstances) a calibration can be carried out as an integral component of the overall photogrammetric orientation process. The latter approach is termed self-calibration since it involves the determination of camera parameters at the same time that 3D object point coordinates are computed within the bundle adjustment.

It must be stressed that camera self-calibration can only be carried out successfully when the multi-image network exhibits certain characteristics. In the context of most accident reconstruction and forensic measurement applications, and close-range photogrammetric measurement in general, these conditions are as follows:

1. The network must display moderate to large convergence angles between different images
2. The network must have a sufficient number of points imaged in three or more images (the threshold is set at 12 points in iWitnessPRO)
3. There must be orthogonal roll angles within the network (i.e., images recorded in both 90° portrait and landscape orientations)
4. The object feature points should, if possible, be well distributed in three dimensions
5. The image point distribution should be such that it occupies a large amount of the format area of each image.

Figure 4.1 illustrates a network that will readily support self-calibration since it possesses all the attributes listed above.

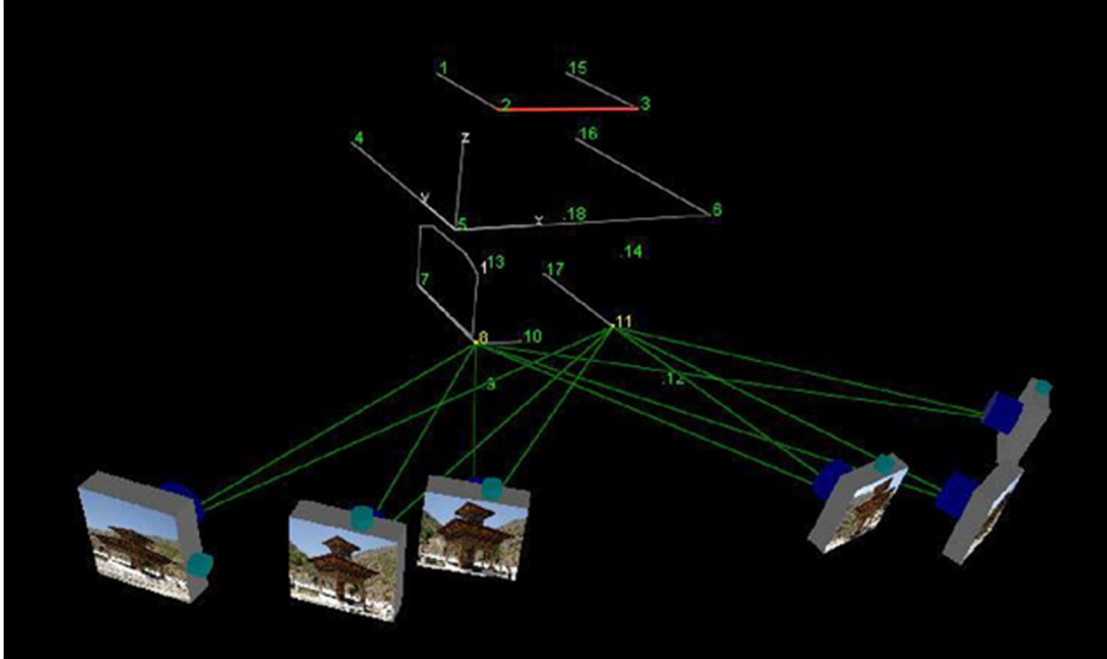


Figure 4.1: Camera calibration (Fraser, 2013)

iWitnessPRO will only perform the computation of camera self-calibration without first warning the operator when the network meets the following requirements:

1. Four or more images from each camera in the project
2. At least one image having a roll angle orthogonal ($\pm 90^\circ$) to that of the other photos
3. There are 12 or more object feature points referenced in each image
4. Angles of intersection between several imaging rays of $>30^\circ$.

These conditions are necessary, but it is noteworthy that they may not always be sufficient to guarantee a successful self-calibration. Care must be taken to make the network comply as closely as possible with the general requirements mentioned above. Through experience, the user will soon learn when self-calibration is feasible and when it is not.

4.2.1 Camera calibration parameters

As shown in Figures 4.2 (a) and (b) the Panasonic Lumix DMC-FZ300 parameters' dialogue box is generated when the calibration process ends successfully. This camera was used to collect the

subjects' photogrammetry data after testing three other cameras (discussed later in this chapter). The groups of camera parameters are as follows:

i- Sensor Specifics: This gives the horizontal (number of columns) and vertical (number of rows) resolution of the camera, along with the pixel size in each direction.

Note: iWitnessPRO assigns a default pixel size of 0.005mm if a size is not specified. Almost always, with modern consumer-grade cameras, the pixel will be square. Choosing the wrong pixel size introduces a scaling effect which is compensated by the computed focal length.

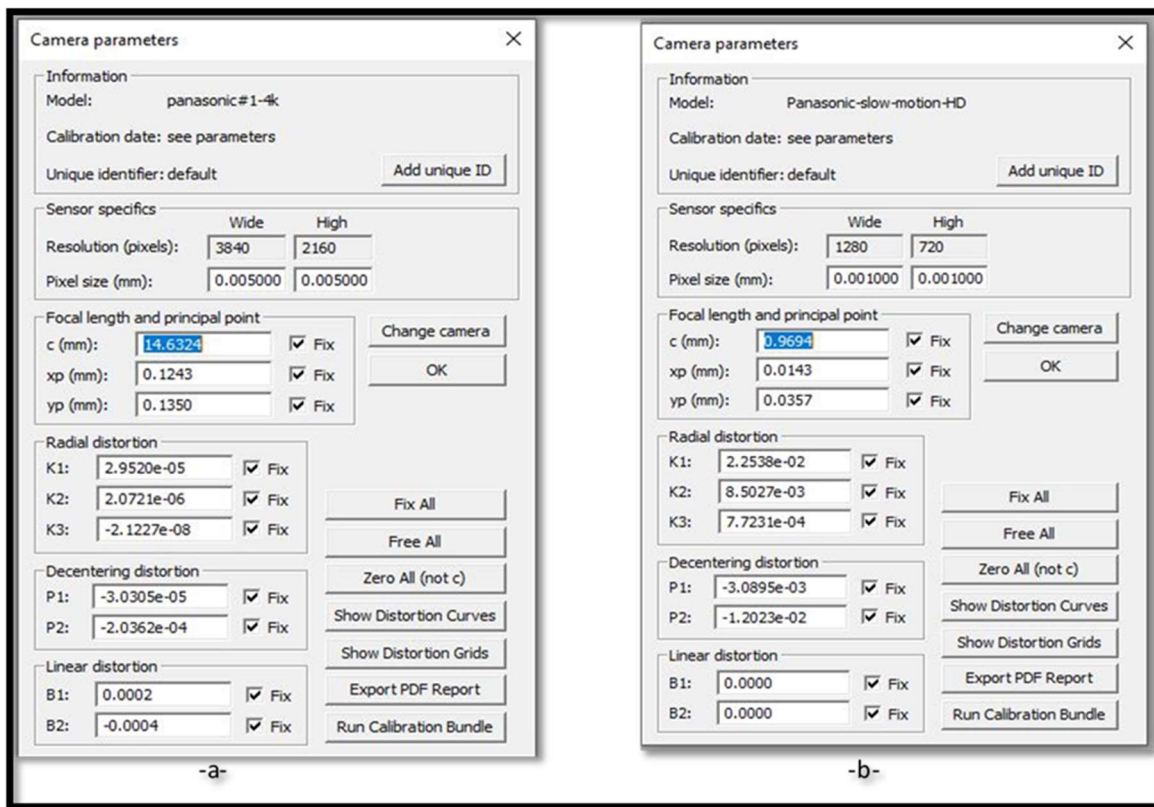


Figure 4.2: (a) and (b) Panasonic Lumix DMC-FZ300 parameters after successful calibration a- at 4K resolution (3840x2160) pixel, b- at low resolution (1280x720) pixel.

ii- Focal Length and Principal Point: This box lists both the focal length and the principal point offsets which indicate how far the optical axis of the lens is displaced from the center of the image format. The 'focal length' refers to the principal distance, which changes with focusing. The nominal lens focal length usually relates to infinity focus. Also, with zoom cameras, this focal length value can vary dramatically, but we seek only one value for the camera used in the survey. Therefore, it

is important not to change the zoom or focus during the photographic session. Generally, x_p and y_p are close to zero (e.g. 0.5mm or less).

iii- Radial Distortion: The three parameters, K_1 , K_2 and K_3 , describe the radial lens distortion of the camera lens. Radial distortion can reach significance levels in digital camera lenses and must be corrected when computing 3D feature point position to even modest accuracy levels. Radial distortion also varies with focusing which is a further reason not to alter focus or zoom within a measurement network.

iv- Decentering Distortion: The parameters, P_1 and P_2 , express the effect of the decentering of optical elements within the lens assembly. This error source is generally quite small and can typically be ignored in all but moderate-to-high accuracy applications.

v- Linear Distortion. The parameters, B_1 and B_2 , effectively model any relative error in the specified pixel size. They can generally be set 'fixed' to zero and ignored.

We started by opening the Camera Parameters Dialogue and set B_1 , B_2 , P_1 and P_2 to zero for this tutorial. These parameters may already have a zero value, with the Fix box being ticked, which locks the value to zero in any calibration. Otherwise, we enter 0.0 and, if necessary, we tick the Fix box for each of these four parameters. In the next section, we will discuss the results of the calibration of each of the four cameras to obtain the most accurate, sufficient, and low-cost camera.

4.2.2 Camera calibration data

4.2.2.1 *Spy camera calibration data results*

This type of camera is small, low resolution and low cost. It is called a Spy camera because of its small size and is ease to hide. Figure 4.3 shows the Parameters Dialogue box of this type of camera. From Figure 4.3 we notice the focal length of this camera is a small value (7.3277 mm) reflecting the low value of photo and video shooting which has a major effect on human identification and the accuracy of data extracted. Figure 4.4 shows the radial and decentering distortion of this camera. As mentioned in Section 3.3.1, we import the diagram again showing the radial and decentering distortion and the area of the distortion on this camera (Figure 4.4).

Camera parameters
✕

Information

Model: Small 4k#1

Calibration date: 02/04/2019 16:56pm

Unique identifier: default Add unique ID

Sensor specifics

	Wide	High
Resolution (pixels):	1920	1088
Pixel size (mm):	0.005000	0.005000

Focal length and principal point

c (mm):	7.3277	<input checked="" type="checkbox"/>	Fix		
xp (mm):	-0.1116	<input checked="" type="checkbox"/>	Fix		
yp (mm):	-0.0719	<input checked="" type="checkbox"/>	Fix		

Change camera
OK

Radial distortion

K1:	1.0277e-02	<input checked="" type="checkbox"/>	Fix		
K2:	1.8509e-04	<input checked="" type="checkbox"/>	Fix		
K3:	1.9526e-06	<input checked="" type="checkbox"/>	Fix		

Fix All
Free All
Zero All (not c)
Show Distortion Curves
Show Distortion Grids
Export PDF Report
Run Calibration Bundle

Decentering distortion

P1:	-3.1854e-04	<input checked="" type="checkbox"/>	Fix		
P2:	-4.0345e-04	<input checked="" type="checkbox"/>	Fix		

Linear distortion

B1:	0.0000	<input checked="" type="checkbox"/>	Fix		
B2:	0.0000	<input checked="" type="checkbox"/>	Fix		

Figure 4.3: Spy Camera parameters.

Table 4.1 below shows the calibration parameters and their values.

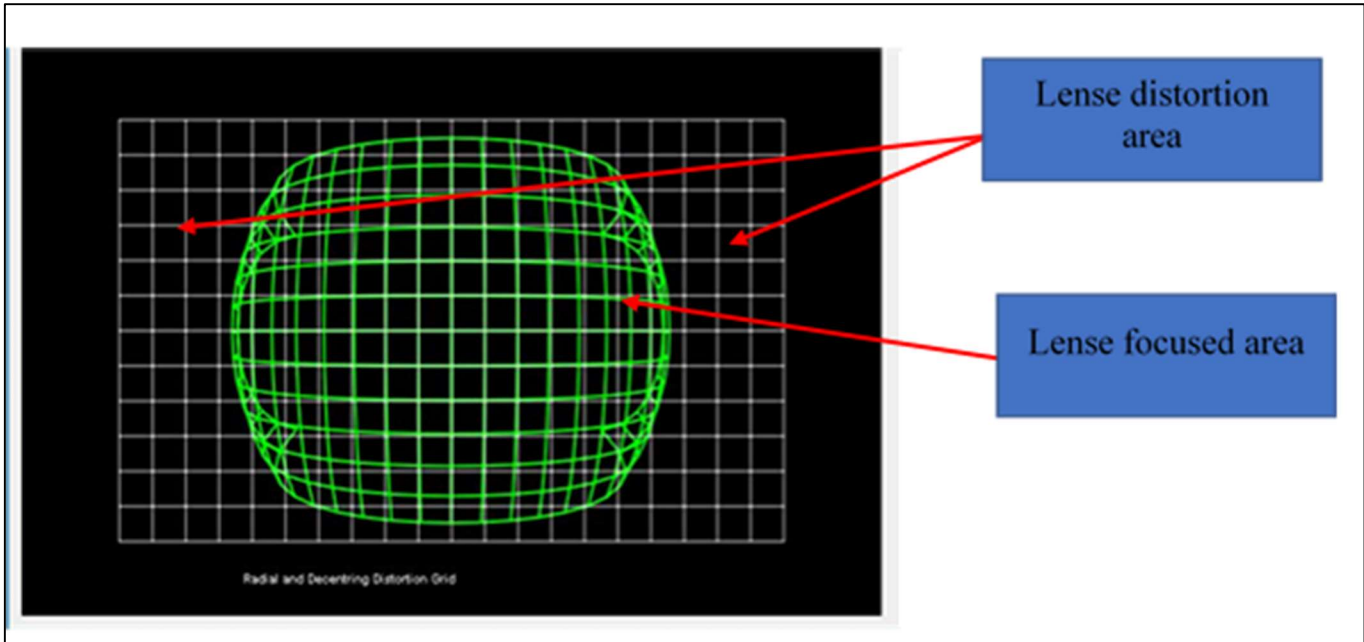


Figure 4.4: Radial and decentering distortion for Spy camera.

Table 4.1: Spy camera parameters

No.	Parameter name	Symbol	Value
1.	Principal distance	C	7.3277mm
2.	Principal point offset in x-image coordinate	Xp	-0.1116mm
3.	Principal point offset in y-image coordinate	Yp	-0.0719mm
4.	3rd-order term of radial distortion correction	K1	1.02768e-02
5.	5th-order term of radial distortion correction	K2	.85087e-04
6.	7th-order term of radial distortion correction	K3	1.95258e-06
7.	Coefficient of decentering distortion	P1	-3.1854e-04
8.	Coefficient of decentering distortion	P2	-4.0345e-04
9.	No significance differential scaling present	B1	0.0000e+00
10.	No significance non-orthogonality present	b	0.0000e+00

For 'balanced' principal distance c_b , radial distortion correction dr (microns) is given for any radial distance r (mm) as:

$$dr = K_0 \cdot r + K_1 \cdot r^3 + K_2 \cdot r^5 + K_3 \cdot r^7 \dots \dots \dots (4.1) \text{ (Lopez et al., 2019).}$$

Table 4.2: Spy camera radius with the corresponding radial distortion according to formula (4.1).

Radius (mm)	Radial distortion dr (microns)
0.00	0.0
0.50	-84.
1.00	-162.1
1.50	-226.3
2.00	-268.3
2.50	-277.9
3.00	-241.5
3.50	-141.5
4.00	45
4.50	351.6
5.00	817.2
5.50	1497.2

According to Figure 4.3 we can notice that the distortion of the lens starts after a 4mm radius (the red line). This value indicates the limitation of the lens distance for close-range photogrammetry. In conclusion, this camera will not be suitable for this research due to the high range of distortion. The analysis of these cameras addresses Objective 1 of this research which requires choice of the most accurate digital video camera available for use in this research.

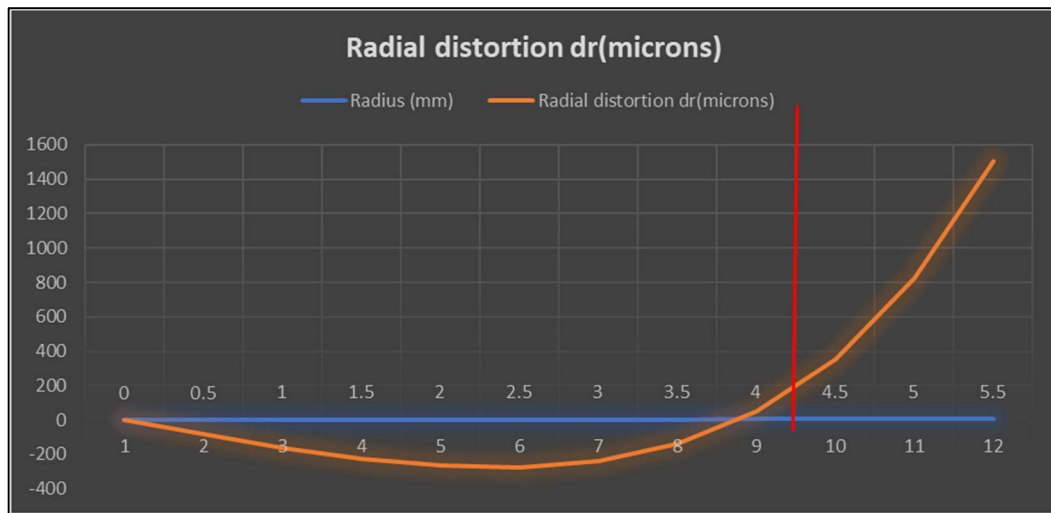


Figure 4.5 : Radial distortion curve for Spy camera.

4.2.2.2 JVC digital camera calibration data results

The second type of digital video camera used in this research is JVC GZ-HD260, specifications in Table 4.3.

Table 4.3: JVC GZ-HD260 video camera specification (<http://everio.jvc.com/>)

Internal storage media	120GB HDD	
Memory card slot	microSD/SDHC	
Image sensor	1/4" 3.32M CMOS (back-illuminated)	
Full HD 1920x1080 recording	●	
1080/60P output	●	
HDMI® (V.1.3 with x.v.Color™)	●	
24Mbps high bit rate recording	●	
Zoom ratios	Optical	30x
	Dynamic	
	Digital	200x

This camera has better specifications than the previous Spy camera. it has a larger value of focal length. Calibration parameters are shown in Figure 4.6 (a) and (b).

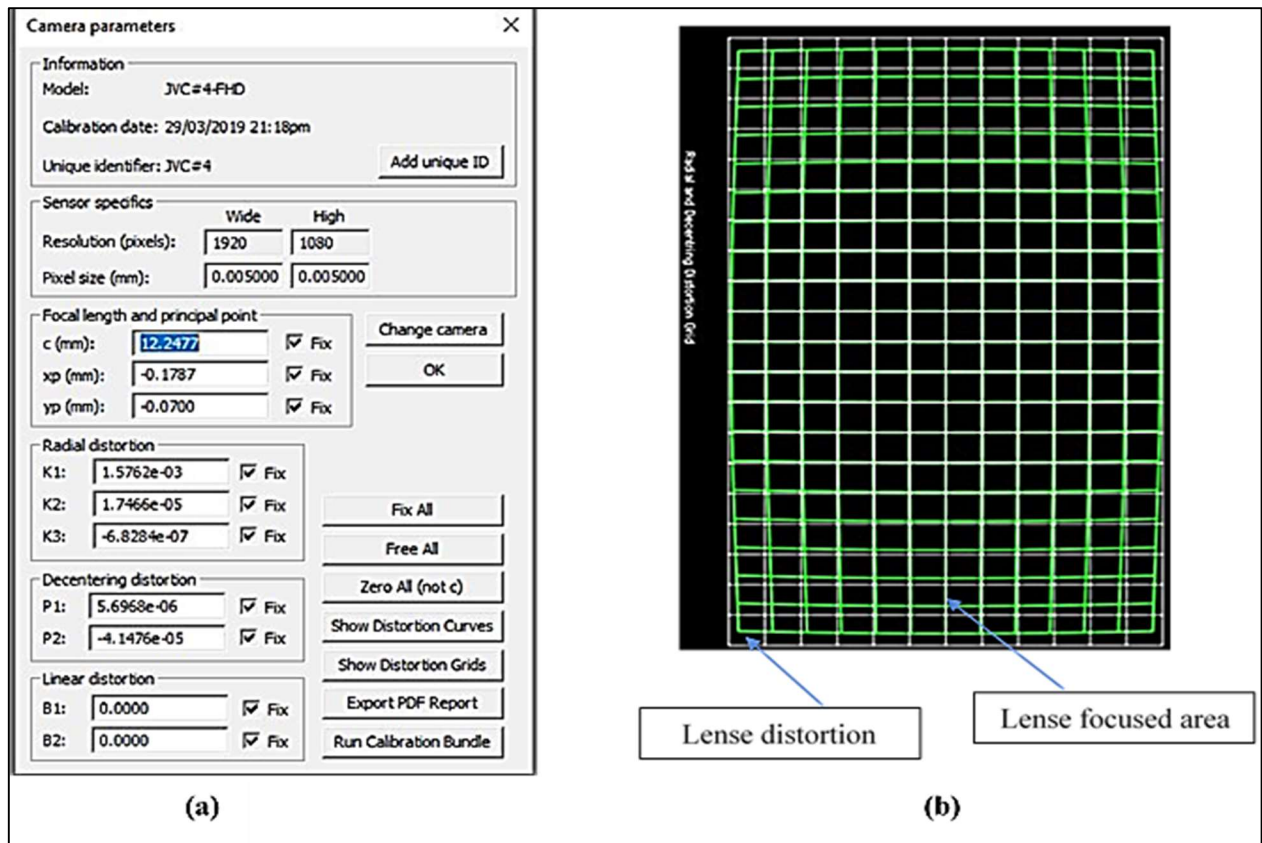


Figure 4.6: (a) Calibration parameters for JVC GZ-HD260 digital video camera as appears in iWitnessPRO, (b) Radial distortion grid for JVC GZ-HD260 digital video camera as appears in iWitnessPRO.

To check the value of this camera, we repeated the procedure and calculations used for the Spy camera in Section 4.3.2.1. Table 4.5 shows the calibration parameters of the JVC digital video camera.

Table 4.4: Calibration parameters for JVC GZ-HD260 digital video camera

No.	Parameter name	Symbol	Value
1.	Principal distance	C	12.2477mm
2.	Principal point offset in x-image coordinate	Xp	-0.1787mm
3.	Principal point offset in y-image coordinate	Yp	-0.0700mm
4.	3rd-order term of radial distortion correction	K1	1.57621e-03
5.	5th-order term of radial distortion correction	K2	1.74659e-05
6.	7th-order term of radial distortion correction	K3	-6.82840e-07
7.	Coefficient of decentering distortion	P1	5.6968e-06
8.	Coefficient of decentering distortion	P2	-4.1476e-05
9.	No significance differential scaling present	B1	0.0000e+00
10.	No significance non-orthogonality present	b	0.0000e+00

Using the formula (4.2), we can obtain the radial distortion factor dr in microns as in Table 4.6. For principal distance c , radial distortion correction dr (microns) is given for any radial distance r (mm) as: $dr = K1 \cdot r^3 + K2 \cdot r^5 + K3 \cdot r^7 \dots \dots \dots$ (4.2)

Table 4.5: Radial distortion correction parameter for JVC GZ-HD260 digital video camera

Radius (mm)	Radial distortion dr (microns)
0.00	0.0
0.50	0.2
1.00	1.6
1.50	5.4
2.00	13.1
2.50	25.9
3.00	45.3
3.50	72.4
4.00	107.6
4.50	150.3
5.00	198.3
5.50	246.2

From Figure 4.7, the red line indicates the maximum radial distance encountered in the calibration. This limit is above 5 mm which is higher than the Spy camera which indicates that this camera is suitable for testing the individuals. However, this camera has limited memory and cannot record for a long time. Also, the distortion grid shows an area of distortion which affects the accuracy of the measurements when we analyse the footage.

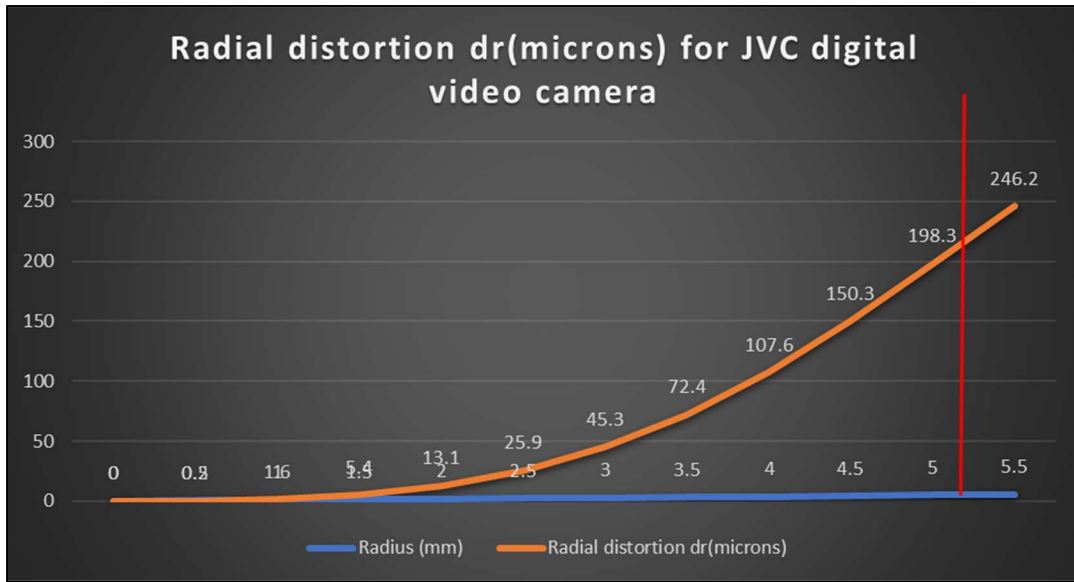


Figure 4.7: Radial distortion parameter plot for JVC GZ-HD260 digital video, redline after 5mm.

4.2.2.3 Calibration results of closed-circuit television (CCTV) camera

This is the most common type of camera used to record in public places. These analogue cameras use a digital video recorder to transfer and store footage on a hard disk. UNIDEN CCTV GDVR 10440 cameras were used in this research and its calibration parameters are shown in Figure 4.8 (a) and (b).

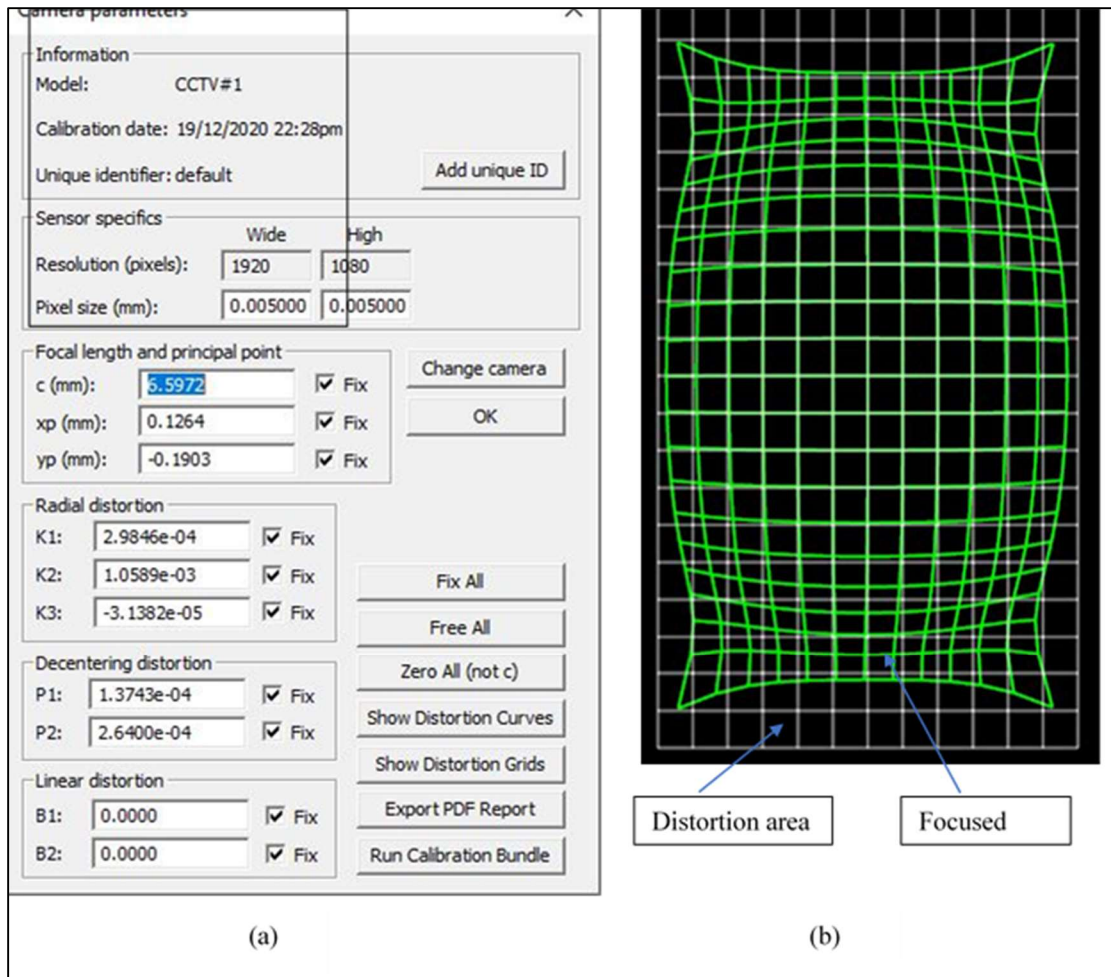


Figure 4.8: (a) UNIDEN cctv calibration parameters as resulted with iWitnessPRO, (b) UNIDEN cctv distortion grid.

For this camera, we can see the low value of focal length in Figure 4.8 (b). Also, the distortion grid (Figure 4.8 (b)) shows a high range of distortion (the black area). To calculate the distortion factor (dr), we used the same process as the previous cameras. Table 4.6 shows the parameters of radius and radial distortion factor (dr). For 'balanced' principal distance c_b , radial distortion correction dr (microns) is given for any radial distance r (mm) as:

$$dr = K_0 \cdot r + K_1 \cdot r^3 + K_2 \cdot r^5 + K_3 \cdot r^7 \dots \dots \dots (4.3).$$

Table 4.6: Radial distortion correction parameter for UNIDEN CCTV digital video camera.

Radius (mm)	Radial distortion dr (microns)
0.00	0.0
0.50	-66.4
1.00	-126.6
1.50	-174.4
2.00	-203.2
T3.00	-173.6
3.50	-98.3
4.00	30.6
4.50	225.1
5.00	498.7
5.50	867.4

From Table 4.6, we can obtain a plot showing the distortion range of the cameras as shown in Figure 4.9.

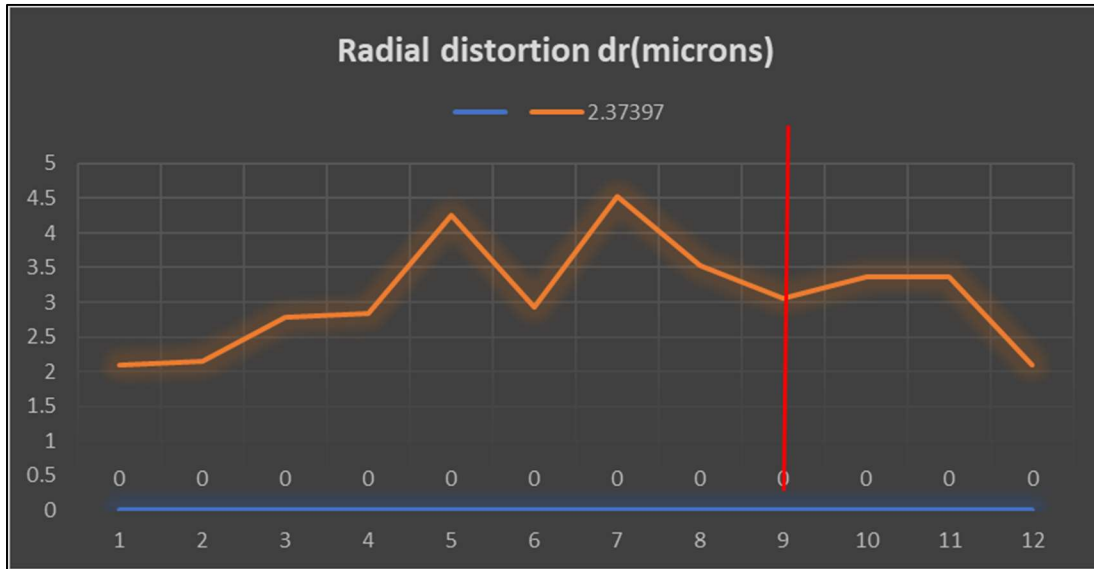


Figure 4.9: Radial distortion plot for UNIDEN CCTV cameras.

According to Figure 4.9, the red line indicates that the maximum radial distance encountered in the calibration is located at 4mm which indicates a high range of lens distortion and low resolution which has consequences for human identification using these types of cameras.

4.2.2.4 Calibration results of Panasonic Lumix DMC-FZ300 digital video camera

Data from this camera have been used to analyse subjects' photogrammetry data for human identification. The specifications of this camera is shown in Table 4.7.

Table 4.7: Specifications of Panasonic Lumix DMC-FZ300 digital camera used to collect subjects' data

Specification	Dimensions
Focal length (equiv.)	25–600 mm
Max resolution	4000 x 3000
Effective pixels	12 megapixels
Videography resolutions	3840 x 2160 (30p, 24p), 1920 x 1080 (60p, 60i, 30p, 24p), 1280 x 720 (30p), 640 x 480 (30p)
Storage types	SD/SDHC/SDXC card

This camera has a high value of focal length (25-600) mm as shown in Table 4.8. It can record a 4K video streaming which means a video with resolution (4000x3000) pixel/cm². These cameras have limited battery power and limited memory size. We can solve this by connecting a high capacity external hard drive such as 4 terabytes (4TB) with a direct connection to a power source. The calibration parameters for the Panasonic cameras were obtained from iWitnessPRO and after successful calibration are shown in Figure 4.10. Figure 4.9 indicates the calibration parameters for the highest resolution (4000x3000) p/cm². This resolution allows a successful calibration with high resolution and low lens distortion as shown in Figure 4.11.

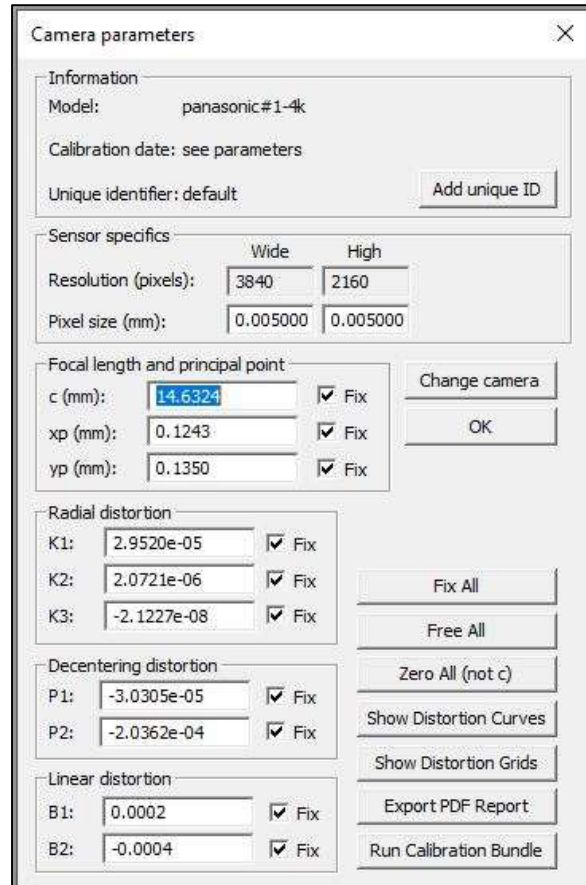


Figure 4.10: Panasonic calibration parameters.

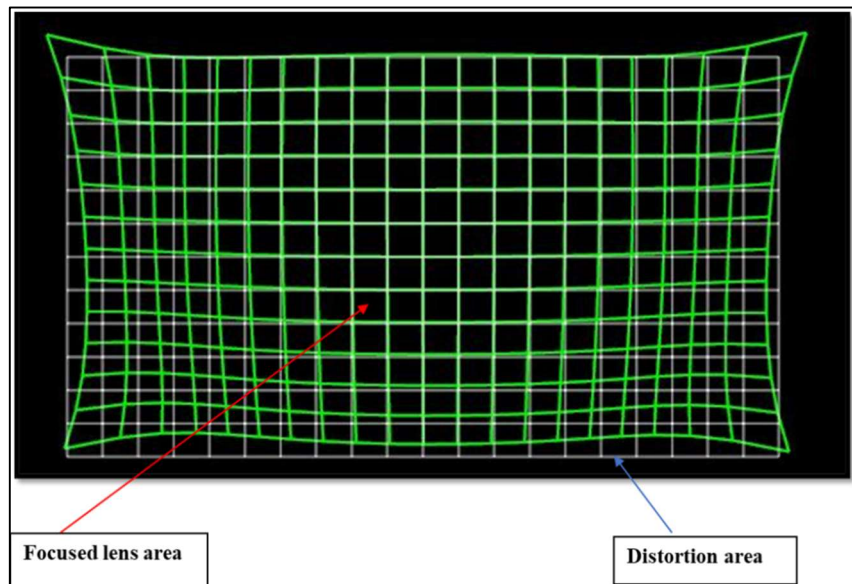


Figure 4.11: Radial distortion grid for Panasonic Lumix DMC-FZ300 after calibration using iWitnessPRO.

Calculation of radial distortion factor (rd) according to equation 4.4 is shown in Table 4.8.

given for any radial distance r (mm) as:

$$dr = K0 \cdot r + K1 \cdot r^3 + K2 \cdot r^5 + K3 \cdot r^7 \dots \dots \dots (4.4)$$

Table 4.8: Radial correction parameters calculated using equation 4.4 for the Panasonic digital camera

Radius (mm)	Radial distortion dr (microns)
0.00	0.0
0.50	-3.7
1.00	-7.4
1.50	-10.6
2.00	-12.5
2.50	-12.3
3.00	-9.1
3.50	-3.6
4.00	0.8
4.50	-5.3
5.00	-39.6
5.50	-133.6

The distortion limit is the highest in this camera which indicates the low value of the distortion, see Figure 4.12. From all of the above, we could choose the Panasonic video camera because it has the lowest lens distortion, high resolution, and less blurry picture with dynamic video streaming. This addresses Objective 1 in this research.

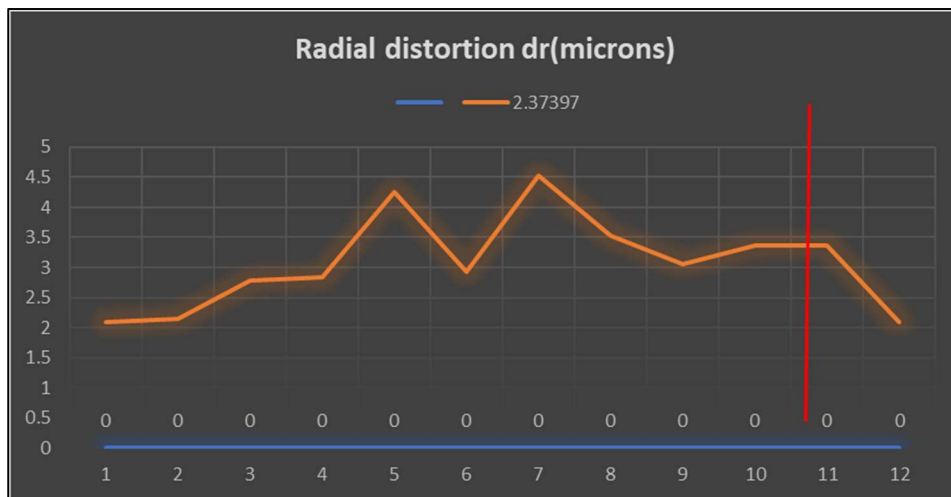


Figure 4.12: Radial distortion plot for Panasonic DMC-FZ300 video camera.

4.3 Photogrammetry results

In this part, we discuss the data obtained from the 23 subjects. We discuss the results obtained from each parameter as shown in Table 3.2. The photogrammetry measures were applied to 23 subjects; each was tested 10 times, so we will show 230 results. The entire results are shown in the appendix of this thesis. We show results for the average of the 10 results of each subject.

The statistical analysis used to obtain the similarities and differences between groups (between individuals) and within groups (same subjects with 10 trials) is the ANOVA calculation. The significance factor (p) value indicates whether there are similarities or differences (Yigit and Mendes, 2018). We put a standard value of 0.005 as a threshold value, if the (p) value is less than the threshold, then the value is significance and there is a high difference between the group of subjects. When the (p) value is larger than 0.005 (threshold), that means the value is insignificance and the individuals have similarities with the measured factor. We can see the insignificance value for the within group (i.e between the trials of the same subjects).

Using iWitnessPRO, we identified the 3-D coordinates (x, y, z) of the target points that were virtually located on the lower limb of the subjects. If the digital video camera filming the subjects' gait was well-calibrated, a true scale model is obtained (Gong et al., 2020). In the next section, we will show the results for each parameter with the ANOVA analysis.

4.3.1 Calculation of photogrammetry three dimensions measurements at heel-down stage

In this part, 3-D measurements were applied at the heel-down posture. Five Panasonic DMC-Fz300 cameras recorded simultaneously. For 3D measurements, only two photos are needed to create 3-D model. For this stage, three factors were measured for the 23 subjects, knee-inner ankle joint distance, knee-outer ankle joint distance and knee angle. First, we will show the knee-inner ankle joint distance for the subjects and the ANOVA analysis for this data.

4.3.1.1 Knee-inner ankle joint 3D distance data with ANOVA analysis

The data obtained for this position used two cameras, Camera 1 and Camera 3 simultaneously. As shown in figure 4.12 .

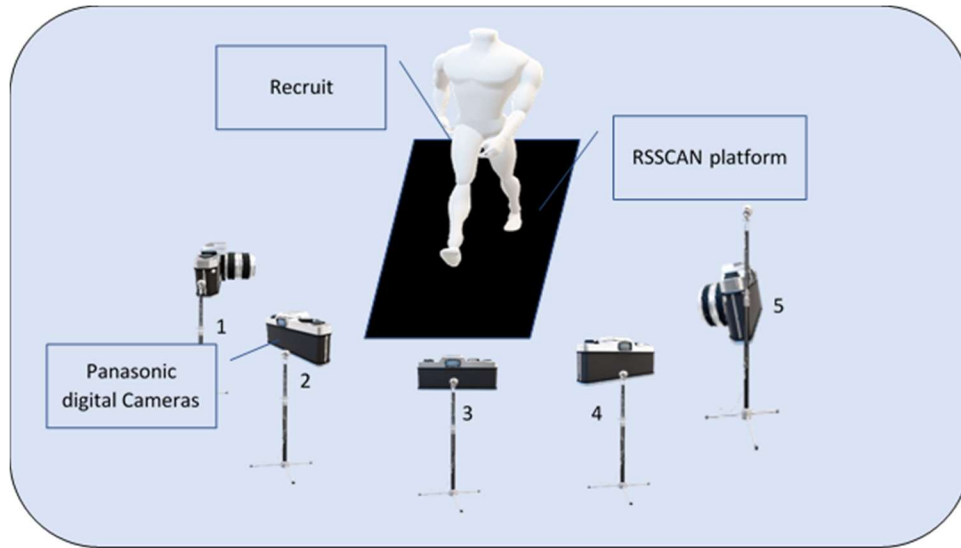


Figure 4.13 : 3-D modelling showing the distribution of Panasonic video cameras. Blue mat refers to RS scan foot pressure mat.

Table 4.9: ANOVA analysis knee-inner ankle joint distance (mm) with standard deviation at heel-down stage

Subjects	Number of trials	Mean (mm)	Std. deviation	Std. error	Minimum (mm)	Maximum (mm)
1.	10	453.7949	1.08532	.34321	452.59	455.87
2.	10	419.6545	.86091	.27224	418.78	420.96
3.	10	400.5754	.73664	.23295	399.16	401.34
4.	10	396.4811	.47801	.15116	395.88	396.97
5.	10	427.2943	.86091	.27224	426.42	428.60
6.	10	392.9907	.73000	.23085	391.52	393.70
7.	10	373.9626	.95136	.30085	372.98	375.16
8.	10	364.5796	.89852	.28414	363.16	365.34
9.	10	389.4462	.95136	.30085	388.25	390.43
10.	10	405.4765	.86091	.27224	404.60	406.79
11.	10	409.0781	.80531	.25466	407.88	410.06
12.	10	415.5143	.88696	.28048	414.43	416.60
13.	10	386.3974	1.03539	.32742	384.98	388.25
14.	10	441.7987	1.30485	.41263	439.51	443.86
15.	10	459.0235	1.30664	.41320	456.95	461.32
16.	10	430.5583	1.00293	.31715	429.69	431.87
17.	10	359.5694	1.15617	.36561	357.71	360.99
18.	10	414.1265	4.02355	1.21315	411.15	422.06
19.	10	378.7576	.89852	.28414	377.34	379.52
20.	10	383.7781	1.30664	.41320	381.70	386.07
21.	10	444.9546	.89112	.28180	443.86	446.05
22.	10	433.8325	.69026	.21828	432.96	435.14
23.	10	368.6178	.89112	.28180	367.53	369.71
Total	230	406.5660	28.43081	1.87061	357.71	461.32

Table 4.10 shows the mean and standard deviation for the inner ankle joint to the knee at initial contact for the twenty three subjects. It also shows the standard deviation for each subject with the minimum and maximum value of each test. The standard deviation shows how the minimum and

maximum values of a sample vary from the average. From Table 4.10, we can see the standard deviation varies from 0.2 to 1.3. This indicates that the photogrammetry measurements of the subjects for every 10 trials are close to each other. Table 4.10 shows the one-way ANOVA calculation with the factors described in Section 3.4.3. The value of the p factor shows there is a significance difference between the group of individuals with a value of 0.001 (~0) and that there is no significance within groups. This means, for the 10 trials of the same subject, the measurement value is almost the same. From the above, we can use this distance factor as one of the human identification factors. These calculations represent Objective 2 of this research.

Table 4.10: ANOVA analysis of Knee_inner_joint_Ankle_Heel_down_distance_(mm) showing the significance value

	Sum of squares	df	Mean square	F	Similarity Significance factor
Between groups	185568.235	22	8434.920	5109.862	0.001
Within groups	343.348	208	1.651		1.000
Total	185911.583	230			

Figure 4.14 shows the mean value of the knee-inner ankle joint value for every recruit with the standard deviation at each point. From this graph, we can see the difference of the recruit's values which refers to the significance of this factor.

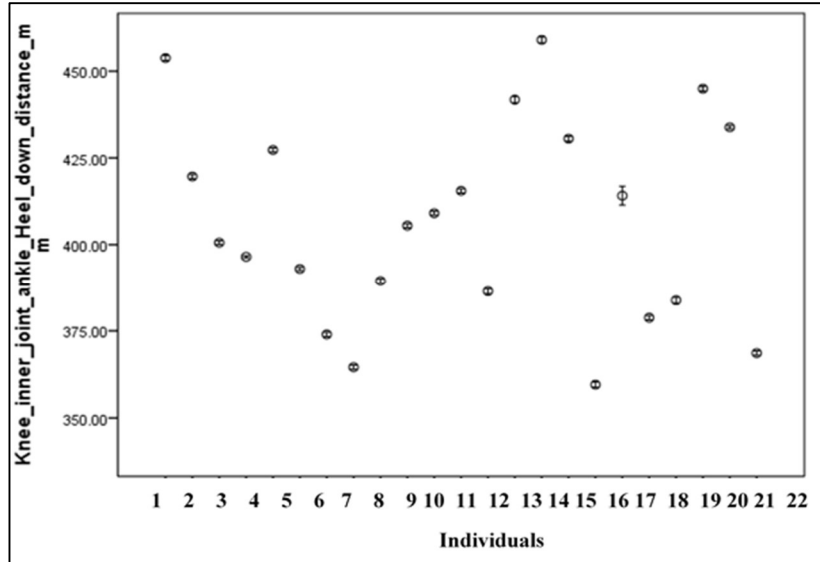


Figure 4.14: Knee-inner ankle joint 3D distance in (mm) at the heel-down stage.

4.3.1.2 Knee-outer ankle joint 3D distance data with ANOVA analysis

Using the same procedure as above, the 3D distance of the knee-outer ankle joint was calculated, see Figure 4.14 (a) and (b). From the result obtained, we see that the outer ankle joint distance to the knee is different from the inner ankle joint to the same knee. This indicates that there is a small 3D deviation of the knee.

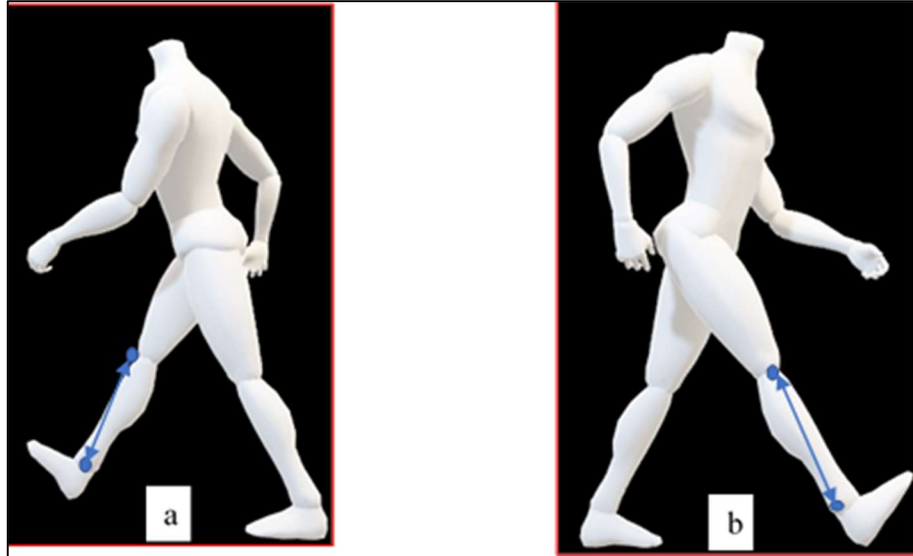


Figure 4.15: Measuring a 3D knee-ankle joint distance; (a) Knee-inner ankle joint, (b) Knee-outer ankle joint.

According to Govsa et al. (2020) the lower limb is unidentical while moving. This explains the difference between the 3D distances of the knee to the inner and outer joint ankle as shown in Figure 4.15. Table 4.11 shows the data from 23 subjects and 10 trials for every subject. Table 4.11 shows the ANOVA analysis for the knee-outer ankle joint. For this parameter, the significance of the similarity between individuals' measurements was very small, i.e. everyone's measurements were very different from the others. However, within groups the significance of similarity within individuals' measurements was very high, i.e. everyone's measurements are uniquely different compared to the others.

Table 4.11: ANOVA analysis knee-outer ankle joint distance (mm) with standard deviation at heel-down stage

Subjects	Number of trials	Mean (mm)	Std. deviation	Std. error	Minimum (mm)	Maximum (mm)
1.	10	455.9685	2.12137	.67084	453.26	459.29
2.	10	422.2005	1.86219	.58888	419.09	425.12
3.	10	413.9040	.94087	.29753	412.05	415.07
4.	10	353.9690	1.21819	.38523	352.23	356.21
5.	10	430.4674	2.52949	.79989	426.54	433.59
6.	10	366.2220	3.79601	1.20040	360.80	370.85
7.	10	326.7580	2.61996	.82850	322.38	330.34
8.	10	402.7035	4.04921	1.28047	395.97	408.03
9.	10	370.5380	3.15345	.99721	366.16	376.11
10.	10	380.7865	2.73700	.86552	377.11	384.07
11.	10	345.1170	3.00381	.94989	340.70	349.74
12.	10	345.1170	3.00381	.94989	340.70	349.74
13.	10	370.9455	1.86219	.58888	366.83	372.86
14.	10	396.8745	2.93770	.92898	392.96	401.00
15.	10	409.1131	.69416	.21951	408.03	409.98
16.	10	392.6183	.91751	.29014	391.82	393.82
17.	10	321.0726	1.03308	.32669	319.41	322.34
18.	10	369.7915	3.59151	1.08288	367.14	376.87
19.	10	345.7213	.81800	.25868	344.43	346.42
20.	10	349.2622	.64204	.20303	348.07	350.06
21.	10	405.7476	.81127	.25655	404.75	406.74
22.	10	387.7782	.61677	.19504	387.00	388.95
23.	10	335.4688	.81127	.25655	334.48	336.46
Total	231	378.1439	34.77043	2.28773	319.41	459.29

Table 4.12 below shows the ANOVA analysis of the outer ankle joint to knee distance. The similarity significance value is too small (0.001) between the group of subjects. This means this factor could help with suspect identification and we will add this parameter to the list of identification parameters shown in Table 3.2. However, within groups, this means that similarities for the subjects' trials is very high (1.000), indicating that the subjects had no similarity for this parameter.

Table 4.12: ANOVA analysis of Knee_outer_joint_ankle_at Heel_down_distance_(mm) showing the significance value

	Sum of squares	df	Mean square	F	Similarity Significance factor
Between groups	276972.598	22	12589.664	2395.024	0.001
Within groups	1093.371	208	5.257		1.000
Total	278065.969	230			

Figure 4.16 indicates the averages values of knee-outer ankle joint 3-D distance in (mm) at the heel-down stage for the 23 subjects. Each point on the graph shows the standard deviation for each measurement. For the heel-down phase, Figure 4.17 shows the variation of inner and outer ankle joints to knee distances for the 23 subjects. There is a slight difference between the two values. These differences are shown in the figure which is the outer ankle joint-knee distance larger than the inner joint distance. On the other hand, some subjects have an inner joint measurement to the knee less than the outer measure.

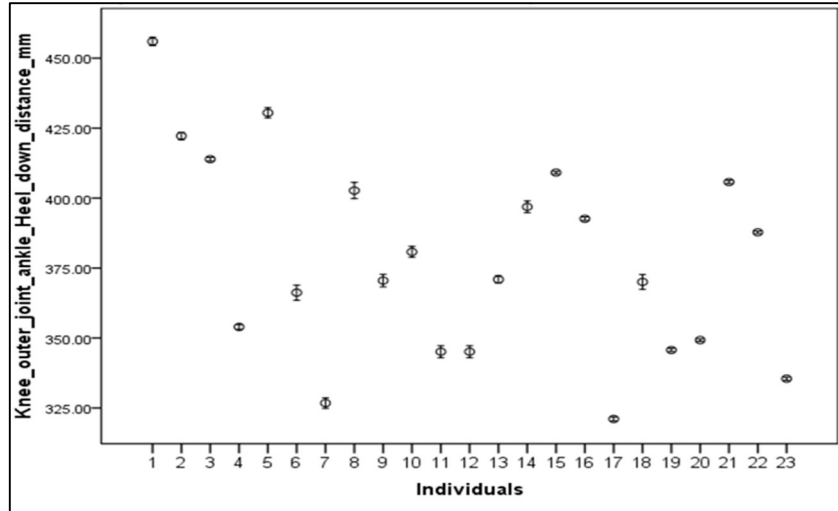


Figure 4.16: Knee-outer ankle joint 3D distance in(mm) at the heel-down stage.

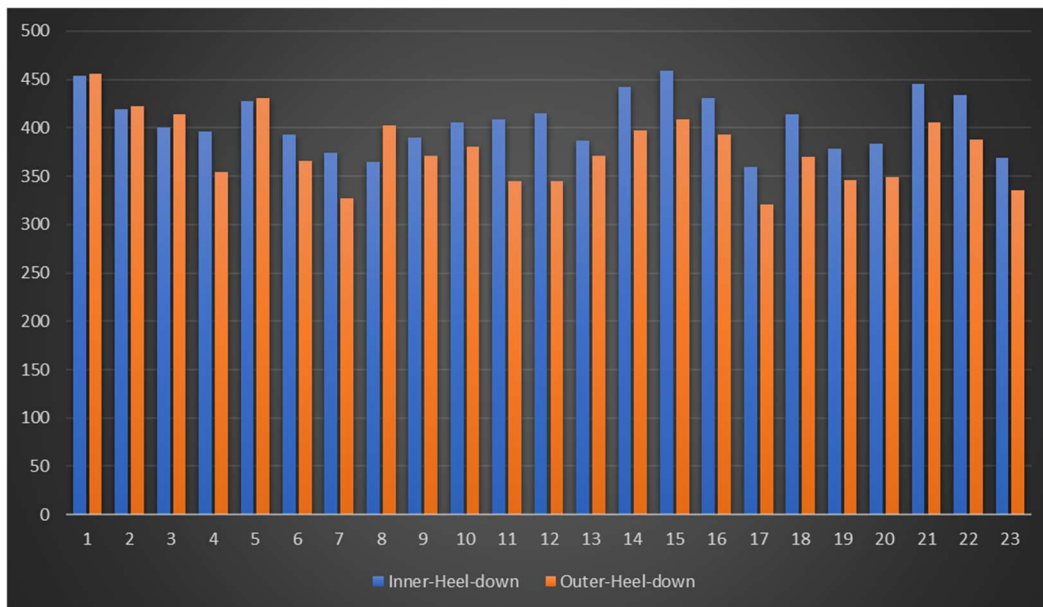


Figure 4.5: Knee-inner and outer joint ankle at heel down stage.

4.3.2 Calculation of 3-D photogrammetry measurements at mid-stance phase

The measurements used in this stage are more reliable as the walking speed is more stable (Yang et al., 2014a). The photos captured for each subject's gait at this stage was less blurry than the other captured moving photos because the foot is stable. The RSSCAN foot scan mat used in this research

has a length of 2 m as shown in the device specification in Chapter 3. Subjects can walk three steps on this mat and some can walk four steps. Data was extracted and analysed for the right second step as the second step is more stable (Govsa et al., 2020). In this part, each of the 23 subjects walked 10 trials.

We analysed 25 parameters to find the most significance factors that could be used in human identification. We isolated the factors that had a low value of similarities significance (less than the threshold value of 0.005). These factors are shown in the Figure 4.18. The significance photogrammetry parameters for the mid-stance were the same as the heel-down parameters as well as the knee angle, the front foot-knee distance and rear foot distance.

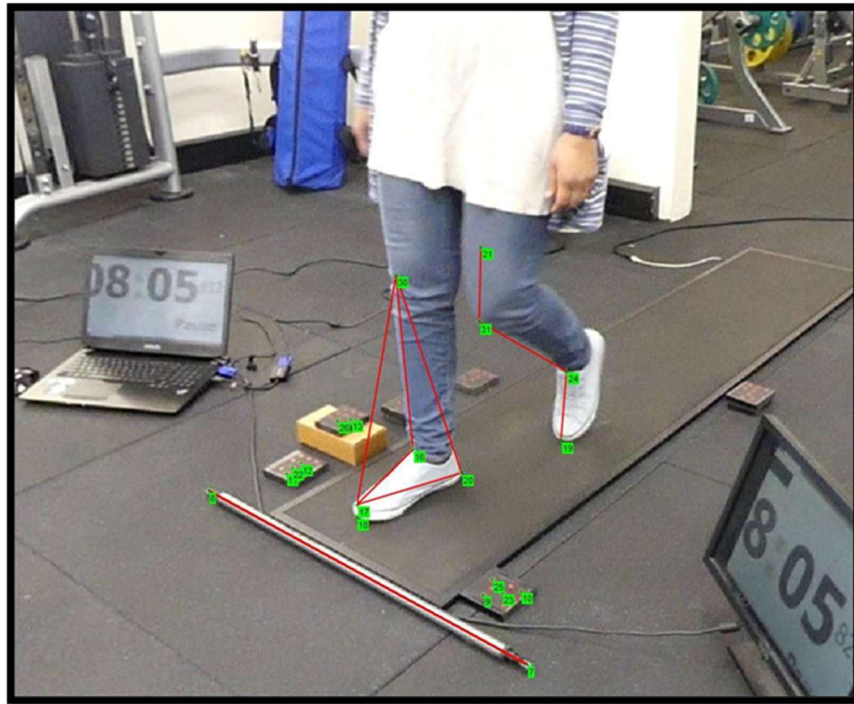


Figure 4.6: 3-D distance parameters at mid-stance stage.

4.3.2.1 Calculation of knee-inner ankle joint 3-D dimensions distance parameter at midstance stage

Results extracted for this parameter show a very low similarity significance factor using the ANOVA calculation. After testing the 23 subjects with 20 trials for each subject. Ten trials started with the right foot and the second ten trials started with the left foot. Table 4.14 shows the ANOVA

calculation for the 10 trials starting with the left foot. The measurements were applied for the mid-stance of the second step which is the right foot. The second step is more stable than the first (Govsa et al., 2020). We can see the low values of the standard deviation. Table 4.13 show the significance factor of similarity for subjects in both cases between groups and within a group. The difference between the two groups was explained in Section 4.3.1.2.

Table 4.13: ANOVA analysis knee-inner ankle joint distance (mm) with standard deviation at mid-stance stage

Subjects	Number of trials	Mean	Std. deviation	Std. error	Minimum	Maximum
1.	10	444.8941	1.06324	.33623	443.72	446.93
2.	10	411.4282	.84340	.26671	410.57	412.71
3.	10	392.7172	.72165	.22821	391.33	393.47
4.	10	388.7077	.46809	.14802	388.12	389.19
5.	10	418.9126	.84340	.26671	418.06	420.20
6.	10	385.2862	.71502	.22611	383.84	385.98
7.	10	366.6287	.93619	.29605	365.67	367.80
8.	10	357.4336	.88024	.27836	356.04	358.18
9.	10	381.8113	.93619	.29605	380.64	382.77
10.	10	397.5286	.84340	.26671	396.67	398.81
11.	10	401.0569	.78893	.24948	399.88	402.02
12.	10	407.3652	.87300	.27607	406.30	408.43
13.	10	378.8176	1.01433	.32076	377.43	380.64
14.	10	433.1329	1.28007	.40479	430.89	435.16
15.	10	450.0263	1.28007	.40479	447.99	452.27
16.	10	422.1202	.98253	.31070	421.26	423.40
17.	10	352.5152	1.13266	.35818	350.70	353.91
18.	10	406.0044	3.94565	1.18966	403.09	413.78
19.	10	371.3332	.88024	.27836	369.94	372.08
20.	10	376.2515	1.28007	.40479	374.22	378.50
21.	10	436.2336	.87300	.27607	435.16	437.30
22.	10	425.3278	.67622	.21384	424.47	426.61
23.	10	361.3896	.87300	.27607	360.32	362.46
Total	231	398.5941	27.87379	1.83396	350.70	452.27

According to Table 4.14, the similarity significance factor between groups is 0.001. This means that, for the 23 subjects, the average value of the knee-inner ankle joint 3-D measurements is different from each subject of the subjects group. If the value is 0.001 this means there is a small overlap in the standard deviation (which can be neglected).

Table 4.14: ANOVA calculation for Knee to Inner-Joint_Ankle_Mid-stance

	Sum of squares	df	Mean square	F	Similarity Significance factor
Between groups	178367.957	22	8107.634	5109.106	0.001
Within groups	330.075	208	1.587		1.000
Total	178698.032	230			

Figure 4.19 below shows the standard deviation of the average value for this parameter. We can see the small value of the standard deviations and no overlaps between each other.

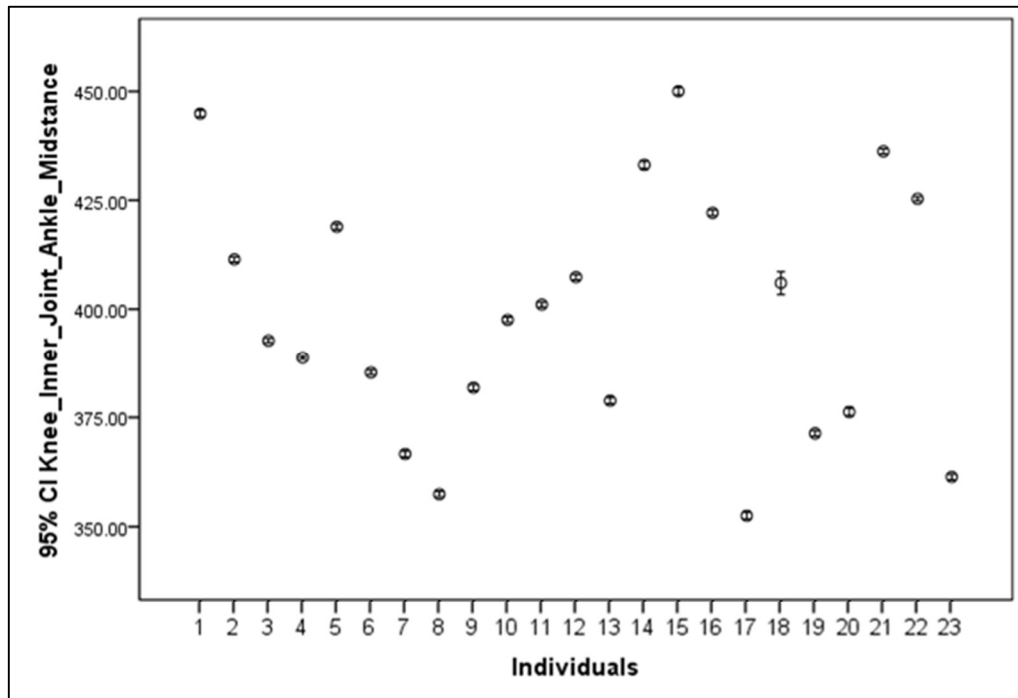


Figure 4.7: Scatter plot of knee-inner ankle joint mean distance (mm) with standard deviation at mid-stance stage.

4.3.2.2 Calculation of knee-outer ankle joint 3-D distance parameter at mid-stance stage

Another vital parameter that could be used in human identification is the knee to outer ankle joint 3-D measurements. Table 4.16 shows the mean value of the 3-D measurements of these parameters. Table 4.15 gives the ANOVA analysis knee-outer ankle joint distance (mm) with standard deviation at Midstance stage.

Table 4.15: The mean value of the 3-D measurements of knee-outer ankle joint parameters

Subjects	Number of trials	Mean	Std. deviation	Std. error	Minimum	Maximum
1.	10	447.1000	1.28668	.40689	445.00	449.00
2.	10	408.7000	1.94651	.61554	405.00	411.00
3.	10	381.4000	.84327	.26667	380.00	383.00
4.	10	384.6000	1.07497	.33993	383.00	387.00
5.	10	417.4000	.96609	.30551	416.00	419.00
6.	10	374.2000	1.87380	.59255	371.00	376.00
7.	10	350.1000	1.37032	.43333	348.00	352.00
8.	10	344.4000	1.26491	.40000	342.00	346.00
9.	10	376.8000	1.13529	.35901	375.00	378.00
10.	10	394.9000	1.59513	.50442	393.00	398.00
11.	10	394.5000	1.17851	.37268	392.00	396.00
12.	10	414.2000	.78881	.24944	413.00	415.00
13.	10	367.9000	1.19722	.37859	366.00	370.00
14.	10	428.8046	1.26647	.40049	426.58	430.81
15.	10	445.5228	1.26821	.40104	443.51	447.75
16.	10	426.7593	.99408	.31436	425.89	428.06
17.	10	348.9938	1.12217	.35486	347.19	350.37
18.	10	402.2350	3.99079	1.26200	399.06	409.64
19.	10	375.7870	.89147	.28191	374.38	376.54
20.	10	380.3918	1.29512	.40955	378.34	382.66
21.	10	441.0285	.88326	.27931	439.95	442.11
22.	10	421.4981	.67064	.21207	420.65	422.77
23.	10	364.6425	.88151	.27876	363.56	365.72
Total	230	395.2984	30.55512	2.01474	342.00	449.00

The values of the standard deviation are higher than the last parameters shown in Table 4.15, but are still small according to the normal values. Also, according to Table 4.16, the ANOVA calculation shows the similarity significance factor to be very small (0.001) which indicates that this factor is useful in human identification.

Table 4.16: ANOVA Knee_outer_Joint_Ankle_Mid-stance

	Sum of squares	df	Mean square	F	Sig.
Between groups	213362.533	22	9698.297	4610.954	0.000
Within groups	435.387	207	2.103		1.000
Total	213797.919	229			

According to Figure 4.20, the standard deviation is small which means small variations of the average value of the knee-outer ankle joint 3-D distance parameter. The small variations of the standard deviations reduced the overlap values of the average of these parameters. This reduction leads to the similarity significance factor being small. This could help this parameter (knee-outer ankle joint measurement) to be a valuable factor for human identification or suspect from perpetrator recognition.

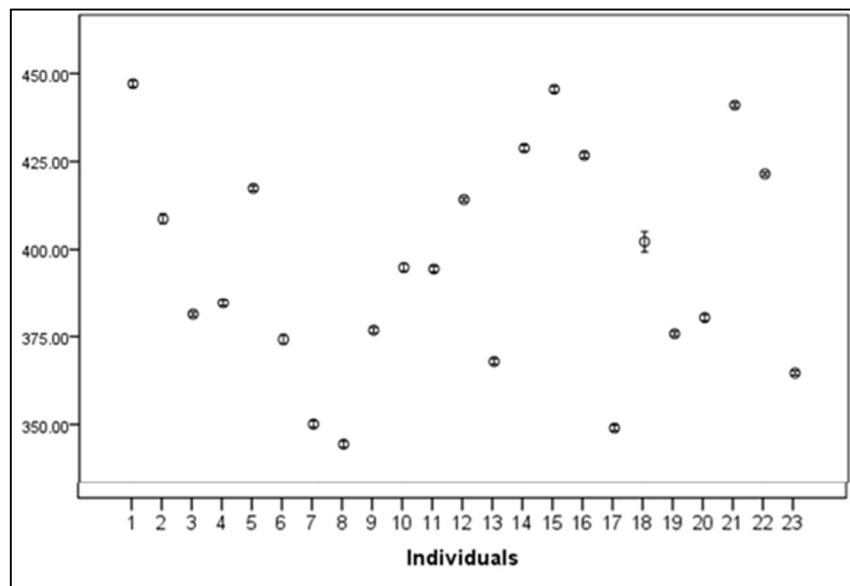


Figure 4.20: SPSS graph knee-outer ankle joint mean distance (mm) plot with standard deviation at mid-stance stage.

Figure 4.21 show the average 3-D distance measurements for the knee-inner and outer ankle joint at the mid-stance phase. The differences between the two factors indicate that there are non-identical measurements for the body during gait (Govsa et al., 2020). The outer ankle joint-knee distance measure is larger than the inner ankle joint-knee value for some subjects. On the other hand, for

some other subjects, the inner ankle joint-knee is less than the other value. This variation belongs to the variations of knee angle and ankle angle during gait.

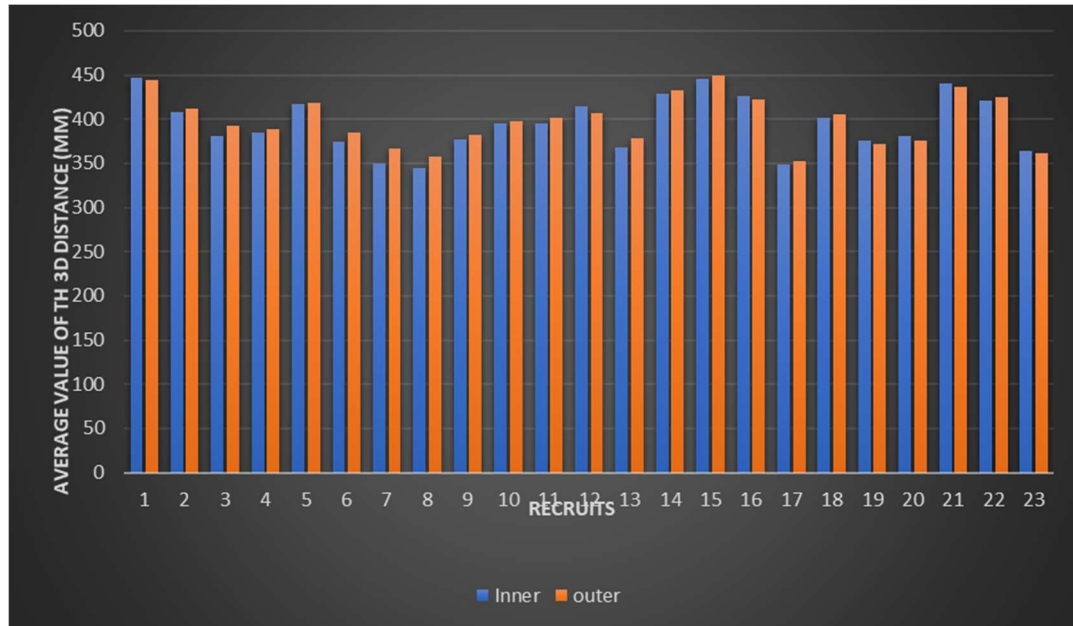


Figure 4.21: Knee to inner and outer ankle joint 3-D distance average parameters at mid-stance stage. On the x axis, “SUBJECTS” is sitting on the numbers

4.3.2.3 Calculation of knee-angle in 3-D measurements at mid-stance phase

There is another factor that helps with person identification is the knee angle using the mid-stance phase. The calculation of the three dimensions of knee kinematics varies between humans but it not difference between the right and left leg (Clément et al., 2018). This variation of the knee angle measurement has motivated researchers to use this factor in human identification (Favre et al., 2008). The calculation of knee angle in 3-D space using two vectors is on the thigh and shank segments (Favre et al., 2008; Hanley et al., 2018). The results obtained from the 23 subjects in this research are shown in Table 4.17 below. From the results in Tables 4.17 and 4.18, we can see that the 3-D knee angle could be used in human identification. From Table 4.18, we can see that the similarity significance value is too low between the subjects. However, this factor is too high when we calculate the same subjects for the ten trials.

This indicates that this factor could be used as an identification factor for suspects from perpetrators. Table 4.18 indicates that the similarity significance factor is the same as previous factors; that the (p) value from Table 4.18 is 0.001 between the group of subjects while this factor has a high value if we compare within same subjects. The standard deviation shown in Figure 4.22 is small in value indicating that the variation of data extracted from each recruit for the 10 trials is small. At the end of this factor analysis, we will move to another photogrammetry factor, the toe-off phase.

Table 4.17: 3-D knee angle at mid-stance phase with a standard deviation

Subjects	Number of trials	Mean(mm)	Std. deviation	Std. error	Min(mm)	Max(mm)
1.	10	56.1000	.73786	.23333	55.00	57.00
2.	10	35.1000	.73786	.23333	34.00	36.00
3.	10	52.8000	.63246	.20000	52.00	54.00
4.	10	27.6000	.51640	.16330	27.00	28.00
5.	10	36.5000	.52705	.16667	36.00	37.00
6.	10	47.5000	.52705	.16667	47.00	48.00
7.	10	41.9000	.87560	.27689	41.00	43.00
8.	10	44.3000	.67495	.21344	43.00	45.00
9.	10	46.8000	.78881	.24944	46.00	48.00
10.	10	38.1000	.73786	.23333	37.00	39.00
11.	10	54.1000	.87560	.27689	53.00	55.00
12.	10	31.1000	.73786	.23333	30.00	32.00
13.	10	59.7000	.67495	.21344	59.00	61.00
14.	10	42.8000	.78881	.24944	42.00	44.00
15.	10	62.2000	.78881	.24944	61.00	63.00
16.	10	54.8000	1.03280	.32660	53.00	56.00
17.	10	29.5000	1.08012	.34157	28.00	31.00
18.	10	58.0909	.70065	.21125	57.00	59.00
19.	10	40.1000	.73786	.23333	39.00	41.00
20.	10	62.3000	.82327	.26034	61.00	63.00
21.	10	42.0000	.94281	.29814	41.00	44.00
22.	10	57.8000	.78881	.24944	57.00	59.00
23.	10	45.2000	.78881	.24944	44.00	46.00
Total	231	46.4156	10.43450	.68654	27.00	63.00

Table 4.18: ANOVA analysis for 3-D knee angle at mid-stance phase

	Sum of squares	df	Mean square	F	Sig.
Between groups	24917.495	22	1132.613	1890.581	0.002
Within groups	124.609	208	.599		1.000
Total	25042.104	230			

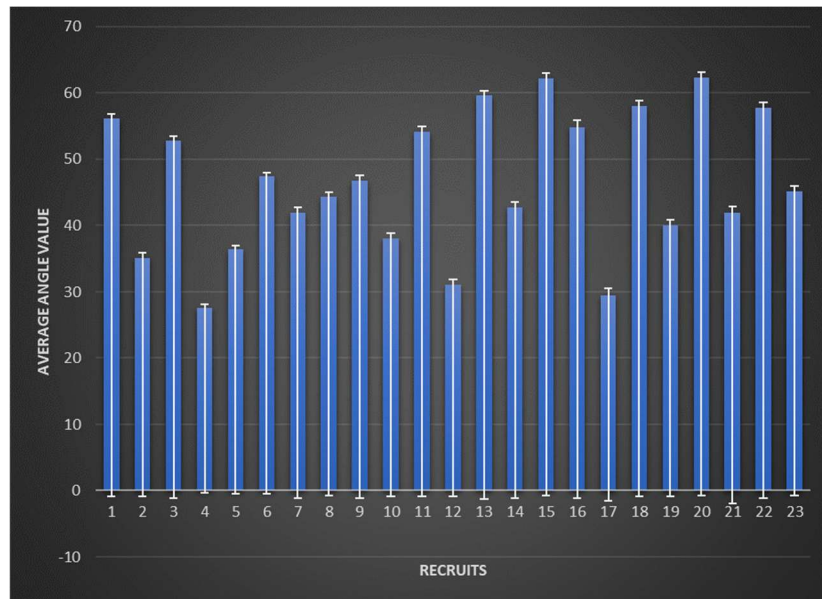


Figure 4.22: Analysis for 3-D knee angle at mid-stance phase. Average angle values showing the standard deviations.

4.3.3 Calculation of 3-D photogrammetry measurements at toe-off phase

In this section, we will describe the two 3-D distances of this stage (knee-inner ankle joint) and (knee-outer ankle joint) in one paragraph. Tables 4.20 and 4.21 show the average 3-D distances for these two factors. Tables 4.21 and 4.22 show the ANOVA analysis and the similarity significance value between the group of subjects and within the same recruit. According to Figure 4.23, There are variations in the two factors as shown in blue and orange. The two factors shown in Figure 4.23 indicate that some subjects have a larger distance from the knee-inner ankle joint than the outer ankle joint, while the other subjects have the opposite. These differences are because of the deviation of the knee and ankle during the toe-off phase. From Tables 4.19 and 4.20, the standard deviation of subjects is larger than its value at the mid-stance stage. This points to a variation in the

3-D distance measurements of the knee-inner and outer ankle joint for the subjects in each trial. The similarity significance factors data in Tables 4.21 and 4.22 show the 3D measure of the knee to interior ankle at the heel-down phase of gait while Table VI shows the group comparison for the trial. The overall standard deviation for the trial was $\pm 1.4\text{mm}$. The individual group comparison statistics at $P=0.05$ and DF of 207 as 1.000 while the between group result at DF of 22 was ≥ 0.001 . Figure 4.22 shows the scatter plot of the 3-D measurements. The figure shows that the measurement error of one individual (Subject 18) was notably larger and this was because this subject had 11 trials instead of 10 however, the value kept showing its unique location in the overall scatter plot. Again, the value of all 23 measurements of the randomly selected individual was unrelated spatially.

Table 4.19: ANOVA analysis knee-inner ankle joint distance (mm) with standard deviation at toe-off stage

Subjects	Number of trials	Mean	Std. deviation	Std. error	Minimum	Maximum
1-	10	509.7646	1.46459	.46314	507.37	511.93
2-	10	465.9838	2.21915	.70176	461.76	468.61
3-	10	431.2202	.91371	.28894	430.08	432.19
4-	10	438.5046	1.22804	.38834	436.68	441.25
5-	10	475.9026	1.09851	.34738	474.31	477.72
6-	10	426.6494	2.13558	.67533	423.00	428.70
7-	10	399.1702	1.56545	.49504	396.77	401.34
8-	10	392.6709	1.44268	.45621	389.94	394.50
9-	10	429.6130	1.29302	.40889	427.56	430.98
10-	10	450.2478	1.81986	.57549	448.08	453.78
11-	10	449.7931	1.34369	.42491	446.95	451.51
12-	10	472.2525	.90114	.28496	470.88	473.17
13-	9	419.4524	1.44502	.48167	417.30	421.86
14-	10	488.9091	1.44422	.45670	486.37	491.19
15-	10	507.1226	1.27403	.40288	505.12	509.30
16-	10	486.5784	1.13755	.35972	485.59	488.06
17-	10	397.9091	1.28139	.40521	395.85	399.48
18-	11	458.2816	4.45052	1.34188	454.99	467.05
19-	10	428.4560	1.01427	.32074	426.85	429.32
20-	10	433.7088	1.47497	.46643	431.37	436.30
21-	10	502.8464	1.00592	.31810	501.61	504.08
22-	10	480.5741	.76502	.24192	479.61	482.03
23-	10	415.7440	1.00592	.31810	414.51	416.98
Total	230	450.6625	34.79877	2.29456	389.94	511.93

Table 4.20: ANOVA analysis knee-outer ankle joint distance (mm) with standard deviation at toe-off stage.

Subjects	Number of trials	Mean	Std. deviation	Std. error	Minimum(mm)	Maximum(mm)
1-	10	510.2315	2.37397	.75071	507.20	513.95
2-	10	472.4463	2.08389	.65898	468.96	475.71
3-	10	461.1992	2.14968	.67979	457.72	464.46
4-	10	394.5919	2.78802	.88165	389.69	398.60
5-	10	481.6937	2.83231	.89565	477.30	485.19
6-	10	409.8058	4.24833	1.34344	403.74	414.98
7-	10	365.6444	2.93183	.92713	360.74	369.65
8-	10	450.6269	4.53213	1.43318	443.09	456.59
9-	10	414.6343	3.52918	1.11603	409.73	420.87
10-	10	426.1029	3.06214	.96833	421.99	429.77
11-	10	386.1882	3.36052	1.06269	381.24	391.36
12-	10	386.1882	3.36052	1.06269	381.24	391.36
13-	10	415.0919	2.08423	.65909	410.48	417.23
14-	10	444.1054	3.28655	1.03930	439.72	448.72
15-	10	458.6557	1.30646	.41314	456.59	460.95
16-	10	439.3418	1.02829	.32517	438.45	440.68
17-	10	359.2807	1.15713	.36592	357.42	360.70
18-	10	414.0971	4.10594	1.29841	410.83	421.72
19-	10	386.8629	.91732	.29008	385.42	387.64
20-	10	391.6064	1.33045	.42072	389.49	393.94
21-	10	454.0309	.90910	.28748	452.92	455.14
22-	10	433.9225	.68885	.21783	433.05	435.24
23-	10	375.3909	.90452	.28604	374.28	376.50
Total	230	423.1191	38.95723	2.56876	357.42	513.95

Table 4.21: ANOVA analysis for the Knee_Inner_Joint_Ankle at Toe-off_stage

	Sum of squares	df	Mean square	Similarity significance factor
Between groups	276735.813	22	12578.901	0.001
Within groups	572.720	207	2.767	1.000
Total	277308.534	229		

Table 4.22: ANOVA analysis for the Knee_outer_Joint_Ankle at Toe-off_stage

	Sum of squares	df	Mean square	Similarity significance factor
Between groups	346079.919	22	15730.905	0.001
Within groups	1465.512	207	7.080	1.000
Total	347545.430	229		

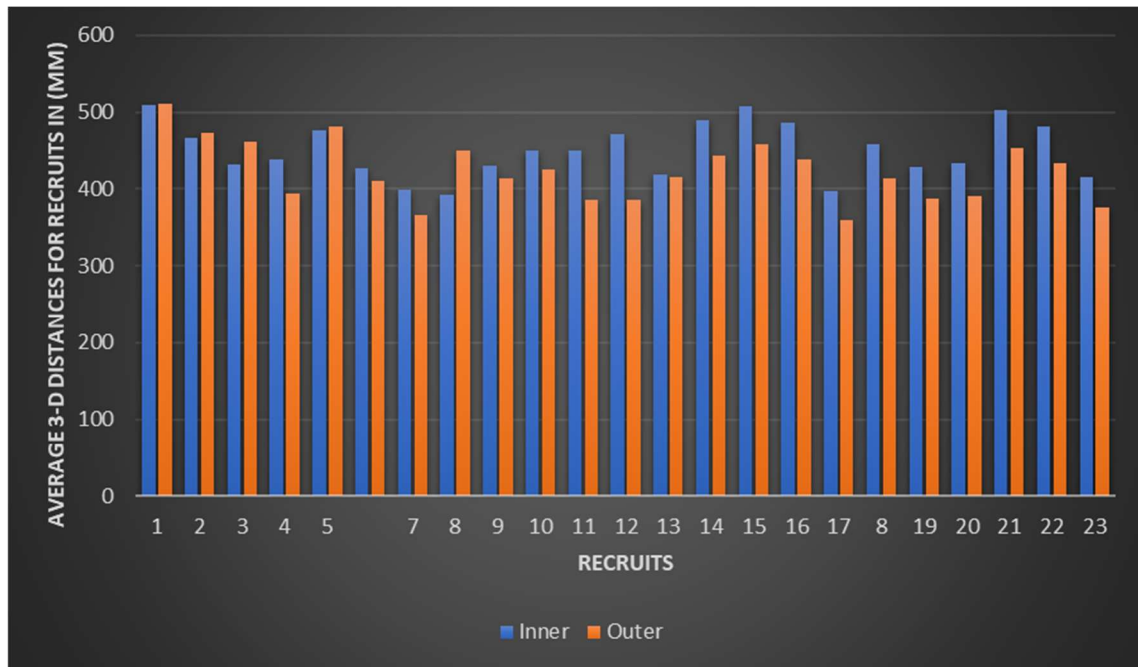


Figure 4.23: Variation of two factor distances (knee-inner and outer ankle joint).

4.4 Data results and analysis of the footprint using RSSCAN International platform

In this section, we will describe the data collected for the 23 subjects during their walking trials on the RSSCAN platform as discussed in Section 3.5. The data collected using this technique is synchronised with the photogrammetry technique used in this research. In this part, five different identification parameters are extracted using Foot Scan version 7. Many parameters were tested for use as valid identification factors, but the similarity factor calculated using SPSS ANOVA analysis was very high. However, these five parameters were the most significance value that can be used in human identification. As mentioned in Section 3.5, the five identification parameters are:

- 1- Force (KN): This parameter is the sum of force in Kilo Newton for the foot from initial contact to the toe-off posture
- 2- Force distance (mm): The RSSCAN Platform recording data during gait. In each recorded frame, the coordinates of each frame are obtained by calculating the distance between each frame (point), we can calculate the total length
- 3- Temporal parameter (ms): Calculations of gait cycle time in (ms) for subjects with all trials
- 4- Spatial parameter (mm): Calculation of gait cycle length in (mm) for the subjects and normalised with ambulation time and total pressure of step for each individual
- 5- Total foot pressure data (N/m²): Calculation of the sum of foot pressure from initial contact to shoe-off for each subject and connected with ambulation time and gait cycle to obtain new results.

4.4.1 Calculating of the Ground Reaction Force (GRF) of a foot during walking

In this part, we calculate the Ground Reaction Force (GRF) of the subjects from initial contact (heel-down) to the final contact (toe-off) for the right step. The values are extracted in KN (Table 4.23).

Table 4.23: Calculating foot force of one recruit for one step, value shown for each frame.

Frame	ms	X	Y	Force (N)
1.	0	6.36	21.7	71
2.	7.94	4.37	22.33	140
3.	15.87	1.24	27.52	193
4.	23.81	-1.31	33.12	245
5.	31.74	-2.06	39.03	318
6.	39.68	-1.92	43.91	393
7.	47.61	-0.92	48.98	469
8.	55.55	0.52	54.79	530
9.	63.49	2.74	61.11	575
10.	71.42	4.92	67.51	611
11.	79.36	6.71	73.65	635
12.	87.29	7.84	79.33	657
13.	95.23	8.6	84.96	676
14.	103.16	8.9	89.42	699
15.	111.1	9.11	93.29	720
16.	119.04	9.16	96.61	743
17.	126.97	8.96	99.45	765
18.	134.91	8.66	101.89	782
19.	142.84	8.38	104.04	795
20.	150.78	8.14	105.66	805
21.	158.71	7.89	106.88	813
22.	161.65	7.56	107.45	819
23.	167.67	8.56	108.56	827
Sum				55514

The total force value shown in Table 4.24 is 55514 N (5.5 KN). This value represents the force at each frame starting from Frame 1 at heel-down and ends with Frame 90 at the toe-off stage. The number of frames vary for each recruit depending on the length of the foot. Table 4.24 shows the average value of the total foot force with the corresponding standard deviation (Std) and the standard error. The similarity factor shown in Table 4.25 is 0.001 between a group of subjects which indicates that this similarity factor is significance while being too high within the group of subjects.

Table 4.24: Indicates that this similarity factor is significance while s too high within the group of subjects.

Subjects	Number of trials	Mean(mm)	Std. deviation	Std. error	Minimum(mm)	Maximum(mm)
1.	10	70.96500	.676413	.213901	70.145	72.014
2.	10	65.63310	.045128	.014271	65.581	65.721
3.	10	38.50200	.041798	.013218	38.436	38.566
4.	10	66.63290	.027209	.008604	66.594	66.687
5.	10	51.33350	.025431	.008042	51.305	51.387
6.	10	60.61690	.013626	.004309	60.594	60.635
7.	10	58.55600	.457377	.144635	57.965	59.326
8.	10	22.02610	.019785	.006256	21.996	22.069
9.	10	61.55195	.404222	.127826	60.895	62.158
10.	10	68.55430	.028775	.009100	68.520	68.591
11.	10	53.12240	.020657	.006532	53.091	53.163
12.	10	46.58850	.018805	.005947	46.557	46.611
13.	10	32.48150	.037080	.011726	32.412	32.515
14.	10	56.28730	0.0152	0.148	54.368	56.147
15.	10	59.49910	.479611	.151666	58.654	60.254
16.	10	42.01120	.897703	.283879	40.489	42.954
17.	10	49.33370	.691551	.218688	47.654	49.874
18.	10	63.05416	.605899	.182685	62.354	63.959
19.	10	57.70970	.563515	.178199	57.145	58.654
20.	10	69.32120	.524024	.165711	68.354	69.851
21.	10	45.46010	.560000	.177088	44.214	46.354
22.	10	41.53260	.836025	.264374	40.012	42.365
23.	10	35.73064	.512328	.162012	35.031	36.684
Total	230	52.93547	12.842224	.844956	21.996	72.014

Table 4.25: ANOVA analysis for foot force_(KN)

	Sum of squares	df	Mean square	F	Similarity significance factor
Between groups	37801.174	22	1718.235	2727.100	0.001
Within groups	131.052	208	.630		1.000
Total	37932.226	230			

The low value of this similarity factor indicates that we can use this parameter for human identification. The 23 subjects were tested with their shoes on. We repeated the tests 10 times for each subject and the subjects wore the same shoes for each test. In a forensic case, if we want to check a perpetrator from a suspect and we want to use this parameter, the suspect will wear the same shoes as shown in the recording footage. After that, the foot force data will be extracted for comparison with the perpetrator. ANOVA analysis will show the similarity significance factor which will help to decide if a person is a perpetrator or not.

4.4.2 Calculation and analysis of foot force/pressure distance identification factor

This identification factor is correlated to the Foot force identification factor described in Section 4.4.2. In Table 4.26, each frame has a force value and two dimension coordinates (x,y). In this section, the calculation of the distance between frames shows that it is a significance factor to be used as one of the human identification factors. The methodology of this part was described in Section 3.5.2. The distances used in this factor are calculated using formula 4.5 below which is mentioned in Chapter 3.

$$D = \sqrt{(X_n - X_{n-1})^2 + (Y_n - Y_{n-1})^2} \dots \dots \dots (4.5)$$

Where (x,y) represent the two dimension coordinates of each foot force frame during gait and (n) is the number of frames per step. Back to Table 4.21 above, by applying equation 4.6 to the coordinates of the frame shown, the total distance is obtained. Table 4.26 shows the average foot force/pressure distance for the 10 trials for each of the 23 subjects. Standard deviation (Std) is calculated using SPSS statistics ANOVA analysis, as is the standard error. The calculated distances in Table 4.26 represent both foot force and foot pressure distance. In this case, force and pressure have the same distance. This

is according to equation 4.6 to described in the previous chapter and shown below:

$$P=F/A \dots\dots\dots (4.6)$$

where P is pressure, F is a force in Newton, and A is the area in mm².

According to this formula, foot-pressure distance is the same as foot force-distance because they have the same frame coordinates. The means distance in Table 4.28 varies for each recruit and they correlate with foot length. The low range of the standard deviations indicates low variations in measurement for each of the subjects. The low value of standard deviation gives a positive sign to use this factor as a human identification factor.

Table 4.26: Statistical analysis for the foot force-distance with standard deviations

Subjects	Number of trials	Mean distance (mm)	Std. deviation	Std. error	Minimum (mm)	Maximum (mm)
1.	10	320.6160	.64529	.20406	319.00	321.16
2.	10	309.1770	1.67392	.52934	305.87	310.65
3.	10	261.5370	.66695	.21091	260.41	262.59
4.	10	255.7540	.57384	.18146	255.12	256.69
5.	10	281.3080	.70212	.22203	280.06	282.52
6.	10	295.8500	.68435	.21641	295.14	297.37
7.	10	302.0070	1.52172	.48121	299.00	305.00
8.	10	299.7860	.91848	.29045	298.00	301.00
9.	10	275.8320	.32940	.10417	275.14	276.12
10.	10	315.7750	.47014	.14867	315.04	316.36
11.	10	287.8390	.41842	.13232	287.14	288.36
12.	10	251.0070	2.40590	.76081	249.09	256.00
13.	10	248.9604	.61302	.19385	247.99	249.65
14.	10	290.8621	.52222	.16514	290.15	291.58
15.	10	325.8075	.84176	.26619	324.16	326.98
16.	10	291.2246	.48445	.15320	290.36	291.85
17.	10	271.5490	.42302	.13377	270.95	271.98
18.	10	285.1620	.67490	.21342	284.01	285.89
19.	10	292.2102	.61414	.19421	290.98	292.98
20.	10	285.2880	.60050	.18989	284.62	286.32
21.	10	251.6560	.81911	.25902	250.39	252.96
22.	10	333.5290	.73137	.23128	332.15	334.65
23.	10	235.8750	.55997	.17708	235.16	236.84
Total	230	285.5918	25.80762	1.70170	235.16	334.65

Table 4.27: ANOVA analysis for distance_Foot_force_or_Pressure_data with similarity significance factor threshold value 0.005

	Sum of squares	df	Mean square(mm)s	F	Similarity significance factor <i>P=0.005</i>
Between groups	152351.581	22	6925.072	8432.074	0.000
Within groups	170.004	207	.821		1.000
Total	152521.585	229			

From Figure 4.24, we can see that there is no overlap between each point. Also, the standard deviation values are small enough to consider that the measurements are

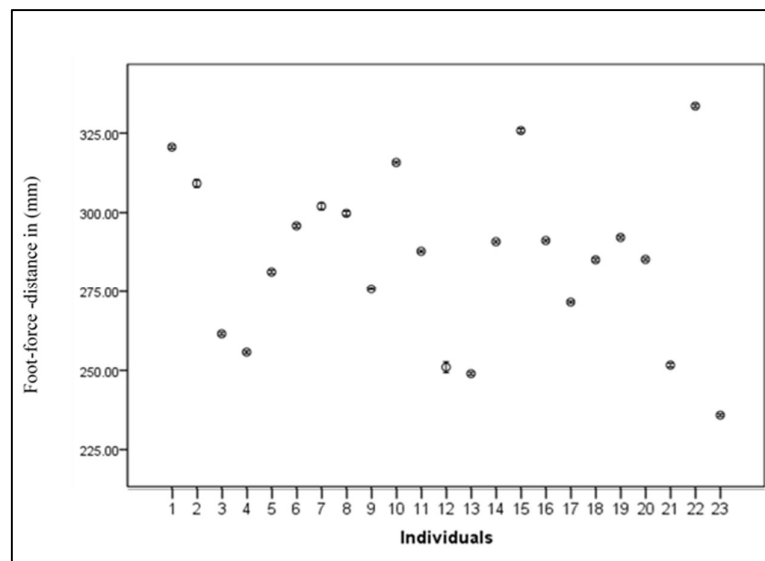


Figure 4.24: Mean values of foot force distance of subjects, each point shows the standard deviation.

4.4.3 Analysis and normalization data of spatial and temporal gait cycle

In this section, we have two sets of data analysis. The first calculates and analyses the gait cycle (mm) for each recruit. The methodology of this part is described in Section 3.5.3.2. The second part represents the temporal parameters of the gait cycle which is the calculation of the ambulation time for one gait cycle. Each set of data is affected by walking speed (DiLiberto et al., 2018). In this case, the normalization of these two sets of data will create new stable data with walking speed. Normalization will be as follows: (Gait cycle / Ambulation time) X total foot pressure.

Table 4.28: Statistical analysis of normalized (Gait cycle /Ambulation time) X total foot pressure.

Subjects	Number of trials	Mean	Std. deviation	Std. error	Minimum (mm)	Maximum (mm)
1.	10	3731.6762	18.94366	5.99051	3698.88	3762.00
2.	10	4347.5000	16.88688	5.34010	4316.00	4366.00
3.	10	1443.5229	14.45827	4.57211	1425.00	1467.00
4.	10	865.5198	9.91988	3.13694	852.00	884.89
5.	10	2659.4532	13.89530	4.39408	2641.00	2684.00
6.	10	1850.9159	15.30754	4.84067	1823.00	1874.00
7.	10	2051.2585	24.53748	7.75943	1999.99	2085.00
8.	10	4232.7000	20.10555	6.35793	4198.00	4258.00
9.	10	2956.1004	13.76397	4.35255	2932.00	2975.00
10.	10	3656.9526	15.96961	5.05003	3625.00	3684.00
11.	10	1757.5092	12.62692	3.99298	1745.00	1784.00
12.	10	2536.0000	16.16581	5.11208	2511.00	2571.00
13.	10	2345.3703	19.22233	6.07864	2299.70	2368.00
14.	10	3434.0000	15.62050	4.93964	3415.00	3456.00
15.	10	4238.5000	11.24722	3.55668	4216.00	4251.00
16.	10	952.8000	8.61265	2.72356	936.00	962.00
17.	10	1967.1000	11.60890	3.67106	1953.00	1984.00
18.	10	2226.4000	10.83410	3.42604	2211.00	2241.00
19.	10	3235.4000	14.10437	4.46019	3214.00	3264.00
20.	10	1536.6000	13.61535	4.30555	1514.00	1561.00
21.	10	4023.5000	20.75920	6.56464	3985.00	4052.00
22.	10	2839.7000	15.25378	4.82367	2814.00	2862.00
23.	10	1652.4000	15.33478	4.84928	1636.00	1687.00
Total	230	2632.2121	1052.45819	69.39704	852.00	4366.00

The results data were tested and analysed using ANOVA statistics. The similarity significance value obtained was too small compared to other values such as step length. From the significance factor shown in Tables 4.29, we can consider this factor as an identification factor.

Table 4.29: ANOVA analysis of gait cycle normalized ambulation time then multiply by total foot pressure

	Sum of squares	df	Mean square	F	significance
Between groups	2.536E8	22	1.153E7	47346.453	0.001
Within groups	50398.673	207	243.472		1.000
Total	2.537E8	229			

The normalized data created a new identification factor that combines three parameters: spatial data represented by gait cycle, temporal data represented by ambulation time, and foot pressure data represented by the total foot pressure. The combined data of these parameters is a new technique to create an authenticated identification factor.

CHAPTER 5

5.1 Discussion

5.1.1 Overview

This research investigated the following main points:

1. **Calculating the most reliable video camera features for human gait recording.** Identified the most suitable digital video cameras, and the best calibration techniques to ensure that accurate data was extracted from the gait recordings
2. **Human identification using gait analysis through close-range photogrammetry .**Demonstrated an innovative alternative methodology to extract human identification parameters through the analysis of gait features using photogrammetry techniques
3. **New protocol to capture more accurate human gait data using footprint features.** Demonstrated the effectiveness of the innovative methodology using footprint features for human identification. This was proved by extracting the footprint features data using the foot force platform
4. **A new technique for human identification .**
Established by correlating the two sets of identification parameters resulting from the photogrammetry and footprint approaches and using them as one set of data for human identification.

5.2 Human gait analysis using photogrammetry

The main aim of this research was to develop a new set of human identification techniques to measure and analyse human movement for forensic purposes. Photogrammetry is mainly based on achieving the best possible camera calibration. The calibration of various cameras was explored following a planned procedure as

explained in Chapter 3 (methodology chapter). Four types of digital cameras were tested for competencies associated with the proposed project. The efficiency and suitability of these cameras were tested based on multiple measured parameters such as lens distortion, focal length and resolution. First, we calibrated the low-cost small size Spy camera. As previously mentioned, the camera had a small lens angle, limited memory capacity and a low-resolution recording.

The calibration results of this spy camera showed that the focal length was approximately 7.32 mm. This focal length value is very low and affects footage accuracy. The radial distortion at 0.5mm radius was -84 microns, while the maximum radial distortion at 5.50 mm radius was 1497.2 microns. According to Fraser (2013), positive radial distortion is mostly referred to as pincushion distortion, while negative distortion is known as barrel distortion. Also, Chong (2014) pointed that the radial distortion magnitude is generally small, and for metric applications, decreases with the increase in focal length. Thus, the highest focal length was achieved from the calibration process with less maximum distortion leading to better camera accuracy.

Our results also found that the maximum radial distortion at 5 mm radius was 198.3microns (12.247 mm focal length) for the JVC digital camera. Despite, these positive results obtained from the JVC digital camera in terms of higher focal length and less distortion at the same radius of 5mm, the camera has limited memory and less recording time and unclear motion capture images. These limitations limit the use of these types of digital cameras for the purpose of this research.

The results obtained from calibrating the CCTV cameras indicated a low value for focal length with a high range of distortion at 5 mm radius (867.4 microns), thus indicating low resolution making it inappropriate for our research.

The results obtained from calibrating the Panasonic Lumix DMC-FZ300 digital video camera indicated the best possible radial distortion of -133.6 microns at 5 mm radius. This camera had a high focal length range of 25-600mm, and recorded 4k video streaming with a resolution of 4000x3000 pixels/cm². Based on these results, the Panasonic Lumix DMC-FZ300 digital video camera was chosen for this research.

To support these findings, (Majeed and Chong, 2020a) compared the Dashcam camera which has similar specification to the previously mentioned Spy camera with the JVC digital camera. They indicated that the JVC digital camera's maximum distortion was

15 μ m while the Dashcam's maximum distortion was 200 μ m. Thus, in comparison, the latter has distortions over 13 times larger. (Majeed and Chong, 2020) concluded that not having calibrated distortion parameters when using the Dashcam, was particularly severe for accurate ground measurement.

The photogrammetric method used in our research has an advantage in that there is a well calibrated digital camera already in place, so the time needed to analyse the perpetrator is less than that needed in previous techniques mentioned in the literature. Furthermore, there was no need to ascertain the location of the subjects in relation to the measuring devices. For example, we measured the set of cardboard (bolted onto the floor) with a scale bar which was already known by the software, and compared this to an actual physical measurement, and the error was less 2mm.

Measurement of stature and bodily proportions has been carried out in numerous investigations where surveillance images of perpetrators could be obtained (Hoogstrate et al., 2001;Stephan, 2015). However, the methods employed up until now are subject to several errors. Usually, images are produced with measuring devices such as vertical rulers placed at the same location as the perpetrator. It is important that these images are produced by the same video cameras as the ones that captured the perpetrator (reverse projection photogrammetry). These images are then overlaid using standard image editing. The major problem is identifying when the measuring device is placed correctly. Ideally, it has to be placed at exactly the same spot where the perpetrator stood in order to result in reliable measurements. This is quite difficult and usually a great many images of the ruler are produced, and only trial and error in terms of overlaying one image after the other enables one to narrow down the most correct superimposition. Likewise, it is very difficult to exactly calculate the error produced if the ruler is not overlaid on exactly the spot where the perpetrator stood.

The techniques used in our research avoids all of these challenges. We can easily test the perpetrator in the same location where the system of cameras is installed. As we had five cameras installed, we could spot the same position for the perpetrator and suspect accurately because, if one or two cameras failed to spot, we still had three other cameras covering the spotting area. Then we used iwitness PRO to obtain 3-D measurements for the parameters described in Chapters 3 and 4. The identification parameter choice in this part of the study were the knee-inner/outer ankle joint and 3-

D knee angle for the following gait phase sequence: (1) heel-down, (2) mid-stance and (3) toe-off. The specific spots on the knee and the inner/outer ankle joint were chosen because this joint is not effected by the change of floor surface and the deviation of the foot while walking (Brockett and Chapman, 2016).

The results were presented according to the gait phase sequences. The three unique measures were analysed, and their statistical quality evaluated. First, the between group's (intrasubject variability) and within group's (intractability, i.e. the variation in gait for each test subject) statistical results were analysed to determine measurement reliability. Next, the results of the three phases were examined for consistency. To evaluate the reliability of these measurements, the mean within a group and between significance group scores ($P=0.05$) were determined, respectively.

Based on the results of the ANOVA statistical tests, it was apparent that the knee-inner ankle joint 3-D measurement accuracy at the heel-down, mid-stance and toe-off phases were within 2mm, i.e., the standard deviation for the individual was approximately 2mm. This accuracy was slightly larger than published human movement for medical applications where the knee was exposed (Chong, 2011;Chong et al., 2014). Thus, the within group measure variation could be established at a 2mm limit however, three standard deviations or 95% CFL was considered a suitable margin of error value. Therefore, the 6mm margin of error could be used to determine whether the between group variation was within this margin of error requirement. By and large, the minimum and maximum values were within the 6mm range. Thus, the knee-inner ankle joint 3-D measurements were determined to exhibit high accuracy for gait characteristics.

The between group test showed that there was very small variation in the three measurements between randomly selected individuals. This indicated that the knee to interior ankle 3-D measurements for all three principal phases could be used to identify the perpetrator successfully. Similarly, these three principal phases were very important gait characteristic markers for everyone. The statistical tests established an important understanding of the accuracy and reliability of the developed advanced photogrammetric techniques and the calculated measure as part of the individual gait characteristics. The technique developed by Bouchrika (2017) was not appropriate for some crime scene video footage, where: (1) the need to set a coordinates system based

on the left ankle joint could be missing from video footage; and (2) accurate body height was not available. The use of accurate pressure-based gait phase markers was precise because: (1) the pressure sensor was very sensitive and (2) timing accuracy was very high at 500th of a second. As the result, the developed technique was very accurate and highly reliable. Therefore, the developed measurements are more likely to survive extensive scrutiny in court. Some other features has been tested and analysed such as Knee-front foot distance , Knee-rear foot distance, the and angle of Knee-ankle joint-front foot . The outcome of These measurements gives 70-80% accuracy of perpetrator identification. By compared to the other results which gives 95% of accuracy, the last measures has been neglected. Also, for the foot pressure techniques , some features has been tested and calculated such as maximum pressure contact area, right stride length ,left stride length and the stance time . These measures give 75-85% of the perpetrator identification of the identification accuracy which also been neglected from the calculation of this thesis.

CHAPTER 6

6.1 Conclusions

The measurement of gait characteristics using a photogrammetric technique has been carried out in numerous investigations to assist the criminal investigators in identifying crime suspects using biomechanical data extracted from static and dynamic gait. However, these methods generate many errors, such as the images not produced by the same video cameras. Thus, the main aim of this research was to introduce a more efficient and reliable technique for the identification of stature and bodily proportions of human movement, correlating two sets of identifications parameters from the photogrammetry and footprint approaches and use them as one set of data for human identification.

The present work compared the effectiveness of different types of digital cameras. The purpose was to select the most suitable digital camera based on calibration results. The Panasonic Lumix DMC-FZ300 digital video camera had the best possible radial distortion of 133.6 microns at 5mm radius, and had high focal length range of (25-600) mm. Three unique measures were studied and analysed, and the statistical analysis showed that the standard deviation of measures was approximately 2mm for all individuals recruited in this study. For example, the knee to inner/outer ankle 3-D measurements was determined to exhibit high accuracy for gait characteristics.

The integration of foot pressure/force data and photogrammetry measurements resulted in more reliable and accurate data for suspect identification. The data were collected and processed at the same time and the subjects were selected randomly from a large group of students, which is significant for criminal identification. We conclude that this new approach can increase the security of interior and exterior locations such as government buildings, banks, etc. It uses low-cost equipment and can be applied to individuals wearing any type of shoes or clothes.

For future work, we recommend using a real-time 3-D coordinate of spotted area for easy analysis. Also, for more subject identification factors, we recommend using the maximum force/pressure area for the right and left feet. Additional identification factors recommended are 3-D distance of the total height of the subject and other biometrics measurements such as arm length, angle of arms while walking, and total length of legs especially at the mid-stance phase.

6.2 Footprint analysis

Utilizing photogrammetry techniques produced high-quality 3-D measurements such as 3-D distances and angles. These were previously explained and analysed in Section 5.1.2. Joint angle and gait cycle characteristics were frequently used to differentiate between suspects and perpetrators thus, in (Black et al., 2017), gait cycle characteristics and joint angles were utilised in an attempt to differentiate between suspects and perpetrators of a criminal scene. However, incomplete gait cycles which were often collected, made evidential gait analysis challenging. These authors argued that perpetrators might have walked differently from the normal walking pattern when the crime was committed, which makes later matching of the gait with a suspect difficult.

In this research, we consider force/pressure measurements which could be exploited to identify an individual through gait characteristics recorded under the shoes by the RSSCAN system. The foot force under the shoes during gait could be used to provide accurate markers. Thus, the same set of gait features could be used for comparing the gait measurements between individuals. The markers were identified and formed part of the research.

As depicted by the statistical results of mean, standard deviation, maximum and minimum values in the Results chapter, individual recruit's gait measurements were very precise. These gait measurements including force, pressure, and force/pressure distance were recorded under the foot in all three phases of gait (heel-down, mid-Stance and toe-off). These parameters were chosen for human identification because they are hard to conceal.

The highlighted identification parameters for this part of the study were obtained after analysing 32 biometric footprint features such as stride length and total gait cycle. The results showed that these are the only parameters with a significant value for identification. The data were recorded at the same time as the photogrammetry measurements were taken, leading to more accurate and reliable data for the identification of the suspects. In addition, these measurements were obtained on separate days, so they represent individual gait characteristics accurately over all periods.

The other important statistic is that the measurement value varied between individuals hugely, thus providing an excellent range of values for further interpretation. This is significant as these individuals were selected randomly from a large group of higher degree research students at the university. The results show that the novel measure is a significant new discovery of the use of gait characteristics for forensic application. The statistical significance of the different measurements was excellent.

This measurement is suitable for the identification of a perpetrator from a group of suspects. As discussed in the review, this significance satisfies the requirement needed for forensic evidence of biometric measures as the research used 23 subjects. The group size is small in statistical terms however, it is suitable for an initial study where we are trying to determine which gait characteristics measurements are suitable for forensic work. Therefore, the next stage is to recruit a larger group. The integration of force/pressure and physical dimension measurements has huge potential for finding suitable ways to separate a perpetrator from suspects. This provides excellent opportunities for crime identification process efficiencies.

7 REFERENCES

- Aboua, G., Oguntibeju, O. O. & du Plessis, S. S. 2013. Can lifestyle factors of diabetes mellitus patients affect their fertility? *Diabetes mellitus—insights and perspectives*, 95.
- Agostini, V., Gastaldi, L., Rosso, V., Knaflitz, M. & Tadano, S. 2017. A wearable magneto-inertial system for gait analysis (h-gait): Validation on normal weight and overweight/obese young healthy adults. *Sensors*, 17, 2406.
- Aich, S., Pradhan, P. M., Park, J., Sethi, N., Vathsa, V. S. S. & Kim, H.-C. 2018. A validation study of freezing of gait (fog) detection and machine-learning-based fog prediction using estimated gait characteristics with a wearable accelerometer. *Sensors*, 18, 3287.
- Akhtaruzzaman, M., Shafie, A. A. & Khan, M. R. Electro-goniometric system: An instrumentation to capture knee movements for forward walking. 2015 10th Asian Control Conference (ASCC), 2015. IEEE, 1-4.
- Allport, G. W. & Vernon, P. E. 1933. The problem of consistency in expressive movement.
- Aminian, K. & Najafi, B. 2004. Capturing human motion using body-fixed sensors: Outdoor measurement and clinical applications. *Computer animation and virtual worlds*, 15, 79-94.
- Andries, M. 2015. *Object and human tracking, and robot control through a load sensing floor*. Université de Lorraine.
- Annamalai, P., Raju, K. & Ranganayakulu, D. 2018. Soft biometrics traits for continuous authentication in online exam using ica based facial recognition. *Int. J. Netw. Secur.*, 20, 423-432.
- Arafsha, F., Hanna, C., Aboualmagd, A., Fraser, S. & El Saddik, A. 2018. Instrumented wireless smartinsole system for mobile gait analysis: A validation pilot study with tekscan strideway. *Journal of Sensor and Actuator Networks*, 7, 36.
- Balazia, M. & Plataniotis, K. N. 2016. Human gait recognition from motion capture data in signature poses. *IET Biometrics*, 6, 129-137.
- Bamberg, S. J. M., Benbasat, A. Y., Scarborough, D. M., Krebs, D. E. & Paradiso, J. A. 2008. Gait analysis using a shoe-integrated wireless sensor system. *IEEE transactions on information technology in biomedicine*, 12, 413-423.
- Bejek, Z., Paróczai, R., Illyés, Á. & Kiss, R. M. 2006. The influence of walking speed

on gait parameters in healthy people and in patients with osteoarthritis. *Knee surgery, sports traumatology, arthroscopy*, 14, 612-622.

- Bell, T., Xu, J. & Zhang, S. 2016. Method for out-of-focus camera calibration. *Applied optics*, 55, 2346-2352.
- Benoit, D. L., Damsgaard, M. & Andersen, M. S. 2015. Surface marker cluster translation, rotation, scaling and deformation: Their contribution to soft tissue artefact and impact on knee joint kinematics. *Journal of biomechanics*, 48, 2124-2129.
- Benson, L. C., Clermont, C. A., Bošnjak, E. & Ferber, R. 2018. The use of wearable devices for walking and running gait analysis outside of the lab: A systematic review. *Gait & posture*, 63, 124-138.
- Bhatia, R. 2013. Biometrics and face recognition techniques. *International Journal of Advanced Research in Computer Science and Software Engineering*, 3.
- Biber, K. 2009. Visual jurisprudence: The dangers of photographic identification evidence: Katherine biber argues that caution is required when using photographic evidence in court. *Criminal Justice Matters*, 78, 35-37.
- Black, S., Wall, M., Abboud, R., Baker, R. & Stebbins, J. 2017. Forensic gait analysis: A primer for courts.
- Bouchrika, I. 2017. Evidence evaluation of gait biometrics for forensic investigation. *Multimedia forensics and security*. Springer.
- Bouchrika, I. 2018. A survey of using biometrics for smart visual surveillance: Gait recognition. *Surveillance in action*. Springer.
- Bouchrika, I., Goffredo, M., Carter, J. & Nixon, M. 2011. On using gait in forensic biometrics. *Journal of forensic sciences*, 56, 882-889.
- Boulgouris, N. V., Hatzinakos, D. & Plataniotis, K. N. 2005. Gait recognition: A challenging signal processing technology for biometric identification. *IEEE signal processing magazine*, 22, 78-90.
- Bravi, M., Gallotta, E., Morrone, M., Maselli, M., Santacaterina, F., Toglia, R., Foti, C., Sterzi, S., Bressi, F. & Miccinilli, S. 2020. Concurrent validity and inter trial reliability of a single inertial measurement unit for spatial-temporal gait parameter analysis in patients with recent total hip or total knee arthroplasty. *Gait & posture*, 76, 175-181.
- Brehm, M.-A., Harlaar, J. & Schwartz, M. 2008. Effect of ankle-foot orthoses on walking efficiency and gait in children with cerebral palsy. *Journal of*

rehabilitation medicine, 40, 529-534.

- Brockett, C. L. & Chapman, G. J. 2016. Biomechanics of the ankle. *Orthopaedics and trauma*, 30, 232-238.
- Brown, E. & Cassells, A. 1971. Induced changes in the nucleotide pattern and metabolic state of pea root tissue. *Phytochemistry*, 10, 1251-1260.
- Buciu, I. 2014. Challenges and specifications for robust face and gait recognition systems for surveillance application. *Journal of Electrical and Electronics Engineering*, 7, 25.
- Buck, U., Buße, K., Campana, L. & Schyma, C. 2018. Validation and evaluation of measuring methods for the 3d documentation of external injuries in the field of forensic medicine. *International journal of legal medicine*, 132, 551-561.
- Burgstaller, B. & Pillichshammer, F. 2009. The average distance between two points. *Bulletin of the Australian Mathematical Society*, 80, 353-359.
- Burns, J., Crosbie, J., Hunt, A. & Ouvrier, R. 2005. The effect of pes cavus on foot pain and plantar pressure. *Clinical Biomechanics*, 20, 877-882.
- Bus, S., Van Deursen, R., Armstrong, D., Lewis, J. E., Caravaggi, C., Cavanagh, P. & Foot, I. W. G. o. t. D. 2016. Footwear and offloading interventions to prevent and heal foot ulcers and reduce plantar pressure in patients with diabetes: A systematic review. *Diabetes/metabolism research and reviews*, 32, 99-118.
- Bus, S. & Waaijman, R. 2013. The value of reporting pressure–time integral data in addition to peak pressure data in studies on the diabetic foot: A systematic review. *Clinical Biomechanics*, 28, 117-121.
- Bus, S. A. & de Lange, A. 2005. A comparison of the 1-step, 2-step, and 3-step protocols for obtaining barefoot plantar pressure data in the diabetic neuropathic foot. *Clinical biomechanics*, 20, 892-899.
- Bzhikhatlov, I., Cheloshkina, K. & Abramchuk, M. Gait phase detection for biped robots. 2019 International Russian Automation Conference (RusAutoCon), 2019. IEEE, 1-6.
- Castelli, A., Paolini, G., Cereatti, A. & Della Croce, U. 2015. A 2d markerless gait analysis methodology: Validation on healthy subjects. *Computational and mathematical methods in medicine*, 2015.
- Castro, M. P. D., Meucci, M., Soares, D. P., Fonseca, P., Borgonovo-Santos, M., Sousa, F., Machado, L. & Vilas-Boas, J. P. 2014. Accuracy and repeatability of the gait analysis by the walkinsense system. *BioMed research international*, 2014.

- Cereatti, A., Rosso, C., Nazarian, A., DeAngelis, J. P., Ramappa, A. J. & Della Croce, U. 2015. Scapular motion tracking using acromion skin marker cluster: In vitro accuracy assessment. *Journal of Medical and Biological Engineering*, 35, 94-103.
- Chaccour, K., Darazi, R., el Hassans, A. H. & Andres, E. Smart carpet using differential piezoresistive pressure sensors for elderly fall detection. 2015 IEEE 11th International Conference on Wireless and Mobile Computing, Networking and Communications (WiMob), 2015. IEEE, 225-229.
- Chatzistergos, P. E., Gatt, A., Formosa, C., Farrugia, K. & Chockalingam, N. 2020. Optimised cushioning in diabetic footwear can significantly enhance their capacity to reduce plantar pressure. *Gait & Posture*, 79, 244-250.
- Cheng, Y. 1995. Mean shift, mode seeking, and clustering. *IEEE transactions on pattern analysis and machine intelligence*, 17, 790-799.
- Cho, S.-H., Park, J. M. & Kwon, O. Y. 2004. Gender differences in three dimensional gait analysis data from 98 healthy korean adults. *Clinical biomechanics*, 19, 145-152.
- Chong, A. K. 2011. Low-cost compact cameras: A medical application in cmt disease monitoring. *The Photogrammetric Record*, 26, 263-273.
- Chong, A. K., Al-Baghdadi, J. A. A. & Alshadli, D. High definition video cameras for measuring movement of vibrating bridge structure. International Conference on Vibration and Vibro-acoustics (ICVV2014), 2014. University of Southern Queensland, 1-10.
- Chong, A. K., Milburn, P., Newsham-West, R. & Voert, M. 2009. High-accuracy photogrammetric technique for human spine measurement. *The Photogrammetric Record*, 24, 264-279.
- Chow, J. Y., Woo, M. T. & Koh, M. 2014. Effects of external and internal attention focus training on foot-strike patterns in running. *International Journal of Sports Science & Coaching*, 9, 307-320.
- Christensen, L. S., Sánchez de Ribera, O. & Trajtenberg, N. 2021. A systematic review of professionals' views about community management policies for individuals convicted of sexual offenses. *Sexual Abuse*, 10790632211000369.
- Chung, M.-J. & Wang, M.-J. J. 2010. The change of gait parameters during walking at different percentage of preferred walking speed for healthy adults aged 20–60 years. *Gait & posture*, 31, 131-135.

- Clément, J., Toliopoulos, P., Hagemeister, N., Desmeules, F., Fuentes, A. & Vendittoli, P.-A. 2018. Healthy 3d knee kinematics during gait: Differences between women and men, and correlation with x-ray alignment. *Gait & posture*, 64, 198-204.
- Cocchi, I., Figari, G., Valeri, N., Paolini, G., Della Croce, U., Cereatti, A., Pantzar, E., Magnuson, A. & Riad, J. A 2d markerless gait analysis protocol to estimate the sagittal joint kinematics of children with cerebral palsy. 2019 IEEE 23rd International Symposium on Consumer Technologies (ISCT), 2019. IEEE, 192-196.
- Coelho, V., Vijay Frederick. 2018. *Characteristics of contralateral plantar pressure distribution in diabetic patients with and without a prosthetic foot: An observational study*. Christian Medical College, Vellore.
- Colyer, S. L., Evans, M., Cosker, D. P. & Salo, A. I. 2018. A review of the evolution of vision-based motion analysis and the integration of advanced computer vision methods towards developing a markerless system. *Sports medicine-open*, 4, 1-15.
- Connor, P. & Ross, A. 2018. Biometric recognition by gait: A survey of modalities and features. *Computer Vision and Image Understanding*, 167, 1-27.
- Costilla-Reyes, O., Vera-Rodriguez, R., Scully, P. & Ozanyan, K. B. 2018. Analysis of spatio-temporal representations for robust footstep recognition with deep residual neural networks. *IEEE transactions on pattern analysis and machine intelligence*, 41, 285-296.
- Cunado, D., Nixon, M. S. & Carter, J. N. 2003. Automatic extraction and description of human gait models for recognition purposes. *Computer vision and image understanding*, 90, 1-41.
- Cutting, J. E. & Kozlowski, L. T. 1977. Recognizing friends by their walk: Gait perception without familiarity cues. *Bulletin of the psychonomic society*, 9, 353-356.
- Cutting, J. E., Proffitt, D. R. & Kozlowski, L. T. 1978. A biomechanical invariant for gait perception. *Journal of Experimental Psychology: Human Perception and Performance*, 4, 357.
- DeBiasio, J. C., Russell, M. E., Butler, R. J., Nunley, J. A. & Queen, R. M. 2013. Changes in plantar loading based on shoe type and sex during a jump-landing task. *Journal of athletic training*, 48, 601-609.

- DeLisa, J. A. 1998. *Gait analysis in the science of rehabilitation*, Diane Publishing.
- DiLiberto, F. E., Nawoczenski, D. A. & Houck, J. 2018. Ankle and midfoot power during walking and stair ascent in healthy adults. *Journal of applied biomechanics*, 34, 262-269.
- Doyle, A., Lippert, R. & Lyon, D. 2013. *Eyes everywhere: The global growth of camera surveillance*, Routledge.
- Ebert, L., Flach, P., Schweitzer, W., Leipner, A., Kottner, S., Gascho, D., Thali, M. & Breitbeck, R. 2016. Forensic 3d surface documentation at the institute of forensic medicine in zurich—workflow and communication pipeline. *Journal of Forensic Radiology and Imaging*, 5, 1-7.
- Edmond, G., Thompson, M. B. & Tangen, J. M. 2014. A guide to interpreting forensic testimony: Scientific approaches to fingerprint evidence. *Law, Probability and Risk*, 13, 1-25.
- Eftekhari, M., Chamsaz, M., Arbab-Zavar, M. H. & Eftekhari, A. 2015. Vortex-assisted surfactant-enhanced emulsification microextraction based on solidification of floating organic drop followed by electrothermal atomic absorption spectrometry for speciation of antimony (u, v). *Environmental monitoring and assessment*, 187, 1-8.
- Eisenberg, P. & Reichline, P. B. 1939. Judging expressive movement: Ii. Judgments of dominance-feeling from motion pictures of gait. *The Journal of Social Psychology*, 10, 345-357.
- Elharrouss, O., Almaadeed, N., Al-Maadeed, S. & Bouridane, A. 2021. Gait recognition for person re-identification. *The Journal of Supercomputing*, 77, 3653-3672.
- Favre, J., Jolles, B., Aissaoui, R. & Aminian, K. 2008. Ambulatory measurement of 3d knee joint angle. *Journal of biomechanics*, 41, 1029-1035.
- Figueiredo, J., Felix, P., Costa, L., Moreno, J. C. & Santos, C. P. 2018. Gait event detection in controlled and real-life situations: Repeated measures from healthy subjects. *IEEE Transactions on Neural Systems and Rehabilitation Engineering*, 26, 1945-1956.
- Foster, J. P., Nixon, M. S. & Prügel-Bennett, A. 2003. Automatic gait recognition using area-based metrics. *Pattern Recognition Letters*, 24, 2489-2497.
- Franklyn-Miller, A., Bilzon, J., Wilson, C. & McCrory, P. 2014. Can rscan footscan® d3d™ software predict injury in a military population following plantar

- pressure assessment? A prospective cohort study. *The Foot*, 24, 6-10.
- Fraser, C. S. 2013. Automatic camera calibration in close range photogrammetry. *Photogrammetric Engineering & Remote Sensing*, 79, 381-388.
- Fuchs, M., Hermans, M., Kars, H., Hendriks, J. & van der Steen, M. 2020. Plantar pressure distribution and wearing characteristics of three forefoot offloading shoes in healthy adult subjects. *The Foot*, 45, 101744.
- García-Soidán, J. L., Leirós-Rodríguez, R., Romo-Pérez, V. & García-Liñeira, J. 2021. Accelerometric assessment of postural balance in children: A systematic review. *Diagnostics*, 11, 8.
- Gautam, P., Sunkaria, R. K. & Sharma, L. D. 2019. Digitization of paper electrocardiogram: A review. *Design and Implementation of Healthcare Biometric Systems*, 212-228.
- Gong, P., Chen, B., Li, X., Liu, H., Wang, J., Bai, Y., Chen, J., Chen, X., Fang, L. & Feng, S. 2020. Mapping essential urban land use categories in china (euluc-china): Preliminary results for 2018. *Science Bulletin*, 65, 182-187.
- Govsa, F., Chatzioglou, G. N., Hepguler, S., Pinar, Y. & Bedre, O. 2020. Variable lower limb alignment of clinical measures with digital photographs and the footscan pressure system. *Journal of Sport Rehabilitation*, 1, 1-8.
- Granieri, J. P., Crabtree, J. & Badler, N. I. 1995. Production and playback of human figure motion for visual simulation. *ACM Transactions on Modeling and Computer Simulation (TOMACS)*, 5, 222-241.
- Grayson, B. & Stein, M. I. 1981. Attracting assault: Victims' nonverbal cues. *Journal of Communication*, 31, 68-75.
- Gunns, R. E., Johnston, L. & Hudson, S. M. 2002. Victim selection and kinematics: A point-light investigation of vulnerability to attack. *Journal of Nonverbal Behavior*, 26, 129-158.
- Hanley, B., Tucker, C. B. & Bissas, A. 2018. Differences between motion capture and video analysis systems in calculating knee angles in elite-standard race walking. *Journal of sports sciences*, 36, 1250-1255.
- Harrati, N., Bouchrika, I. & Mahfouf, Z. 2017. Investigating the uptake of educational systems by academics using the technology to performance chain model. *Library Hi Tech*.
- Hennekes, H. & Nigg, E. A. 1994. The role of isoprenylation in membrane attachment of nuclear lamins. A single point mutation prevents proteolytic cleavage of the

- lamin a precursor and confers membrane binding properties. *Journal of cell science*, 107, 1019-1029.
- Heo, K. H., Jeong, S. Y. & Kang, S. J. 2019. Real-time user identification and behavior prediction based on foot-pad recognition. *Sensors*, 19, 2899.
- Hoogstrate, A., Van den Heuvel, H. & Huyben, E. 2001. Ear identification based on surveillance camera images. *Science & justice: journal of the Forensic Science Society*, 41, 167-172.
- Hullfish, T. J. & Baxter, J. R. 2020. A simple instrumented insole algorithm to estimate plantar flexion moments. *Gait & posture*, 79, 92-95.
- Hurd, W. J. & Snyder-Mackler, L. 2007. Knee instability after acute acl rupture affects movement patterns during the mid-stance phase of gait. *Journal of Orthopaedic Research*, 25, 1369-1377.
- Hutton, D., Newman-Casey, P. A., Tavag, M., Zacks, D. & Stein, J. 2014. Switching to less expensive blindness drug could save medicare part b \$18 billion over a ten-year period. *Health affairs*, 33, 931-939.
- Iwashita, Y., Kurazume, R. & Ogawara, K. Expanding gait identification methods from straight to curved trajectories. 2013 IEEE Workshop on Applications of Computer Vision (WACV), 2013. IEEE, 193-199.
- Jafarnejadgero, A. A., Anvari, M. & Granacher, U. 2020. Long-term effects of shoe mileage on ground reaction forces and lower limb muscle activities during walking in individuals with genu varus. *Clinical Biomechanics*, 73, 55-62.
- Jain, A. K., Ross, A. & Prabhakar, S. 2004. An introduction to biometric recognition. *IEEE Transactions on circuits and systems for video technology*, 14, 4-20.
- James, M. R., Chandler, J. H., Eltner, A., Fraser, C., Miller, P. E., Mills, J. P., Noble, T., Robson, S. & Lane, S. N. 2019. Guidelines on the use of structure-from-motion photogrammetry in geomorphic research. *Earth Surface Processes and Landforms*, 44, 2081-2084.
- Jia, Z., Yang, J., Liu, W., Wang, F., Liu, Y., Wang, L., Fan, C. & Zhao, K. 2015. Improved camera calibration method based on perpendicularity compensation for binocular stereo vision measurement system. *Optics express*, 23, 15205-15223.
- Johnson, K. L., Gill, S., Reichman, V. & Tassinary, L. G. 2007. Swagger, sway, and sexuality: Judging sexual orientation from body motion and morphology. *Journal of personality and social psychology*, 93, 321.

- Jokisch, D., Daum, I. & Troje, N. F. 2006. Self recognition versus recognition of others by biological motion: Viewpoint-dependent effects. *Perception*, 35, 911-920.
- Jung, H.-W., Jang, I.-Y., Lee, C. K., Yu, S. S., Hwang, J. K., Jeon, C., Lee, Y. S. & Lee, E. 2018. Usual gait speed is associated with frailty status, institutionalization, and mortality in community-dwelling rural older adults: A longitudinal analysis of the aging study of pyeongchang rural area. *Clinical interventions in aging*, 13, 1079.
- Jung, J.-W., Bien, Z., Lee, S.-W. & Sato, T. Dynamic-footprint based person identification using mat-type pressure sensor. Proceedings of the 25th Annual International Conference of the IEEE Engineering in Medicine and Biology Society (IEEE Cat. No. 03CH37439), 2003. IEEE, 2937-2940.
- Jung, J. W., Sato, T. & Bien, Z. 2004. Dynamic footprint-based person recognition method using a hidden markov model and a neural network. *International journal of intelligent systems*, 19, 1127-1141.
- Karatsidis, A., Bellusci, G., Schepers, H. M., De Zee, M., Andersen, M. S. & Veltink, P. H. 2017. Estimation of ground reaction forces and moments during gait using only inertial motion capture. *Sensors*, 17, 75.
- Kaufman, K. R., Brodine, S. K., Shaffer, R. A., Johnson, C. W. & Cullison, T. R. 1999. The effect of foot structure and range of motion on musculoskeletal overuse injuries. *The American journal of sports medicine*, 27, 585-593.
- Keijsers, N., Stolwijk, N., Louwerens, J. & Duyens, J. 2013. Classification of forefoot pain based on plantar pressure measurements. *Clinical biomechanics*, 28, 350-356.
- Keijsers, N., Stolwijk, N., Nienhuis, B. & Duyens, J. 2009. A new method to normalize plantar pressure measurements for foot size and foot progression angle. *Journal of Biomechanics*, 42, 87-90.
- Kelly, H. D. 2020. *Forensic gait analysis*, CRC Press.
- Kerkum, Y. L., Buizer, A. I., Van Den Noort, J. C., Becher, J. G., Harlaar, J. & Brehm, M.-A. 2015. The effects of varying ankle foot orthosis stiffness on gait in children with spastic cerebral palsy who walk with excessive knee flexion. *PloS one*, 10, e0142878.
- Khamsemanan, N., Nattee, C. & Jianwattanapaisarn, N. 2017. Human identification from freestyle walks using posture-based gait feature. *IEEE Transactions on Information Forensics and Security*, 13, 119-128.

- Kich, G. K. 1992. The developmental process of asserting a biracial, bicultural identity. *Racially mixed people in America*, 304, 317.
- Kim, D. & Paik, J. 2009. Gait recognition using active shape model and motion prediction. *IET Computer Vision*, 4, 25-36.
- Kleissen, R., Buurke, J., Harlaar, J. & Zilvold, G. 1998. Electromyography in the biomechanical analysis of human movement and its clinical application. *Gait & posture*, 8, 143-158.
- Kobayashi, H., Kakihana, W. & Kimura, T. 2014. Combined effects of age and gender on gait symmetry and regularity assessed by autocorrelation of trunk acceleration. *Journal of neuroengineering and rehabilitation*, 11, 1-6.
- Koch, M., Lunde, L.-K., Ernst, M., Knardahl, S. & Veiersted, K. B. 2016. Validity and reliability of pressure-measurement insoles for vertical ground reaction force assessment in field situations. *Applied ergonomics*, 53, 44-51.
- Koeva, M. N. 2016. 3d modelling and interactive web-based visualization of cultural heritage objects. *International Archives of the Photogrammetry, Remote Sensing & Spatial Information Sciences*, 41.
- Kovacs, C. R. 2005. Age-related changes in gait and obstacle avoidance capabilities in older adults: A review. *Journal of applied gerontology*, 24, 21-34.
- Kozlow, P., Abid, N. & Yanushkevich, S. 2018. Gait type analysis using dynamic bayesian networks. *Sensors*, 18, 3329.
- Kozlowski, L. T. & Cutting, J. E. 1977. Recognizing the sex of a walker from a dynamic point-light display. *Perception & psychophysics*, 21, 575-580.
- Lanitis, A. 2010. A survey of the effects of aging on biometric identity verification. *International Journal of Biometrics*, 2, 34-52.
- Larsen, P. K., Simonsen, E. B. & Lynnerup, N. 2008. Gait analysis in forensic medicine. *Journal of forensic sciences*, 53, 1149-1153.
- Larsen, P. K., Simonsen, E. B. & Lynnerup, N. Use of photogrammetry and biomechanical gait analysis to identify individuals. 2010 18th European Signal Processing Conference, 2010. IEEE, 1660-1664.
- Lebleu, J., Gosseye, T., Detrembleur, C., Mahaudens, P., Cartiaux, O. & Penta, M. 2020. Lower limb kinematics using inertial sensors during locomotion: Accuracy and reproducibility of joint angle calculations with different sensor-to-segment calibrations. *Sensors*, 20, 715.
- Lee, N., Goonetilleke, R. S., Cheung, Y. S. & So, G. M. 2001. A flexible encapsulated

- mems pressure sensor system for biomechanical applications. *Microsystem technologies*, 7, 55-62.
- Lee, T. K., Belkhatir, M. & Sanei, S. 2014. A comprehensive review of past and present vision-based techniques for gait recognition. *Multimedia tools and applications*, 72, 2833-2869.
- Leipold, A. D. 2021. The puzzle of clearance rates, and what they can tell us about crime, police reform, and criminal justice. *Wake Forest L. Rev.*, 56, 47.
- Lemoyne, R., Coroian, C., Mastroianni, T. & Grundfest, W. 2009. Wireless accelerometer assessment of gait for quantified disparity of hemiparetic locomotion. *Journal of Mechanics in Medicine and Biology*, 9, 329-343.
- LeMoyne, R. & Mastroianni, T. 2015. Use of smartphones and portable media devices for quantifying human movement characteristics of gait, tendon reflex response, and parkinson's disease hand tremor. *Mobile health technologies*. Springer.
- Li, J. & Liu, Z. 2018. Efficient camera self-calibration method for remote sensing photogrammetry. *Optics express*, 26, 14213-14231.
- Liu, T., Inoue, Y., Shibata, K., Yamasaki, Y. & Nakahama, M. A six-dimension parallel force sensor for human dynamics analysis. IEEE Conference on Robotics, Automation and Mechatronics, 2004., 2004. IEEE, 208-212.
- Lopez-Nava, I. H. & Munoz-Melendez, A. 2016. Wearable inertial sensors for human motion analysis: A review. *IEEE Sensors Journal*, 16, 7821-7834.
- Lopez, M., Mari, R., Gargallo, P., Kuang, Y., Gonzalez-Jimenez, J. & Haro, G. Deep single image camera calibration with radial distortion. Proceedings of the IEEE/CVF Conference on Computer Vision and Pattern Recognition, 2019. 11817-11825.
- Losciale, J. M., Ithurnburn, M. P., Paterno, M. V. & Schmitt, L. C. 2021. Does passing return-to-sport criteria coincide with normalized landing biomechanics in young athletes following primary anterior cruciate ligament reconstruction? *Journal of Orthopaedic Research®*.
- Luhmann, T., Fraser, C. & Maas, H.-G. 2016. Sensor modelling and camera calibration for close-range photogrammetry. *ISPRS Journal of Photogrammetry and Remote Sensing*, 115, 37-46.
- Lynnerup, N. & Vedel, J. 2005. Person identification by gait analysis and photogrammetry. *Journal of Forensic science*, 50, JFS2004054-7.

- Machado, Á. S., Bombach, G. D., Duysens, J. & Carpes, F. P. 2016. Differences in foot sensitivity and plantar pressure between young adults and elderly. *Archives of gerontology and geriatrics*, 63, 67-71.
- MacWilliams, B. & Armstrong, P. Clinical applications of plantar pressure measurement in pediatric orthopedics. *Pediatric Gait: A New Millennium in Clinical Care and Motion Analysis Technology*, 2000. IEEE, 143-150.
- Maetzler, M., Bochdansky, T. & Abboud, R. 2010. Normal pressure values and repeatability of the emed® st2 system. *Gait & posture*, 32, 391-394.
- Majeed, A. & Chong, A. K. Advanced computing and image processing utilised in dashcam imagery study. 2020 IEEE 10th Symposium on Computer Applications & Industrial Electronics (ISCAIE), 2020a. IEEE, 211-214.
- Majeed, A. & Chong, A. K. Two measures of foot pressure image to detect foot drop of elderly diabetes sufferers. 2020 IEEE 10th Symposium on Computer Applications & Industrial Electronics (ISCAIE), 2020b. IEEE, 224-228.
- Majeed, A., Chong, A. K. & Abdulla, S. Person identification by gait analysis using photogrammetry techniques and foot pressure sensing matt. *Proceedings of the 1st MoHESR and HCED Iraqi Scholars Conference in Australasia 2017 (ISCA 2017)*, 2017. Swinburne University of Technology, 282-288.
- Mariani, B. 2012. Assessment of foot signature using wearable sensors for clinical gait analysis and real-time activity recognition. EPFL.
- Martínez, M., Villagra, F., Castellote, J. M. & Pastor, M. A. 2018. Kinematic and kinetic patterns related to free-walking in parkinson's disease. *Sensors*, 18, 4224.
- McKean, K. A., Landry, S. C., Hubble-Kozey, C. L., Dunbar, M. J., Stanish, W. D. & Deluzio, K. J. 2007. Gender differences exist in osteoarthritic gait. *Clinical Biomechanics*, 22, 400-409.
- Melai, T., IJzerman, T. H., Schaper, N. C., de Lange, T. L., Willems, P. J., Meijer, K., Lieveerse, A. G. & Savelberg, H. H. 2011. Calculation of plantar pressure time integral, an alternative approach. *Gait & posture*, 34, 379-383.
- Menant, J. C., Steele, J. R., Menz, H. B., Munro, B. J. & Lord, S. R. 2009. Effects of walking surfaces and footwear on temporo-spatial gait parameters in young and older people. *Gait & posture*, 29, 392-397.
- Montefiori, E., Modenese, L., Di Marco, R., Magni-Manzoni, S., Malattia, C., Petrarca, M., Ronchetti, A., de Horatio, L. T., van Dijkhuizen, P. & Wang, A.

2019. An image-based kinematic model of the tibiotalar and subtalar joints and its application to gait analysis in children with juvenile idiopathic arthritis. *Journal of biomechanics*, 85, 27-36.
- Morris, R. & Lawson, S. 2010. A review and evaluation of available gait analysis technologies, and their potential for the measurement of impact transmission. *Newcastle University*.
- Mostayed, A., Kim, S., Mazumder, M. M. G. & Park, S. J. Foot step based person identification using histogram similarity and wavelet decomposition. 2008 International Conference on Information Security and Assurance (isa 2008), 2008. IEEE, 307-311.
- Moustakas, K., Tzovaras, D. & Stavropoulos, G. 2010. Gait recognition using geometric features and soft biometrics. *IEEE Signal processing letters*, 17, 367-370.
- Muro-De-La-Herran, A., Garcia-Zapirain, B. & Mendez-Zorrilla, A. 2014. Gait analysis methods: An overview of wearable and non-wearable systems, highlighting clinical applications. *Sensors*, 14, 3362-3394.
- Murphy, D. F., Beynnon, B. D., Michelson, J. D. & Vacek, P. M. 2005. Efficacy of plantar loading parameters during gait in terms of reliability, variability, effect of gender and relationship between contact area and plantar pressure. *Foot & ankle international*, 26, 171-179.
- Murray, M. P., Drought, A. B. & Kory, R. C. 1964. Walking patterns of normal men. *JBJS*, 46, 335-360.
- Mutsavi, T. 2018. *The reliability of firearm identification in south africa: A comparative perspective*. University of Fort Hare.
- Nagwanshi, K. K. & Dubey, S. 2018. Statistical feature analysis of human footprint for personal identification using bigml and ibm watson analytics. *Arabian Journal for Science and Engineering*, 43, 2703-2712.
- Nagymáté, G. & Kiss, R. M. 2019. Affordable gait analysis using augmented reality markers. *PloS one*, 14, e0212319.
- Nakajima, K., Mizukami, Y., Tanaka, K. & Tamura, T. 2000. Foot-based personal recognition, ieee: Tr. *On Biomedical Engineering*, 47.
- Niu, W., Feng, T., Jiang, C. & Zhang, M. 2014. Peak vertical ground reaction force during two-leg landing: A systematic review and mathematical modeling. *BioMed research international*, 2014.

- Norman, G. R. 1988. Problem-solving skills, solving problems and problem-based learning. *Medical education*, 22, 279-286.
- Nurse, J. R., Creese, S. & De Roure, D. 2017. Security risk assessment in internet of things systems. *IT professional*, 19, 20-26.
- Orr, R. J. & Abowd, G. D. The smart floor: A mechanism for natural user identification and tracking. CHI'00 extended abstracts on Human factors in computing systems, 2000. 275-276.
- Peyer, K. E., Morris, M. & Sellers, W. I. 2015. Subject-specific body segment parameter estimation using 3d photogrammetry with multiple cameras. *PeerJ*, 3, e831.
- Piriyaprasarth, P., Morris, M. E., Winter, A. & Bialocerkowski, A. E. 2008. The reliability of knee joint position testing using electrogoniometry. *BMC musculoskeletal disorders*, 9, 1-10.
- Pirttikangas, S., Suutala, J., Riekkilä, J. & Rönning, J. Footstep identification from pressure signals using hidden markov models. Proc. Finnish Signal Processing Symposium (FINSIG'03), 2003. Citeseer, 124-128.
- Poon, C. C., Zhang, Y.-T. & Bao, S.-D. 2006. A novel biometrics method to secure wireless body area sensor networks for telemedicine and m-health. *IEEE Communications Magazine*, 44, 73-81.
- Porter, G. 2009. Cctv images as evidence. *Australian Journal of Forensic Sciences*, 41, 11-25.
- Prakash, C., Kumar, R. & Mittal, N. 2018. Recent developments in human gait research: Parameters, approaches, applications, machine learning techniques, datasets and challenges. *Artificial Intelligence Review*, 49, 1-40.
- Preatoni, E., Hamill, J., Harrison, A. J., Hayes, K., Van Emmerik, R. E., Wilson, C. & Rodano, R. 2013. Movement variability and skills monitoring in sports. *Sports biomechanics*, 12, 69-92.
- Provost, M. P., Troje, N. F. & Quinsey, V. L. 2008. Short-term mating strategies and attraction to masculinity in point-light walkers. *Evolution and Human Behavior*, 29, 65-69.
- Qian, G., Zhang, J. & Kidané, A. People identification using gait via floor pressure sensing and analysis. European Conference on Smart Sensing and Context, 2008. Springer, 83-98.
- Qiu, H. & Xiong, S. 2015. Center-of-pressure based postural sway measures:

- Reliability and ability to distinguish between age, fear of falling and fall history. *International Journal of Industrial Ergonomics*, 47, 37-44.
- Qiu, S., Liu, L., Zhao, H., Wang, Z. & Jiang, Y. 2018. Mems inertial sensors based gait analysis for rehabilitation assessment via multi-sensor fusion. *Micromachines*, 9, 442.
- Raj, R., Chen, V. & Lipps, R. 2010. Analysis of radar human gait signatures. *IET Signal Processing*, 4, 234-244.
- Ramirez-Bautista, J. A., Huerta-Ruelas, J. A., Chaparro-Cárdenas, S. L. & Hernández-Zavala, A. 2017. A review in detection and monitoring gait disorders using in-shoe plantar measurement systems. *IEEE reviews in biomedical engineering*, 10, 299-309.
- Ramizuddin, K. & Washimkar, S. 2013. Modelling and measurement of a wireless foot plantar pressure. *International Journal of Engineering Research and Applications (IJERA)*, 3, 104-107.
- Randhavane, T., Bhattacharya, U., Kapsaskis, K., Gray, K., Bera, A. & Manocha, D. 2019. Identifying emotions from walking using affective and deep features. *arXiv preprint arXiv:1906.11884*.
- Rangarajan, S., Kidane, A., Qian, G., Rajko, S. & Birchfield, D. The design of a pressure sensing floor for movement-based human computer interaction. European Conference on Smart Sensing and Context, 2007. Springer, 46-61.
- Rao, S., Baumhauer, J. & Nawoczinski, D. 2011. Is barefoot regional plantar loading related to self-reported foot pain in patients with midfoot osteoarthritis. *Osteoarthritis and cartilage*, 19, 1019-1025.
- Refai, M. I. M., van Beijnum, B. J., Buurke, J. H., Koopman, B. & Veltink, P. Pressure insoles for gait and balance estimation. 6th Dutch Bio-Medical Engineering Conference 2017, 2017.
- Reid, D. A., Samangoei, S., Chen, C., Nixon, M. S. & Ross, A. 2013. Soft biometrics for surveillance: An overview. *Handbook of statistics*, 31, 327-352.
- Ridgewell, E., Dobson, F., Bach, T. & Baker, R. 2010. A systematic review to determine best practice reporting guidelines for afo interventions in studies involving children with cerebral palsy. *Prosthetics and Orthotics International*, 34, 129-145.
- Roberts, M., Mongeon, D. & Prince, F. 2017. Biomechanical parameters for gait analysis: A systematic review of healthy human gait. *Phys. Ther. Rehabil*, 4.

- Roca-Dols, A., Losa-Iglesias, M. E., Sánchez-Gómez, R., Becerro-de-Bengoa-Vallejo, R., López-López, D., Rodríguez-Sanz, D., Martínez-Jiménez, E. M. & Calvo-Lobo, C. 2018. Effect of the cushioning running shoes in ground contact time of phases of gait. *Journal of the mechanical behavior of biomedical materials*, 88, 196-200.
- Roche, B., Simon, A.-L., Guilmin-Crépon, S., Boizeau, P., Andriss, B., Alberti, C., Presedo, A., Ilharreborde, B. & Husson, I. 2018. Test-retest reliability of an instrumented electronic walkway system (gaitrite) for the measurement of spatio-temporal gait parameters in young patients with friedreich's ataxia. *Gait & posture*, 66, 45-50.
- Roetenberg, D. 2006. *Inertial and magnetic sensing of human motion*, These de doctorat.
- Rouzbeh, S. & Babaei, M. 2015. Human gait recognition using body measures and joint angles. *International Journal*, 6, 2305-1493.
- Rucco, R., Agosti, V., Jacini, F., Sorrentino, P., Varriale, P., De Stefano, M., Milan, G., Montella, P. & Sorrentino, G. 2017. Spatio-temporal and kinematic gait analysis in patients with frontotemporal dementia and alzheimer's disease through 3d motion capture. *Gait & posture*, 52, 312-317.
- Rundo, F., Conoci, S., Ortis, A. & Battiato, S. 2018. An advanced bio-inspired photoplethysmography (ppg) and ecg pattern recognition system for medical assessment. *Sensors*, 18, 405.
- Sabhanayagam, T., Venkatesan, V. P. & SenthamaraiKannan, K. 2018. A comprehensive survey on various biometric systems. *International Journal of Applied Engineering Research*, 13, 2276-2297.
- Sakaguchi, K. & Hasegawa, T. 2006. Person perception through gait information and target choice for sexual advances: Comparison of likely targets in experiments and real life. *Journal of Nonverbal Behavior*, 30, 63-85.
- Sant'Anna, A., Wickström, N., Zügner, R. & Tranberg, R. A wearable gait analysis system using inertial sensors part i: Evaluation of measures of gait symmetry and normality against 3d kinematic data. International Conference on Bio-inspired Systems and Signal Processing, BIOSIGNALS 2012, Vilamoura, Algarve, 1-4 February, 2012, 2012. SciTePress, 180-188.
- Schepers, M., Giuberti, M. & Bellusci, G. 2018. Xsens mvn: Consistent tracking of human motion using inertial sensing. *Xsens Technol*, 1-8.

- Schmid, S., Schweizer, K., Romkes, J., Lorenzetti, S. & Brunner, R. 2013. Secondary gait deviations in patients with and without neurological involvement: A systematic review. *Gait & posture*, 37, 480-493.
- Schöllhorn, W., Nigg, B., Stefanyshyn, D. & Liu, W. 2002. Identification of individual walking patterns using time discrete and time continuous data sets. *Gait & Posture*, 15, 180-186.
- Schüle, S., Barth, J., Rampp, A., Rupprecht, R., Eskofier, B. M., Winkler, J., Gaßmann, K.-G. & Klucken, J. 2017. Instrumented gait analysis: A measure of gait improvement by a wheeled walker in hospitalized geriatric patients. *Journal of neuroengineering and rehabilitation*, 14, 1-11.
- Shah, S. & Aggarwal, J. 1996. Intrinsic parameter calibration procedure for a (high-distortion) fish-eye lens camera with distortion model and accuracy estimation. *Pattern Recognition*, 29, 1775-1788.
- Shan, Q., Li, Z., Jia, J. & Tang, C.-K. 2008. Fast image/video upsampling. *ACM Transactions on Graphics (TOG)*, 27, 1-7.
- Shen, Y., Wen, H., Luo, C., Xu, W., Zhang, T., Hu, W. & Rus, D. 2018. Gaitlock: Protect virtual and augmented reality headsets using gait. *IEEE Transactions on Dependable and Secure Computing*, 16, 484-497.
- Sheng, V. S., Provost, F. & Ipeirotis, P. G. Get another label? Improving data quality and data mining using multiple, noisy labelers. Proceedings of the 14th ACM SIGKDD international conference on Knowledge discovery and data mining, 2008. 614-622.
- Shu, L., Hua, T., Wang, Y., Li, Q., Feng, D. D. & Tao, X. 2010. In-shoe plantar pressure measurement and analysis system based on fabric pressure sensing array. *IEEE Transactions on information technology in biomedicine*, 14, 767-775.
- Sivapalan, S., Chen, D., Denman, S., Sridharan, S. & Fookes, C. Gait energy volumes and frontal gait recognition using depth images. 2011 International Joint Conference on Biometrics (IJCB), 2011. IEEE, 1-6.
- Smith-Ray, R. L., Hughes, S. L., Prohaska, T. R., Little, D. M., Jurivich, D. A. & Hedeker, D. 2015. Impact of cognitive training on balance and gait in older adults. *Journals of Gerontology Series B: Psychological Sciences and Social Sciences*, 70, 357-366.
- Song, C., Huang, Y., Huang, Y., Jia, N. & Wang, L. 2019. Gaitnet: An end-to-end network for gait based human identification. *Pattern recognition*, 96, 106988.

- Sprager, S. & Juric, M. B. 2015. Inertial sensor-based gait recognition: A review. *Sensors*, 15, 22089-22127.
- Stamatopoulos, C. 2011. *Orientation and calibration of long focal length cameras in digital close-range photogrammetry*.
- Stephan, C. N. 2015. Accuracies of facial soft tissue depth means for estimating ground truth skin surfaces in forensic craniofacial identification. *International journal of legal medicine*, 129, 877-888.
- Stevenage, S. V., Nixon, M. S. & Vince, K. 1999. Visual analysis of gait as a cue to identity. *Applied Cognitive Psychology: The Official Journal of the Society for Applied Research in Memory and Cognition*, 13, 513-526.
- Sturzenegger, M. & Stead, D. 2009. Close-range terrestrial digital photogrammetry and terrestrial laser scanning for discontinuity characterization on rock cuts. *Engineering Geology*, 106, 163-182.
- Suchomel, T. J., Nimphius, S. & Stone, M. H. 2016. The importance of muscular strength in athletic performance. *Sports medicine*, 46, 1419-1449.
- Świtoński, A., Polański, A. & Wojciechowski, K. Human identification based on gait paths. International Conference on Advanced Concepts for Intelligent Vision Systems, 2011. Springer, 531-542.
- Tahir, A. M., Chowdhury, M. E., Khandakar, A., Al-Hamouz, S., Abdalla, M., Awadallah, S., Reaz, M. B. I. & Al-Emadi, N. 2020. A systematic approach to the design and characterization of a smart insole for detecting vertical ground reaction force (vgrf) in gait analysis. *Sensors*, 20, 957.
- Tang, R. 2013. Mathematical methods for camera self-calibration in photogrammetry and computer vision.
- Tao, D., Li, X., Wu, X. & Maybank, S. J. 2007. General tensor discriminant analysis and gabor features for gait recognition. *IEEE transactions on pattern analysis and machine intelligence*, 29, 1700-1715.
- Tao, W., Liu, T., Zheng, R. & Feng, H. 2012. Gait analysis using wearable sensors. *Sensors*, 12, 2255-2283.
- Tawalbeh, L. a., Muheidat, F., Tawalbeh, M. & Quwaider, M. 2020. Iot privacy and security: Challenges and solutions. *Applied Sciences*, 10, 4102.
- Teufl, W., Lorenz, M., Miezal, M., Taetz, B., Fröhlich, M. & Bleser, G. 2019. Towards inertial sensor based mobile gait analysis: Event-detection and spatio-temporal parameters. *Sensors*, 19, 38.

- Teymouri, M., Halabchi, F., Mirshahi, M., Mansournia, M. A., Mousavi Ahranjani, A. & Sadeghi, A. 2017. Comparison of plantar pressure distribution between three different shoes and three common movements in futsal. *PloS one*, 12, e0187359.
- Tistarelli, M., Grosso, E. & Meuwly, D. Biometrics in forensic science: Challenges, lessons and new technologies. International Workshop on Biometric Authentication, 2014. Springer, 153-164.
- Tong, J. W. & Ng, E. Y. 2010. Preliminary investigation on the reduction of plantar loading pressure with different insole materials (srp–slow recovery poron®, p–poron®, ppf–poron®+ plastazote, firm and pps–poron®+ plastazote, soft). *The Foot*, 20, 1-6.
- Troje, N. F., Westhoff, C. & Lavrov, M. 2005. Person identification from biological motion: Effects of structural and kinematic cues. *Perception & Psychophysics*, 67, 667-675.
- Tvoroshenko, I. & Kukharchuk, V. 2021. Current state of development of applications for recognition of faces in the image and frames of video captures.
- Urbanová, P., Hejna, P. & Jurda, M. 2015. Testing photogrammetry-based techniques for three-dimensional surface documentation in forensic pathology. *Forensic science international*, 250, 77-86.
- van Mastrigt, N. M., Celie, K., Mieremet, A. L., Ruifrok, A. C. & Geradts, Z. 2018a. Critical review of the use and scientific basis of forensic gait analysis. *Forensic sciences research*, 3, 183-193.
- van Mastrigt, N. M., Celie, K., Mieremet, A. L., Ruifrok, A. C. C. & Geradts, Z. 2018b. Critical review of the use and scientific basis of forensic gait analysis. *Forensic Sci Res*, 3, 183-193.
- Vasconcelos, M. J. M. & Tavares, J. M. R. 2008. Human motion analysis: Methodologies and applications. *CMBBE 2008*.
- Vienne, A., Barrois, R. P., Buffat, S., Ricard, D. & Vidal, P.-P. 2017. Inertial sensors to assess gait quality in patients with neurological disorders: A systematic review of technical and analytical challenges. *Frontiers in psychology*, 8, 817.
- Viteckova, S., Kutilek, P., Svoboda, Z., Krupicka, R., Kauler, J. & Szabo, Z. 2018. Gait symmetry measures: A review of current and prospective methods. *Biomedical Signal Processing and Control*, 42, 89-100.
- Wafai, L., Zayegh, A., Woulfe, J., Aziz, S. M. & Begg, R. 2015. Identification of foot

- pathologies based on plantar pressure asymmetry. *Sensors*, 15, 20392-20408.
- Wahab, Y. & Bakar, N. A. Gait analysis measurement for sport application based on ultrasonic system. 2011 IEEE 15th international symposium on consumer electronics (ISCE), 2011. IEEE, 20-24.
- Wang, H., An, L., Feng, X., Zhao, J., Merryweather, A. & Xu, H. 2020. Ground reaction force adaptation during cross-slope walking on railroad ballast. *Gait & posture*, 75, 66-71.
- Wang, X. & Yan, W. Q. 2020. Human gait recognition based on frame-by-frame gait energy images and convolutional long short-term memory. *International journal of neural systems*, 30, 1950027.
- Wang, Y., Chen, Y., Bhuiyan, M. Z. A., Han, Y., Zhao, S. & Li, J. 2018. Gait-based human identification using acoustic sensor and deep neural network. *Future Generation Computer Systems*, 86, 1228-1237.
- Wilken, J. M., Rodriguez, K. M., Brawner, M. & Darter, B. J. 2012. Reliability and minimal detectable change values for gait kinematics and kinetics in healthy adults. *Gait & posture*, 35, 301-307.
- Wolff, G. 1935. Increased bodily growth of school-children since the war. *Lancet*, 1006-11.
- Woollacott, M. & Shumway-Cook, A. 2002. Attention and the control of posture and gait: A review of an emerging area of research. *Gait & posture*, 16, 1-14.
- Wright, D., Friedewald, M., Gutwirth, S., Langheinrich, M., Mordini, E., Bellanova, R., De Hert, P., Wadhwa, K. & Bigo, D. 2010. Sorting out smart surveillance. *Computer Law & Security Review*, 26, 343-354.
- Xu, C., Wen, X.-X., Huang, L.-Y., Shang, L., Yang, Z., Yan, Y.-B. & Lei, W. 2017. Reliability of the footscan® platform system in healthy subjects: A comparison of without top-layer and with top-layer protocols. *BioMed research international*, 2017.
- Yamin, N., Amran, M. A., Basaruddin, K., Salleh, A. & Rusli, W. 2017. Ground reaction force response during running on different surface hardness. *ARPN J. Eng. Appl. Sci*, 12, 2313-2318.
- Yang, G., Tan, W., Jin, H., Zhao, T. & Tu, L. 2019. Review wearable sensing system for gait recognition. *Cluster Computing*, 22, 3021-3029.
- Yang, S. X., Larsen, P. K., Alkjær, T., Lynnerup, N. & Simonsen, E. B. 2014a. Influence of velocity on variability in gait kinematics: Implications for

- recognition in forensic science. *Journal of forensic sciences*, 59, 1242-1247.
- Yang, S. X., Larsen, P. K., Alkjær, T., Simonsen, E. B. & Lynnerup, N. 2014b. Variability and similarity of gait as evaluated by joint angles: Implications for forensic gait analysis. *Journal of forensic sciences*, 59, 494-504.
- Yigit, S. & Mendes, M. 2018. Which effect size measure is appropriate for one-way and two-way anova models? A monte carlo simulation study. *Revstat Statistical Journal*, 16, 295-313.
- Yun, J.-S., Lee, S.-H., Woo, W.-T. & Ryu, J.-H. 2003. The user identification system using walking pattern over the ubifloor. *제어로봇시스템학회: 학술대회논문집*, 1046-1050.
- Yun, J., Woo, W. & Ryu, J. User identification using user's walking pattern over the ubifloor. *International Conference on Computational and Information Science*, 2005. Springer, 949-956.
- Zang, Y., Zhang, F., Di, C.-a. & Zhu, D. 2015. Advances of flexible pressure sensors toward artificial intelligence and health care applications. *Materials Horizons*, 2, 140-156.
- Zhang, S. & Li, L. 2013. The differential effects of foot sole sensory on plantar pressure distribution between balance and gait. *Gait & posture*, 37, 532-535.
- Zhou, H. & Hu, H. 2008. Human motion tracking for rehabilitation—a survey. *Biomedical signal processing and control*, 3, 1-18.
- Zhou, Y., Zia Ur Rehman, R., Hansen, C., Maetzler, W., Del Din, S., Rochester, L., Hortobágyi, T. & Lamothe, C. J. 2020. Classification of neurological patients to identify fallers based on spatial-temporal gait characteristics measured by a wearable device. *Sensors*, 20, 4098.
- Zhu, Y., Lan, Z., Newsam, S. & Hauptmann, A. Hidden two-stream convolutional networks for action recognition. *Asian conference on computer vision*, 2018. Springer, 363-378.
- Zijlstra, W. & Aminian, K. 2007. Mobility assessment in older people: New possibilities and challenges. *European Journal of Ageing*, 4, 3-12.

8 Appendix

		Knee_outer_joint_ankle_Heel_down_distance_mm																				
		Subset for alpha = 0.05																				
Subjects	N	1	2	3	4	5	6	7	8	9	10	11	12	13	14	15	16	17	18	19		
Tukey HSD ^a																						
Subjects_17	10	321.0726																				
Subjects_7	10		326.7580																			
Subjects_23	10			335.4688																		
Subjects_11	10				345.1170																	
Subjects_12	10				345.1170																	
Subjects_19	10				345.7213	345.7213																
Subjects_20	10					349.2622																
Subjects_4	10						353.9690															
Subjects_6	10							366.2220														
Subjects_18	10								370.0571													
Subjects_9	10									370.5380												
Subjects_13	10										370.9455											
Subjects_10	10											380.7865										
Subjects_22	10												387.7782									
Subjects_16	10													392.6183								
Subjects_14	10														396.8745							
Subjects_8	10															402.7035						
Subjects_21	10																405.7476	405.7476				
Subjects_15	10																	405.1131				
Subjects_3	10																		413.9040			
Subjects_2	10																			422.2005		
Subjects_5	10																				430.4674	
Subjects_1	10																					455.9685

		Knee_inner_joint_ankle_Heel_down_distance_mm																						
		Subset for alpha = 0.05																						
Subjects	N	1	2	3	4	5	6	7	8	9	10	11	12	13	14	15	16	17	18	19	20	21	22	23
Tukey HSD ^a																								
Subjects_17	1000	359.5884																						
Subjects_9	1000		364.5796																					
Subjects_23	1000			368.6178																				
Subjects_7	1000				373.9526																			
Subjects_19	1000					378.7576																		
Subjects_20	1000						383.7781																	
Subjects_13	1000							386.3974																
Subjects_9	1000								389.4462															
Subjects_6	1000									392.9307														
Subjects_4	1000										396.4811													
Subjects_3	1000											400.5734												
Subjects_10	1000												405.4765											
Subjects_11	1000													409.0781										
Subjects_10	1000														414.4240									
Subjects_12	1000															415.5143								
Subjects_2	1000																419.5345							
Subjects_5	1000																	427.2943						
Subjects_16	1000																		430.5583					
Subjects_22	1000																			433.8325				
Subjects_14	1000																				441.7967			
Subjects_21	1000																					444.9546		
Subjects_1	1000																						453.7949	
Subjects_15	1000																							459.02

		Knee_angle_Heel_down																						
		Subset for alpha = 0.95																						
Subjects	N	1	2	3	4	5	6	7	8	9	10	11	12	13	14	15	16	17	18	19	20	21	22	
Tukey HSD ^a																								
Subjects_11	10	3.1000																						
Subjects_7	10		4.3000																					
Subjects_2	10			6.0500																				
Subjects_14	10				6.5300																			
Subjects_19	10					7.3800																		
Subjects_10	10						8.2700																	
Subjects_5	10							9.0900																
Subjects_3	10								10.8400															
Subjects_12	10									12.1300														
Subjects_21	10										13.7200													
Subjects_8	10											14.0200												
Subjects_8	10												15.6300											
Subjects_19	10													16.6300										
Subjects_16	10														17.6000									
Subjects_1	10															19.7900								
Subjects_15	10																20.7100							
Subjects_22	10																	21.5300						
Subjects_4	10																		22.0000					
Subjects_9	10																			23.8200				
Subjects_13	10																				24.6200			
Subjects_17	10																					25.4900		
Subjects_23	10																						26.2900	
Subjects_20	10																							27.4600
Sig.		1.000	1.000	1.000	1.000	1.000	1.000	1.000	1.000	1.000	1.000	1.000	1.000	1.000	1.000	1.000	1.000	1.000	1.000	1.000	1.000	1.000	1.000	1.000

Means for groups in homogeneous subsets are displayed.
^a Uses Harmonic Mean Sample Size = 10.000.

Knee_Inner_Joint_Ankle_Midstance

Tukey HSD* Subset for alpha = 0.05

Subjects	N	1	2	3	4	5	6	7	8	9	10	11	12	13	14	15	16	17	18	19	20	21	22
Subjects_17	10	352.5152																					
Subjects_8	10		357.4238																				
Subjects_23	10			361.3896																			
Subjects_7	10				366.6287																		
Subjects_19	10					371.3332																	
Subjects_20	10						376.2515																
Subjects_13	10							378.8176															
Subjects_6	10								381.9113														
Subjects_4	10									385.2962													
Subjects_3	10										388.7077												
Subjects_10	10											392.7172											
Subjects_11	10												397.5286										
Subjects_18	10													401.0569									
Subjects_12	10														406.2960								
Subjects_2	10															407.3652							
Subjects_5	10																411.4282						
Subjects_16	10																	418.9126					
Subjects_22	10																		422.1202				
Subjects_14	10																			425.3278			
Subjects_21	10																				430.1329		
Subjects_1	10																					436.2336	
Subjects_15	10																						444.8941
Sig.		1.000	1.000	1.000	1.000	1.000	1.000	1.000	1.000	1.000	1.000	1.000	1.000	1.000	1.000	1.000	1.000	1.000	1.000	1.000	1.000	1.000	1.000

Means for groups in homogeneous subsets are displayed.
a. Uses Harmonic Mean Sample Size = 10.000.

Knee_outer_Joint_Ankle_midstance

Tukey HSD* Subset for alpha = 0.95

Subjects	N	1	2	3	4	5	6	7	8	9	10	11	12	13	14	15	16	17	18	19		
Subjects_8	10	344.4000																				
Subjects_17	10		348.8938																			
Subjects_7	10			350.1000																		
Subjects_23	10				364.6425																	
Subjects_13	10					367.9000																
Subjects_6	10						374.2000															
Subjects_19	10							375.7870														
Subjects_9	10								376.8000													
Subjects_20	10									380.3918												
Subjects_3	10										381.4000											
Subjects_4	10											384.6000										
Subjects_11	10												394.5000									
Subjects_10	10													394.9000								
Subjects_18	10														402.2350							
Subjects_2	10															408.7000						
Subjects_12	10																414.2000					
Subjects_5	10																	417.4000				
Subjects_22	10																		421.4981			
Subjects_16	10																			426.7593		
Subjects_14	10																				428.8046	
Subjects_21	10																					441.0285
Subjects_15	10																					445.5228
Subjects_1	10																					447.1000
Sig.		1.000	.998	1.000	1.000	1.000	.996	.996	1.000	1.000	1.000	1.000	1.000	1.000	1.000	1.000	1.000	1.000	1.000	1.000	1.000	1.000

Means for groups in homogeneous subsets are displayed.
a. Uses Harmonic Mean Sample Size = 10.000.

Knee_angle_midstance

Tukey HSD* Subset for alpha = 0.95

Subjects	N	1	2	3	4	5	6	7	8	9	10	11	12	13	14	15	16	17	18	19	20	
Subjects_4	10	27.6000																				
Subjects_17	10		29.5000																			
Subjects_12	10			31.1000																		
Subjects_2	10				35.1000																	
Subjects_5	10					36.5000																
Subjects_10	10						38.1000															
Subjects_19	10							40.1000														
Subjects_7	10								41.9000													
Subjects_21	10									42.0000												
Subjects_14	10										42.8000											
Subjects_8	10											44.3000										
Subjects_23	10												45.2000									
Subjects_9	10													46.8000								
Subjects_6	10														47.5000							
Subjects_3	10															52.8000						
Subjects_11	10																54.1000					
Subjects_16	10																	54.8000				
Subjects_1	10																		56.1000			
Subjects_22	10																			57.8000		
Subjects_18	10																				58.1000	
Subjects_13	10																					59.7000
Subjects_15	10																					62.2000
Subjects_20	10																					62.3000
Sig.		1.000	1.000	1.000	1.000	1.000	1.000	1.000	1.000	1.000	1.000	1.000	1.000	1.000	1.000	1.000	1.000	1.000	1.000	1.000	1.000	1.000

Means for groups in homogeneous subsets are displayed.
a. Uses Harmonic Mean Sample Size = 10.000.

		Knee_outer_Joint_Ankle_Toeoff_distance_mm																		
Tukey HSD*		Subset for alpha = 0.95																		
Subjects	N	1	2	3	4	5	6	7	8	9	10	11	12	13	14	15	16	17	18	19
Subjects_17	10	359.2807																		
Subjects_7	10		365.6444																	
Subjects_23	10			375.3909																
Subjects_11	10				386.1892															
Subjects_12	10				386.1892															
Subjects_19	10				386.8629															
Subjects_20	10					391.6064														
Subjects_4	10						394.5919													
Subjects_6	10							409.8058												
Subjects_18	10								414.0971											
Subjects_9	10								414.6343											
Subjects_13	10								415.0919											
Subjects_10	10									426.1029										
Subjects_22	10										433.9225									
Subjects_16	10											439.3419								
Subjects_14	10												444.1054							
Subjects_8	10													450.8269						
Subjects_21	10														454.0309					
Subjects_15	10															458.6557				
Subjects_3	10																481.1992			
Subjects_2	10																	472.4463		
Subjects_5	10																		481.6937	
Subjects_1	10																			510.2315
Sig.		1.000	1.000	1.000	1.000	1.000	1.000	1.000	1.000	1.000	1.000	1.000	1.000	1.000	1.000	1.000	1.000	1.000	1.000	1.000

Means for groups in homogeneous subsets are displayed.
a. Uses Harmonic Mean Sample Size = 10.000.

		Knee_inner_Joint_Ankle_Toeoff_distance_mm																			
Tukey HSD*		Subset for alpha = 0.95																			
Subjects	N	1	2	3	4	5	6	7	8	9	10	11	12	13	14	15	16	17	18	19	20
Subjects_8	10	392.6709																			
Subjects_17	10		397.9091																		
Subjects_7	10			399.1702																	
Subjects_23	10				415.7440																
Subjects_13	10					419.5592															
Subjects_6	10						426.6494														
Subjects_19	10							429.4560													
Subjects_9	10								429.6130												
Subjects_3	10									431.2202											
Subjects_20	10										433.7089										
Subjects_4	10											439.5046									
Subjects_11	10												448.7931								
Subjects_10	10													450.2478							
Subjects_18	10														458.6109						
Subjects_2	10															485.9938					
Subjects_12	10																472.2525				
Subjects_5	10																	475.9026			
Subjects_22	10																		480.5741		
Subjects_16	10																			486.5784	
Subjects_14	10																				488.9091
Subjects_21	10																				502.8464
Subjects_15	10																				507.1226
Subjects_1	10																				509.7646
Sig.		1.000	.998	1.000	1.000	1.000	.996	1.000	1.000	1.000	1.000	1.000	1.000	1.000	1.000	1.000	1.000	1.000	1.000	1.000	1.000

Means for groups in homogeneous subsets are displayed.
a. Uses Harmonic Mean Sample Size = 10.000.

		Knee_angle_Toe_off																					
Tukey HSD*		Subset for alpha = 0.95																					
Subjects	N	1	2	3	4	5	6	7	8	9	10	11	12	13	14	15	16	17	18	19	20	21	22
Subjects_23	10	9.9200																					
Subjects_4	10		13.7600																				
Subjects_2	10			19.3600																			
Subjects_11	10				20.8960																		
Subjects_15	10					23.6160																	
Subjects_22	10						26.4040																
Subjects_7	10							29.0980															
Subjects_3	10								34.6990														
Subjects_9	10									38.8160													
Subjects_20	10										43.9040												
Subjects_5	10											44.8640											
Subjects_9	10												48.0960										
Subjects_16	10													53.2160									
Subjects_13	10														56.3200								
Subjects_1	10															63.3280							
Subjects_12	10																66.2720						
Subjects_17	10																	68.8960					
Subjects_6	10																		70.4000				
Subjects_21	10																			76.2240			
Subjects_10	10																				78.7840		
Subjects_14	10																					81.5680	
Subjects_18	10																						84.1280
Subjects_19	10																						87.8720
Sig.		1.000	1.000	1.000	1.000	1.000	1.000	1.000	1.000	1.000	.997	1.000	1.000	1.000	1.000	1.000	1.000	1.000	1.000	1.000	1.000	1.000	1.000

Means for groups in homogeneous subsets are displayed.
a. Uses Harmonic Mean Sample Size = 10.000.